

UNIVERSITY OF MALTA
Faculty of Engineering
Department of Systems and Control Engineering

FINAL YEAR PROJECT
B.ENG. (Hons)

Proportional and Simultaneous Myoelectric Control of a Robotic Arm

by

Christian Grech

A dissertation submitted in partial fulfillment
of the requirements of the award of

Bachelor of Engineering (Hons.) of the University of Malta



UNIVERSITY OF MALTA

FACULTY/INSTITUTE/CENTRE OF/FOR _____ Engineering

DECLARATION OF AUTHENTICITY FOR UNDERGRADUATE STUDENTS

Student's I.D. /Code _____ 11294G

Student's Name & Surname _____ Christian Grech

Course _____ Bachelor of Engineering (Hons.)

Title of Long Essay/Dissertation:

Proportional and Simultaneous Myoelectric Control of a Robotic Arm

I hereby declare that I am the legitimate author of this Long Essay/Dissertation and that it is my original work.

No portion of this work has been submitted in support of an application for another degree or qualification of this or any other university or institution of higher education.

I hold the University of Malta harmless against any third party claims with regard to copyright violation, breach of confidentiality, defamation and any other third party right infringement.

Signature of Student

18/07/2016

Date

Copyright Notice

1. Copyright in text of this dissertation rests with the Author. Copies (by any process) either in full, or of extracts may be made only in accordance with regulations held by the Library of the University of Malta. Details may be obtained from the Librarian. This page must form part of any such copies made. Further copies (by any process) made in accordance with such instructions may not be made without the permission (in writing) of the Author.
2. Ownership of the right over any original intellectual property which may be contained in or derived from this dissertation is vested in the University of Malta and may not be made available for use by third parties without the written permission of the University, which will prescribe the terms and conditions of any such agreement.

Abstract

In the past years, machine and robot technologies have progressed rapidly, improving human life and making tasks much easier to execute. In a world that caters to the able-bodied, someone who has lost his/her upper limb often becomes dependent on other people in order to perform the simplest of tasks. Human-machine interfaces (HMI) are used to help these people perform specific limb movements. HMIs provide control of a device using only signals produced by the body which are called biosignals.

This project's aim is to develop an HMI for the control of a robotic arm manipulator through the use of non-invasive surface electromyography (EMG) signals. These signals can provide information on the limb movement being performed, such as its position in 3D space. Current research is focused on developing a reliable prosthetic device which incorporates simultaneous control of different joints. In this project, a model which converts EMG signals from multiple muscles to elbow and shoulder angles for simultaneous and proportional control is developed and tested in real-time. Furthermore an application to this project is demonstrated where a robotic arm replicates the user's wrist position in real-time as the user moves in the horizontal plane, stops and points towards an object. This system's performance was assessed using the correlation coefficient (CC) measure which was found to be 0.908 ± 0.043 and 0.951 ± 0.015 for the x and y directions respectively.

This project focuses on developing a system which caters for different speeds and flexible variety of movements. In this project seven different sequential and simultaneous movements in different planes were successfully modelled. The average root mean square error (RMSE) for sequential movements varied from 5.43° to 12.34° while the best performing simultaneous joint model resulted with an average cross-validated RMSE of $9.03^\circ \pm 0.33^\circ$ for the elbow angle estimation and $7.30^\circ \pm 0.85^\circ$ for the shoulder angle estimation. Incorporating these models into a single model would be the final step in creating a fully functional prosthetic device which could replace the functions of the elbow and shoulder.

Acknowledgements

First I would like to thank my supervisor, Dr Tracey Camilleri *B.Eng.(Hons.)*, *Ph.D.*, *M.IEEE*, for her invaluable guidance, dedication and support throughout this research. She has provided me with indispensable advice and knowledge without which this project would not have been possible.

I would also like to thank my co-supervisor, Dr Ing. Marvin Bugeja *B.Eng.(Hons.)*, *Ph.D.*, *M.IEEE*, for his assistance and advice throughout the duration of the project.

I would like to further extend my gratitude to the Systems and Control Laboratory technician, Mr. Noel Agius, for always being available to provide the necessary support, for which I am grateful. My sincere thanks also goes to Mr. Norbert Gauci and Ing. Carl Azzopardi who have provided their assistance to utilise the equipment present in the laboratories, around which this project is based.

Finally, I must express my very profound gratitude to all my family, especially my parents for their patience and support they have always shown and which I can never equally repay.

Contents

Declaration of Authorship	i
Copyright Notice	ii
Abstract	iii
Acknowledgements	iv
Contents	v
List of Figures	viii
List of Tables	x
List of Abbreviations and Notation	xi
1 Introduction	1
1.1 Objectives of Dissertation	1
1.2 Outline of Dissertation	2
2 Theoretical Background	4
2.1 Introduction	4
2.2 The source of the EMG signal	4
2.2.1 The Sliding Filament theory	5
2.3 Muscles of the shoulder and upper limb	6
2.4 Why EMG signals?	8
2.5 EMG signal detection	10
2.5.1 Skin surface electrodes	10
2.5.2 Inserted electrodes	11
2.6 Applications of EMG signal	12
2.7 Summary	13
3 Literature Review	14
3.1 Introduction	14
3.2 Characteristics of an EMG control system	14
3.2.1 Myoelectric control	14
3.2.2 The ideal myoelectric control system	15

3.3	EMG-to-joint angle models	16
3.3.1	State space representation	16
3.3.2	Linear regression	18
3.3.2.1	Linearising EMG data	19
3.3.3	Multi-layer perceptron	20
3.4	Transient properties of the EMG signal	22
3.5	Previous work	24
3.6	Concluding Analysis	25
4	Analysis of the EMG-Joint angle system	27
4.1	Introduction	27
4.2	The offline data acquisition system	27
4.2.1	ZeroWire EMG acquisition box	28
4.2.2	Vicon motion capture system	29
4.2.3	Inverse kinematics	30
4.3	Overview of the real-time system	31
4.3.1	Introduction	31
4.3.2	CRS Catalyst-5T robot system	32
4.3.3	Robot Simulink model	33
4.3.4	Forward kinematics	34
4.4	Testing the Catalyst-5T robot system	35
4.4.1	Tests	35
4.4.2	Discussion of Results	38
4.5	State space model	39
4.5.1	Experimental and Analysis procedure	39
4.5.2	Order variation and filter changes	41
4.5.3	Results without cross-validation	42
4.5.4	Results with cross-validation	43
4.5.5	Discussion of Results	46
4.6	Summary	48
5	System Identification	49
5.1	Introduction	49
5.2	Data acquisition and Pre-processing	49
5.2.1	Effect of feature transformation and window size	50
5.3	Linear regression	52
5.3.1	Procedure	52
5.3.2	Results without cross-validation	53
5.3.3	Results with cross-validation	54
5.3.4	Discussion of Results	55
5.4	Multi-layer perceptron	55
5.4.1	Procedure	56
5.4.2	Defining the architecture of the network	57
5.4.3	Results without cross-validation	58

5.4.4	Results with cross-validation	59
5.4.5	Discussion of Results	60
5.5	Summary	61
6	Modelling different joint movements	63
6.1	Introduction	63
6.2	Single joint movements	64
6.2.1	Results	65
6.2.1.1	Movement in the x-z plane	65
6.2.1.2	Movement in the x-y plane	66
6.2.1.3	Movement in the y-z plane	67
6.2.2	Performance as a function of training set size	67
6.3	Simultaneous joint movements	69
6.3.1	Results	71
6.3.1.1	Movement in the x-z plane	71
6.3.1.2	Movement in the x-y plane	72
6.3.1.3	Movement in the y-z plane	74
6.4	Discussion of Results	74
6.5	Summary	77
7	Real-time Application	78
7.1	Introduction	78
7.2	Elbow joint angle replication	78
7.2.1	Experimental Procedure	79
7.2.2	Results	79
7.3	Simultaneous movement replication	81
7.3.1	Application Procedure	82
7.3.2	Results	83
7.4	Summary	85
8	Conclusion	86
8.1	Project Objectives and Achievements	86
8.2	Accomplishments and Recommendations	88
References		91

List of Figures

2.1	The composition of a muscle fibre	5
2.2	Myofibril contraction	6
2.3	Anatomy of the shoulder and upper limb	7
2.4	Movements of the forearm	8
2.5	Relation between EMG signal and elbow joint angle	9
2.6	Passive surface electrode	10
2.7	The two types of inserted electrodes	11
3.1	State space model example	17
3.2	Linear regression example	19
3.3	Effect of non-linear transformations on the estimation of joint angles	20
3.4	Structure of a multi-layer perceptron	21
4.1	Offline data acquisition system diagram	28
4.2	ZeroWire EMG amplifier box and probes	28
4.3	Vicon motion capture system at the Biomedical Engineering Lab . .	29
4.4	Position of the Vicon markers	30
4.5	Online data acquisition system diagram	31
4.6	CRS Catalyst-5T robot system	32
4.7	Joint-level position control flow diagram	33
4.8	Arm model	34
4.9	Range of robotic arm's elbow joint	36
4.10	Testing the CRS Catalyst-5T robot system	37
4.11	Analysing the currents sent to the motors	38
4.12	Elbow flexion/extension motion and markers' position	40
4.13	Effect of changing filter cutoff frequency	41
4.14	Effect of order variation on the RMSE	42
4.15	Actual and estimated elbow joint angle using biceps brachii EMG for Trial 7	43
4.16	Actual and estimated elbow joint angle using triceps brachii EMG for Trial 7	44
4.17	Biceps brachii results (forward cross-validation) for Trial 7	46
4.18	Triceps brachii results (reverse cross-validation) for Trial 7	46
5.1	Electrode and position marker placement	50
5.2	Pre-processing biceps brachii EMG data	51

5.3	Comparing how performance (RMSE), varies with window size and feature used	51
5.4	Actual and estimated angles for Trial 6	54
5.5	Actual and estimated angles for Trials 5 and 6	55
5.6	Training the MLP	56
5.7	MLP structure for elbow movement	58
5.8	Actual and estimated angles for Trial 2	59
5.9	Actual and estimated angles for Trials 5 and 6	60
5.10	Comparing performance of the three models	61
6.1	EMG electrode and plane references	63
6.2	The three types of shoulder single joint movements	64
6.3	Actual and estimated angles for Trials 5 and 6	66
6.4	Actual and estimated angles for Trials 1 and 2	67
6.5	Actual and estimated angles for Trials 1 and 2	68
6.6	The RMSE obtained for different training set sizes	69
6.7	The three types of simultaneous joint movements	70
6.8	MLP structure for simultaneous control	70
6.9	The three EMG sources with the corresponding joint angle	71
6.10	Actual and estimated joint angles for Trials 7 and 8	72
6.11	Actual and estimated joint angles for Trials 1 and 2	73
6.12	Actual and estimated joint angles for Trials 3 and 4	75
6.13	Comparing performance of the three single joint movements	76
6.14	Comparing performance of the three simultaneous movements	77
7.1	Human and robotic arm elbow angle for Trial 1	80
7.2	Robotic arm's position control Simulink model	81
7.3	Real-time wrist position control application	82
7.4	MLP structure for the real-time, simultaneous joint movement application	83
7.5	Human and robotic arm's x-y position for Trial 3	84

List of Tables

4.1	Joint specifications for the CataLyst-5T arm	32
4.2	Non cross-validation results for model	43
4.3	Cross-validation results for biceps brachii EMG	45
4.4	Cross-validation results for triceps brachii EMG	45
4.5	State Space model analysis- Summary of results	47
5.1	Linear regression non cross-validation results	53
5.2	Linear regression cross-validation results	54
5.3	MLP elbow angle non cross-validation results	59
5.4	MLP elbow angle cross-validation results	60
6.1	Shoulder angle in x-z plane cross-validation results	65
6.2	Shoulder angle in x-y plane cross-validation results	66
6.3	Shoulder angle in y-z plane cross-validation results	67
6.4	MLP average elbow and shoulder angle performance	68
6.5	Simultaneous movement in x-z plane cross-validation results	72
6.6	Simultaneous movement in x-y plane cross-validation results	73
6.7	Simultaneous movement in y-z plane cross-validation results	74
7.1	Human and robotic arm elbow angles performance	80
7.2	Human and robotic arm simultaneous control performance	84

List of Abbreviations and Notation

ANN	Artificial Neural Network
BPNN	Back-Propagation Neural Network
CC	Correlation Coefficient
CV	Cross-Validation
EMG	Electromyography
HMI	Human Machine Interface
LR	Linear Regression
MLP	Multi-Layer Perceptron
N4SID	Numerical Subspace State Space System IDentification
R²	Coefficient of determination
RMS	Root Mean Square
RMSE	Root Mean Square Error
SD	Standard Deviation

Chapter 1

Introduction

Biosignals are becoming increasingly important in many practical uses including biomedical and clinical applications, control of prosthetic devices, human machine interfaces (HMIs) and more. HMIs are used mostly to help people with reduced mobility who cannot use a standard joystick or keyboard as a control input, to control a machine. Besides this application, HMIs have other uses, such as tele-operation, where robots can be controlled from remote places.

An HMI is possible through the extraction of features from biosignals such as electroencephalography (EEG) and electromyography (EMG) which are both physical quantities that vary in time. This project focuses solely on EMG-based control where muscle activity is recorded through surface electrodes placed at strategic positions on the subject's muscles. Many commercial EMG-based devices use a discrete form of robotic arm control called gesture recognition techniques, where EMG signals are used to identify a discrete number of movements. This dissertation, however, focuses on developing an HMI to control a robotic arm's position continuously in time through EMG signals from the upper limb. Furthermore, the ability of the model to control more than one degree of freedom in a natural manner will be evaluated. This type of control is known as proportional and simultaneous myoelectric control.

1.1 Objectives of Dissertation

This project continues from two previous projects by Paul Bezzina [1] titled ‘EMG-Based Control of a Robotic Arm’ and by Sean Grech [2] titled ‘Analysis of EMG Signals for Real-Time Control of a Robotic Arm’. The former project focused on developing a state space model which converts EMG data from five muscles to

elbow, shoulder and wrist joint angles. Results show that this model performed well in replicating the movement, however errors in joint angle estimation increased drastically when cross-validated data was considered. In the latter project, the state space model was improved and a real-time system was implemented. Finally, one movement, elbow flexion and extension was replicated in real-time by using biceps brachii EMG. These two projects will be analysed in more depth in the literature review.

In this project, the aim is to improve the accuracy of the EMG-to-joint angle model, and extend it to replicate movements in different planes. A literature review is to be carried out to study the different techniques used in previous works which make use of EMG signals in order to control a robotic arm. After tests are carried out on the current and new techniques, the best model will be extended to mimic movements in different 2D planes. The movements replicated in previous projects were cyclic sequential movements performed at a specific speed using a metronome. In this project, intermittent and simultaneous movement replication will be included. Finally the replication of an everyday movement will be performed, so as to emphasise the practicality of such a system in real life.

1.2 Outline of Dissertation

Following this introduction, Chapter 2 provides background information about the EMG signal, anatomy and physiology of the human upper limb and applications of the EMG signal. In Chapter 3 a thorough literature review is carried out in order to study the different system identification techniques used by researchers to control devices remotely using EMG signals. Following this review, the best methods to carry out this project are determined.

Chapter 4 provides the results of the analysis carried out on the existing control system. The state space model is tested, and results are compared with those of previous projects. This is followed by Chapter 5 which presents two alternative EMG-joint angle models, both of which are tested and discussed.

Chapter 6 makes use of the best-performing model to extend the control system to six additional movements, with the inclusion of three simultaneous movements in three different 2D planes. Chapter 7 focuses on the replication of the movements

modelled in real-time, with an emphasis given to a real life application which replicates a simultaneous, intermittent proportional movement.

Chapter 8 concludes this dissertation and provides potential ideas and improvements for possible future work on myoelectric control systems.

Chapter 2

Theoretical Background

2.1 Introduction

This chapter provides a brief outline on electromyography (EMG) signals, giving information on the source of this signal, the anatomy of the upper limb, the benefits and weaknesses of using EMG signals in our analysis, and several methods used to detect the signal. Furthermore, a quick overview on the applications of the signal will be provided.

2.2 The source of the EMG signal

Electromyography (EMG) is the study of muscle activity based on the analysis of electrical signals which originate from the muscles. This signal is a complex signal, as it concerns both the anatomical and physiological characteristics of the muscles, in addition to the properties of the instrumentation used for detecting and recording the signal.

EMG signals are caused by motor unit action potentials. Action potentials are discharged by each of the motor units activated during a contraction. The structural unit of contraction is the muscle fibre. Each muscle compartment has fibres grouped together into narrow sub-compartments separated by a connective tissue which holds the muscle cells together in their parallel arrangement. Best described as a very fine thread, the muscle fibre has a length of up to 30mm but is less than 0.1mm wide. On contracting, it shortens to about 57 per cent of its resting length [3]. The individual fibres may be broken down into clusters of individual *myofibrils*, which are tiny strands, as can be seen in Figure 2.1.

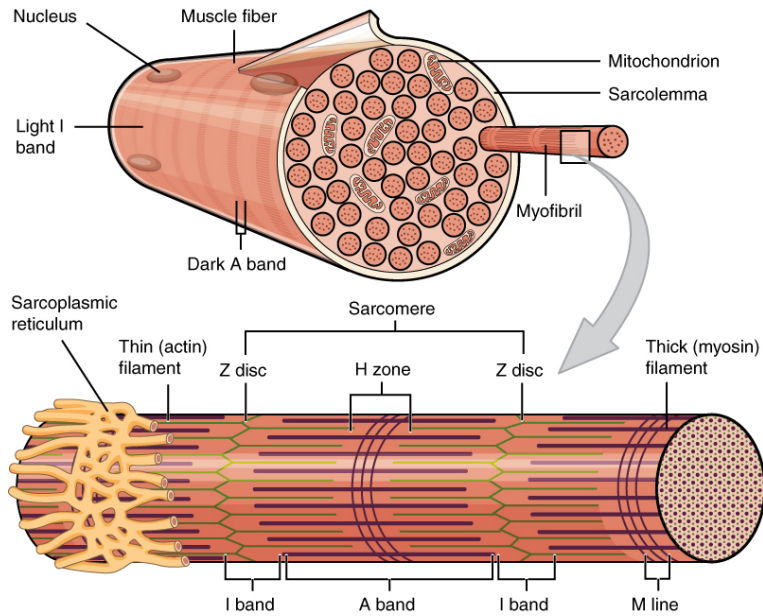


FIGURE 2.1: The composition of a muscle fibre [4]

The basic anatomical structure from which all muscles are made is called a *sarcomere*. Each myofibril consists of a number of *myosin* and *actin* filaments which make up the sarcomere, which is basically a unit of overlapping myosin and actin filaments. Every sarcomere is around $2 \mu\text{m}$ in length with a three-dimensional cylindrical arrangement and is bordered by structures called Z-discs, to which the actin filaments are attached (see Figure 2.1).

2.2.1 The Sliding Filament theory

The sliding filament theory is the model by which muscles are thought to contract. The process of muscle contraction can be divided into four segments:

1. When an impulse arrives at the myoneural junction (where a motor neuron can transmit a signal to the muscle fibre), a chemical called acetylcholine is discharged. This causes Calcium (Ca^+) to be released and as a result a bridge is created as the myosin filaments bind to the actin.
2. Discharge of energy (by the breakdown of Adenosine triphosphate (ATP)) enables the myosin to pull the actin filaments inwards and as a result the muscle is shortened. This happens along every myofibril in the muscle cell as can be seen in Figure 2.2.
3. When an ATP molecule attaches to the myosin head, the myosin separates from the actin and the bridge is demolished. When the ATP is broken

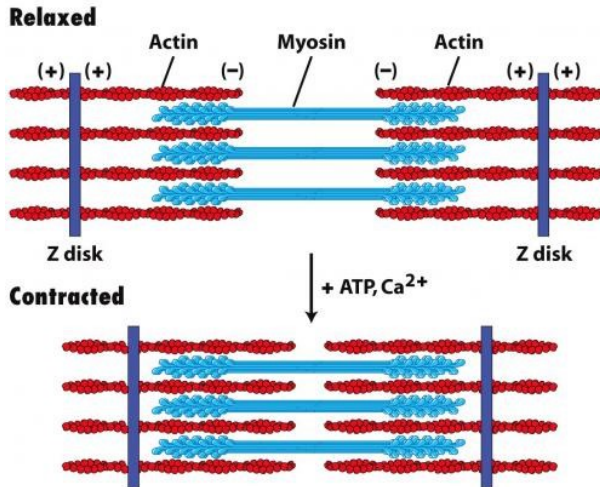


FIGURE 2.2: Myofibril contraction [6]

down the myosin head attaches to another actin binding site and repeats the process. This repeated movement of the actin over the myosin is referred to as the *ratchet mechanism*.

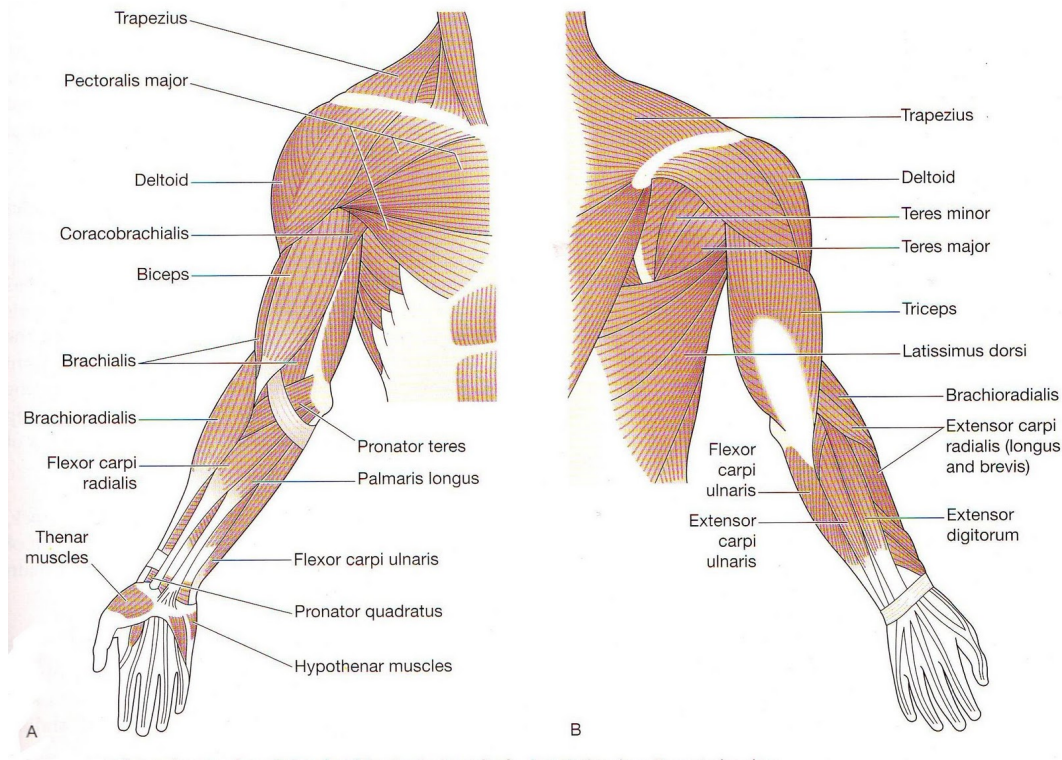
4. This process of contraction can keep going on until there is sufficient ATP and Ca+ supply. When the impulse stops, the actin returns to its initial position causing the muscle to lengthen and relax [5].

2.3 Muscles of the shoulder and upper limb

Muscles of the shoulder and upper limb can be classified into four categories: muscles which stabilise and position the pectoral girdle, muscles which move the arm, muscles which move the forearm, and those that move the wrist and hand. Figure 2.3 shows all the muscles discussed in each group below.

Muscles that position the pectoral girdle:

The pectoral girdle joins the upper limbs to the axial skeleton and it is the point where the muscles of the upper back, chest and neck are attached. The main muscle involved in the elevation and depression of the shoulder is the *Trapezius*.



The main muscles of the shoulder and upper limb. A: anterior view. B: posterior view.

FIGURE 2.3: Anatomy of the shoulder and upper limb [7]

Muscles that move the humerus:

The humerus (the bone of the upper arm) can be moved by muscles which cross the shoulder joint. The two axial muscles are the *Pectoralis major*, which covers much of the superior part of the anterior thorax and the *Latissimus dorsi*, which is located in the posterior part of the upper limb [8]. The *Deltoid*, the muscle on the rounded section of the shoulder is the major abductor of the arm, but it also enables flexion/extension and medial/lateral rotation. This muscle has three heads: the anterior, lateral and posterior heads. The *Teres major* muscle is inferior to the *Teres minor* as it extends the arm, and is involved in adduction and medial rotation of the arm. The long *Teres minor* revolves laterally and extends the arm while the *Coracobrachialis* adducts and flexes the arm.

Muscles that move the forearm:

The forearm has four main types of movements at the elbow joint: extension, flexion, supination and pronation (see Figure 2.4). The muscles involved in flexing include the *Biceps brachii*, *Brachioradialis* and *Brachialis*. The muscles involved in extending are the *Triceps brachii* and *Anconeus*. The pronator muscles are the *Pronator teres* and the *Pronator quadratus*, and the *Supinator* muscle is the only

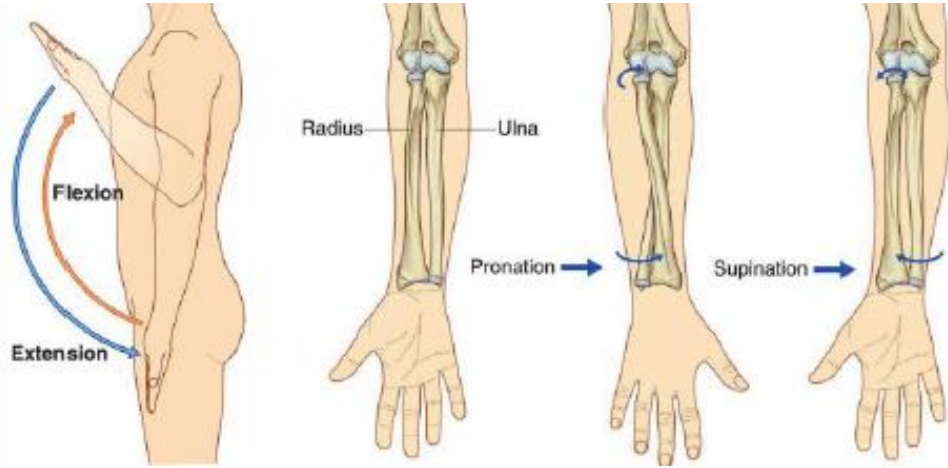


FIGURE 2.4: Movements of the forearm [9]

one that turns the forearm anteriorly.

Muscles that move the hand and wrist:

The muscles in the anterior part of the forearm stem from the humerus and insert onto different parts of the hand. The anterior part of the forearm includes the *Flexor carpi radialis*, *Flexor carpi ulnaris* and *Palmaris longus*. The muscles in the posterior part of the forearm include the *Extensor carpi radialis brevis*, *Extensor digitorum* and the *Extensor carpi ulnaris* [8].

2.4 Why EMG signals?

Using surface EMG signals in robot control applications has many benefits. Surface EMG recordings are an easy and non-invasive way to obtain information on the energy of a particular muscle. Current technology allows processing and amplification of the signal to occur in the electrode, and the possibility for the signal to be transmitted to a remote location.

Besides giving a measurement on the energy of a particular muscle, the EMG signal provides a range of other information. For example, as can be seen in Figure 2.5, there is a relation between the position of the upper limb and the EMG signal observed from the biceps brachii and triceps brachii EMG. Moreover, EMG signals can give information about the intention of a certain motion, 50-100ms before the motion actually happens [10]. Activation and musculoskeletal dynamics are the main sources of this Electro Mechanical Delay (EMD), and this feature is beneficial in applications where such time delays in action can play an important role [11].

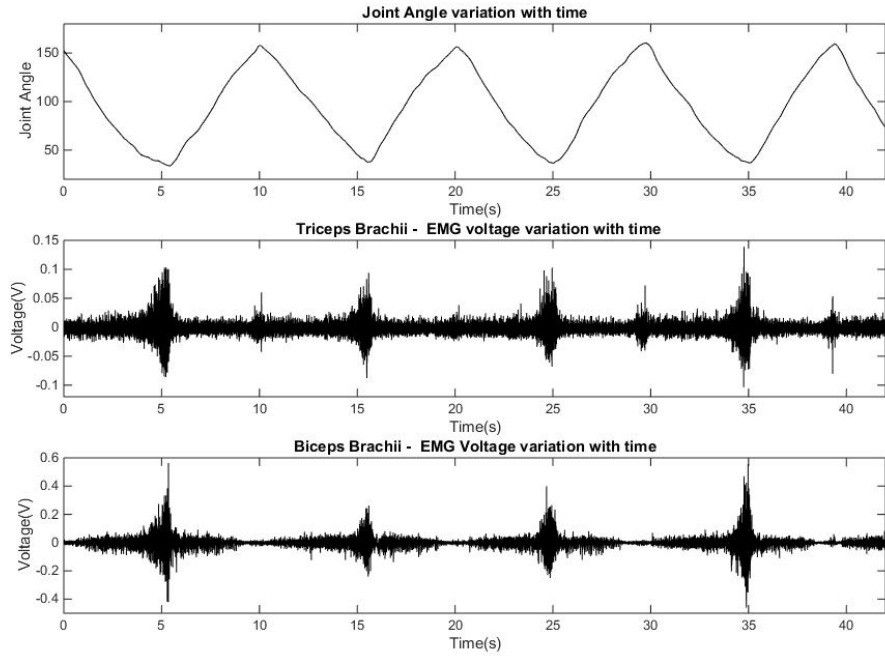


FIGURE 2.5: Relation between EMG signal and the elbow joint angle

The EMG signal can also provide information about the fatigue of the muscle and limb impedance.

The weakness of the surface EMG signal lies in the signal's non-stationarity. Since the signal is measured over layers of muscle, fat and tissue, the features of the signal change significantly. The main causes for the change in signal include changing the position of the electrode, changing the impedance of the electrode and muscle fatigue. This disadvantage can be compensated for both in the hardware and software level. In the next chapter, this issue will be discussed in more detail. Besides this fact, the EMG signal is also subject-specific, meaning that the signal changes from one subject to another.

Another difficulty with the EMG signal is the crosstalk phenomenon. Crosstalk occurs when the energy from one group of muscles travels over into the recording range of another muscle group [12]. This makes it very difficult to isolate the signal of a particular muscle from the other signals. This is the reason why electrode placement is very important when trying to record the signal from a single muscle.

2.5 EMG signal detection

There are several types of electrodes available on the market which are used to obtain EMG recordings. The two main types of electrodes are skin surface electrodes and inserted electrodes, which will be described in the sub-sections below.

2.5.1 Skin surface electrodes

The skin surface electrodes can be divided into two main groups: active and passive electrodes. Active electrodes, have built-in amplifiers at the electrode site to improve the impedance and as a result, they require no gel. Since they reside directly on the skin, they are more prone to movement artifacts, and hence are not recommended for recording of dynamic movements [13].

Passive electrodes (see Figure 2.6), on the other hand, detect the EMG signal without a built-in amplifier, and hence it is essential to reduce any skin resistance if possible. Hence, these require conducting gels and thorough skin preparation. Passive electrodes are usually created in such a way that the electrode is housed inside a cup and a gel provides the bridge between the electrode and the skin. These electrodes may take more time to prepare and usually they are more expensive than direct contact electrodes. They are recommended for the recording of dynamic movements.

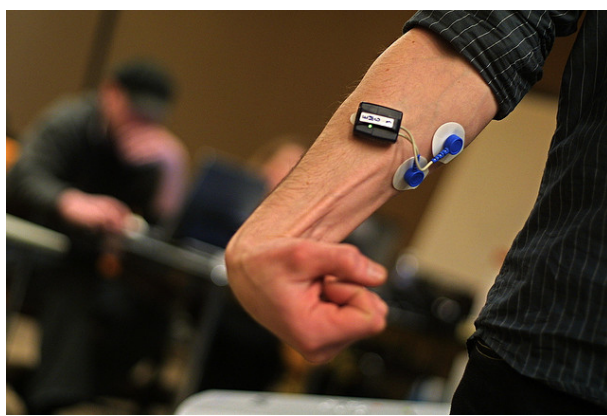


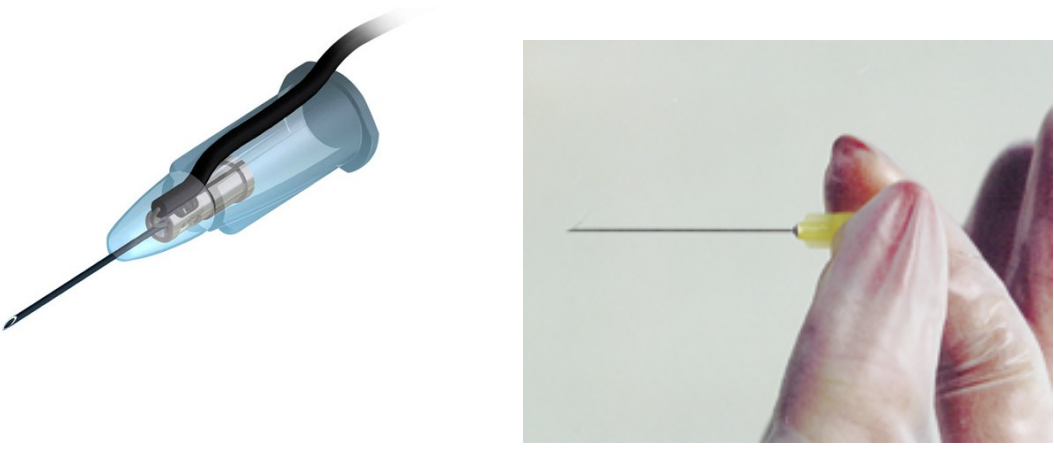
FIGURE 2.6: Passive skin surface electrodes [14]

The advantages of surface electrodes are that there is no pain with application and they are easy to apply. On the other hand, surface electrodes have a large pick-up

area and therefore, there is a bigger possibility for crosstalk from nearby muscles. Moreover, these electrodes can only be used for surface muscles.

2.5.2 Inserted electrodes

The two most common inserted electrodes are needle and fine wire electrodes. Needle electrodes consist of a simple stainless steel hypodermic needle which has an insulated wire in its barrel as can be seen in Figure 2.7(a). The tip of the wire is bared and acts as one electrode while the barrel of the needle acts as the other. Fine wire electrodes (see Figure 2.7(b)) are placed in site using a hypodermic needle and consist of a pair of extremely fine nylon-coated wires (diameter of $50\mu\text{m}$ or less) The needle is withdrawn and a small hook or barb at the end of the wires keeps them in the muscle [15].



(a) Needle electrode [16]

(b) Fine wire electrode [17]

FIGURE 2.7: The two types of inserted electrodes

The advantages of inserted electrodes include the possibility of a more specific recording area, the possibility of testing deep muscles, isolating specific muscle parts from large muscles and testing small muscles which would be impossible to detect with a surface electrode due to crosstalk. The disadvantages are that the needle insertion can cause discomfort which can increase the tightness in the muscles and the electrodes become less repeatable as it is difficult to place the electrode in the same area of the muscle every time. However, for deep muscles, fine wires are needed for detecting useful information.

2.6 Applications of EMG signal

As discussed in Section 2.5, surface EMG signals provide a useful source of information of a person’s intention of movement. Moreover, by using surface passive electrodes, the signal can be obtained quickly and in a very practical manner. To date, there has been considerable research on the use of EMG signals as control interfaces for robots. The studies in this area can be classified into three groups: controlling prosthetic arms and hands, applying orthoses for rehabilitation purposes and controlling robots remotely [11].

EMG controlled prosthetic limbs, as the name suggests, are artificial limbs controlled by EMG signals which replace an amputee’s limb. Since the muscles in the remaining part of the arm function in a normal way, this enables the EMG signals to be used to control the prosthetic device. Therefore, a signal obtained from the patient’s body controls the input to drive motors coupled to the prosthetic limb. Bitzer *et al.* [18] successfully demonstrate EMG-based control of a four-finger hand which can be used to grasp objects. A similar device was created by Okuno *et al.* in [19]. This work describes the development of a myoelectric controlled prosthetic hand. The aim of the experiment was to control the finger angles using EMG signals picked up from two muscles of the right forearm: extensor carpi radialis and flexor carpi radialis. Using this prosthetic hand, an amputee was able to grasp a soft object easily. Fermo *et al.* in [20] present the development of a system which captures the EMG signal using two parallel-bar electrodes in order to control a myoelectric prosthesis of the upper limb. A pattern classification technique is adopted, where the device recognises and replicates several discrete gestures performed by the hand such as opening and closing the hand.

EMG signals provide an efficient approach in the application of orthoses for rehabilitation or extension of human ability. Robot-driven rehabilitation systems can be used to deliver an increased dose of therapy and practice. This includes specificity of movement pattern generation, feedback and repetition in upper limb rehabilitation. In [21], Naft investigated the use of myoelectric orthoses to increase power and range of motion in the arms of patients with severe arm dysfunction. The orthoses uses an electrode on the biceps brachii and triceps brachii in order to read EMG signals. Results were encouraging, with patients noting improvements in doing several activities such as carrying objects. In another case, Kazerooni [22]

proposed a new feature for a robot manipulator worn by humans where, the human in physical contact with the robot manipulator exchanges power and information signals. A similar orthotic device has been developed and presented in [23] by Cavallaro *et al.* where an exoskeleton robot (which acts as an assistive device worn by the person) functions as a human-amplifier, with EMG signals being used as the main control signal. Such exoskeletons can be used to assist nurses while lifting patients or people who work in the building industry and need to carry heavy material.

Furthermore, robotic devices can be controlled remotely using EMG signals. Artemiadis *et al.* in [24] managed to teleoperate a robot arm through signals from the biceps brachii and triceps brachii muscles. In another example, Vogel *et al.*, in [25] describe and demonstrate a robotic arm that is controlled in real time through measured human muscular activity. Muscular control is obtained via surface EMG signals, and a supervised machine learning technique is used to map muscle activity to hand position, orientation and grasping force. Numeric validation shows that the system achieves good movement precision. This project falls within this field of application, with the main outcome being the operation of a robotic arm which is controlled in real-time through several EMG signals in the arm and shoulder.

2.7 Summary

This chapter has presented a thorough introduction to the EMG signal, by describing the origin of the signal in the muscles. Moreover, the sliding filament theory has been identified as the method by which muscles contract. A brief overview on the muscles in the shoulder and arm has been given to introduce the reader to the different muscles which contribute to selected types of movements in the upper limb which are most relevant to this project. The benefits and weaknesses of EMG signals have been identified so as to be aware of all the possibilities that the signals may present when recording EMG data. Different methods by which the signal may be detected have also been described, and the skin surface passive electrodes, which are available at the Biomedical Engineering laboratory at the University of Malta, were chosen to be used in this project. Finally the three main applications of using EMG signals to control external equipment have been identified and a brief literature review was carried out to identify the main research work contributing to the different applications.

Chapter 3

Literature Review

3.1 Introduction

This chapter contains an overview on several systems that allow the control of devices using EMG signals. First of all, the differences between simultaneous proportional control and sequential proportional control will be presented and the ideal characteristics of a myoelectric controller will be discussed. Furthermore, different modelling techniques relating the EMG signals to the subject's joint angles will be analysed in detail. This is followed by a review of the transient properties of the EMG signal and their effects on the EMG to joint angle models. Finally the aims of this project with relation to previous works are presented.

3.2 Characteristics of an EMG control system

3.2.1 Myoelectric control

Myoelectric control consists of using EMG signals to extract control signals to command external devices. Since the 1950s proportional control has been a popular subject in research on upper limb devices. Proportional control is exhibited by a system if the user can control an output quantity of the device (e.g. force, position, velocity) within a finite time period by varying the control input within a corresponding continuous time period [26]. The conventional method for proportional control of myoelectric systems is sequential control, where only one function can be articulated at a time. This prevents the imitation of the user's fluid, life-like motions. Most activities of daily living require simultaneous movement of multiple degrees of freedom. This is the reason simultaneous proportional control is preferred over sequential proportional control.

In recent years, several researchers [27–30] attempted proportional and simultaneous control of a device. An implementation of a control system with simultaneous proportional myoelectric control was made by Fougner *et al.* in [31]. In this study, a system was developed for a prosthetic hand with two functions (hand open/close, and wrist pronation/supination). Proportional and simultaneous control was compared to three other control setups including a more traditional, sequential proportional control system. The practical tests indicate that proportional and simultaneous control performed superiorly to the more traditional sequential control technique in terms of timing and accuracy of certain standard movements. This project was the first proportional and simultaneous myoelectric control system demonstrated on a prosthetic device mounted to the forearm.

Another form of robotic arm myoelectric control involves pattern recognition of different gestures. Gesture recognition control schemes interpret EMG signals from muscles into control outputs by training a model using a dataset which relates a feature of the EMG signal input with the desired output. In [32], Ahsan *et al.* developed a model which decodes certain features of the input signal and classifies this input to a certain class which corresponds to a gesture. While this control system produces satisfactory results, the use of gesture recognition relies on the model created to learn the patterns of activation of the muscles to control the arm. Due to the transient properties of EMG signals, these patterns may not be constant in the short or long term, and this can be the cause for several failed efforts to create a practical myoelectric control system [31].

3.2.2 The ideal myoelectric control system

In [33], Farina *et al.* describe the criteria which must be fulfilled to obtain an ideal system for upper limb control. These are:

1. The movement of the robotic arm should be as natural as possible. This implies that control must be simultaneous and proportional, with the inclusion of multiple degrees-of-freedom if possible.
2. The system should be robust to the transient effects of the EMG signal and range of activities, as well as signal changes over different days of use.
3. It should be based on a minimal number of electrodes, and must not be sensitive to the precise position of the electrodes.

4. The training needed should be simple and short and there should not be need for frequent re-training.
5. The complete system should not be computationally complex, so that it can be implemented using low consumption hardware.
6. The intended motions by the user should be reproduced with negligible delays (usually < 200ms).

Farina *et. al* further indicate that none of the current myoelectric control systems available commercially satisfy all these requirements. They expect that a control system which satisfies all these requirements will have the potential to be used for robust commercial applications, something which has been lacking for more than 60 years in this area.

3.3 EMG-to-joint angle models

This project focuses on the conversion of EMG data directly to output joint angles. Different system identification techniques have been applied by researchers as a solution to this problem. Three types of models that have been used for continuous translation of EMG signals to joint angle position are the state space model, the linear regression representation and a multi-layer perceptron. These models produce varying degrees of reliability, depending on the way that they are applied.

3.3.1 State space representation

Classical control theory methods usually represent single-input single-output (SISO) systems in the form of a transfer function. As systems become more complex, representing them with transfer functions becomes more complicated. The state space method largely alleviates this problem.

In state-space modelling, three types of variables are involved in representing dynamic systems: input variables, output variables and state variables. The state space representation of a system is given by two equations [34]:

$$x_{k+1} = \mathbf{A}x_k + \mathbf{B}u_k + w_k \quad (3.1)$$

$$y_k = \mathbf{C}x_k + v_k \quad (3.2)$$

Equation 3.1 is called the state equation, where \mathbf{A} is the state matrix and \mathbf{B} is the input matrix. The second equation, Equation 3.2 is the output equation, where \mathbf{C} is the output matrix. The size of these matrices depends on the number of inputs, outputs and states of the system. In this model w_k and v_k represent zero-mean Gaussian noise processes with covariances ψ and Γ respectively, i.e. $w_k \sim N(0, \psi)$ and $v_k \sim N(0, \Gamma)$. Model training involves finding values for \mathbf{A} , \mathbf{B} , \mathbf{C} , ψ and Γ . These parameters can model the system states and thus facilitate the correlation between the EMG signal u_k and arm kinematics y_k .

Various researchers [35, 36] have made use of this model for EMG-to-joint translation, using various methods to find the unknown state variables. Artemiadis and Kyriakopoulos make use of this model in [37] where EMG signals from nine electrodes on the upper limb muscles are used to control a robot arm with four degrees of freedom. The signals recorded are translated into low dimensional space using principal component analysis (PCA), on which motion decoding takes place. After projecting back to a higher dimensional space, the required kinematic parameters are found using forward and inverse kinematic equations. The results achieved were promising, with a correlation coefficient up to 0.97 and a root mean square position error of 1.95 cm between the human and robot motion. Figure 3.1 shows the complete system implemented by Artemiadis and Kyriakopolous.

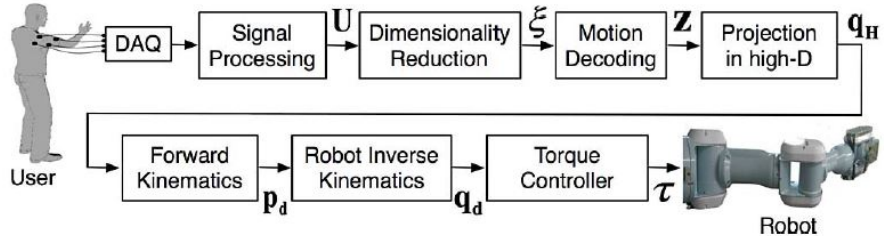


FIGURE 3.1: Diagram of the EMG to robot arm motion system implemented by Artemiadis and Kyriakopoulos [37]

In [38], Artemiadis and Kyriakopolous give their reasons on choosing this model to estimate arm motions. A model which describes the function of the muscles in simulating the human joints would be generally complex, making it difficult to implement real-time decoding. For this reason, the state space model is used as it is a flexible decoding model in which hidden variables could model the unobserved system states and translate arm motions from EMG signals.

3.3.2 Linear regression

Linear regression model structures are a useful method in describing basic linear and non-linear systems. This approach attempts to model the correlation between two variables by fitting a linear equation to the data. The two variables are defined as the *explanatory* variable and the *dependent* variable [39]. In our case, the explanatory variable is the input EMG data and the dependent variable is the output joint angle. An important criterion for using this method is that there must be an existing linear relationship between the two variables. In Section 3.3.2.1, the linear relationship between the EMG data and the joint angle will be explained in detail.

The relationship between the two variables [28] can be described as seen in Equation 3.3, where $\hat{\mathbf{Y}}$ represents the estimation of the dependent variable, and \mathbf{X} represents the explanatory variable. The vector \mathbf{W} represents the weight vector and \mathbf{w}_0 is the bias which can compensate for possible offsets.

$$\hat{\mathbf{Y}} = \mathbf{WX}^T + \mathbf{w}_0 \quad (3.3)$$

One method which is commonly used to fit a regression line is the least mean-squares method. The best fitting line is found by minimizing the sum of squares of the vertical deviations from each point to the regression line. The least mean squares solution for Equation 3.3 including the regularisation constant λ is obtained by minimising the following function [28]:

$$err(\mathbf{w}) = \frac{1}{2} \sum_T [\mathbf{y}(t) - \mathbf{w}^T \mathbf{x}(t)]^2 + \frac{\lambda}{2} \mathbf{w}^T \mathbf{w} \quad (3.4)$$

This can be expressed in closed form by Equation 3.5, where \mathbf{I} is the identity matrix and the regularisation constant is optimised by cross-validation [28].

$$\mathbf{W} = (\mathbf{XX}^T + \lambda \mathbf{I})^{-1} \mathbf{XY}^T \quad (3.5)$$

The linear regression model is a popular method used in simultaneous and proportional myoelectric control. The benefit of this technique is that unlike classification, a regressor does not give a certain class as a result, but provides a continuous

output value. This allows for independent proportional and simultaneous control which can enable fluent and natural control of a device [28]. In fact, Hahne *et al.* in [29] implement a co-adaptive strategy where the instantaneous feedback of the closed-loop system is exploited, which in combination with a real-time learning algorithm allows the user and the device to co-adapt and compensate for errors instantaneously. Due to the common goal, the user and the machine adapt to a consistent and stable control strategy. The system makes use of a linear regression model and a recursive least squares method to train the model.

In another work, Hahne *et al.* [40] develop a regression based embedded system that provides independent and proportional activation of two degrees of freedom and satisfies clinical requirements. The diagram of the whole system is seen in Figure 3.2. The estimated control signal is transmitted back to the embedded system in real-time and is then used to generate four signals to open/close and rotate a prosthetic hand. When the training is finished, the coefficient \mathbf{W} is transferred to the microcontroller and stored in an EEPROM. This allows the system to run in autonomous mode, which directly transfers the EMG signal into prosthetic control commands.

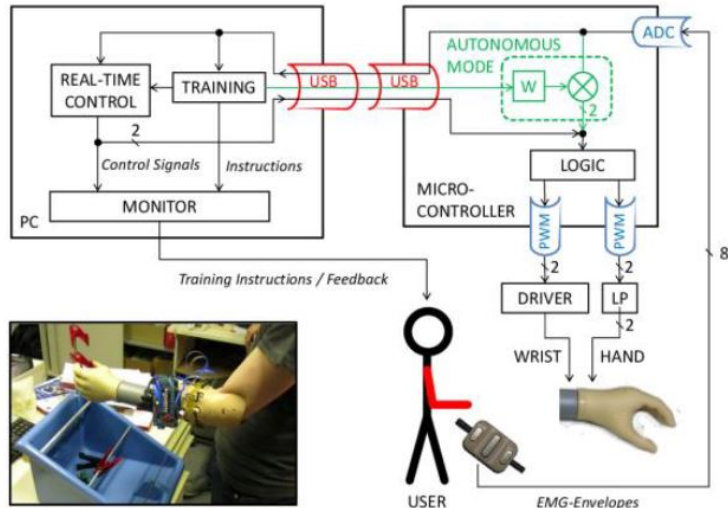


FIGURE 3.2: Block diagram of the developed embedded system by Hahne *et al.* in [40] and evaluation with clothes pin test

3.3.2.1 Linearising EMG data

When using linear methods such as linear regression, the relationship between the EMG signal and the target joint angles should be as linear as possible. In [28],

Hahne *et al.* investigate the use of the variance of the EMG and two other non-linear transformations applied on the variance (var), to linearise the relationship between the EMG signal and the joint angle. The two transformations are the root mean square (rms), defined by $f(x) = \sqrt{x}$ and the log-variance (log-var) described by $f(x) = \log(x)$. The performance of these three methods as obtained in [28] are shown in Figure 3.3 under the linear regression (LR) heading. The performance metric used is the coefficient of determination (R^2). This parameter is a measure of how close the data is to the fitted output. A value of one indicates that the representation explains all the variability of the data around its mean. Hence a higher r-squared value indicates that the model fits the data better. This is defined in Equation 3.6.

$$R^2 = 1 - \frac{\text{Mean Square Error}}{\text{Variance}} \quad (3.6)$$

It can clearly be seen that when using a linear regression technique, the effect of a non-linear transformation on the variance of the EMG is significant. In fact the best results were obtained when using the log-var transformation followed by the rms transformation.

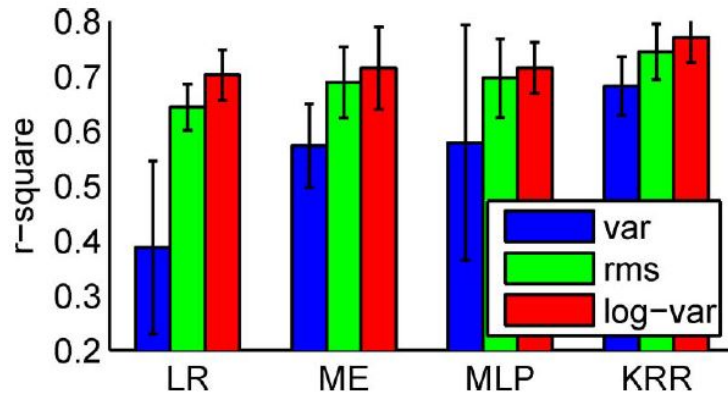


FIGURE 3.3: Effect of non-linear transformations on the estimation of joint angles [28]

3.3.3 Multi-layer perceptron

Another form by which the EMG to joint angle model can be implemented is by making use of artificial neural networks (ANNs). An ANN is made up of a considerable amount of simple processing units, coupled by weighted connections, where each unit receives inputs from several other units and produces a single

output. This then acts as an input to other units. A multi-layer perceptron (MLP) is one such type of neural network made up of simple neurons called perceptrons. As can be seen in Equation 3.7, the perceptron provides a single output y from multiple real-valued inputs x_i by developing a linear combination depending on the input weights w_i and then placing the output through a non-linear activation function φ :

$$y = \varphi(w_0 + \sum_{i=1}^n x_i w_i) \quad (3.7)$$

As can be seen in Figure 3.4, a multi-layer perceptron network has an input layer (on the left), hidden layers (in the middle) and an output layer (on the right). This configuration's key advantages are that it is easy to use and that it can approximate any input-output map. The main disadvantages are that MLPs train slowly and require a large amount of training data. Once the architecture to be used is chosen, the network's weights and thresholds are adjusted to reduce the prediction error. The back-propagation neural network (BPNN) algorithm can be used to train MLPs. The nature of this algorithm is to minimise the error of the network using the derivatives of the error function. The derivatives' flow backwards through the network is calculated.

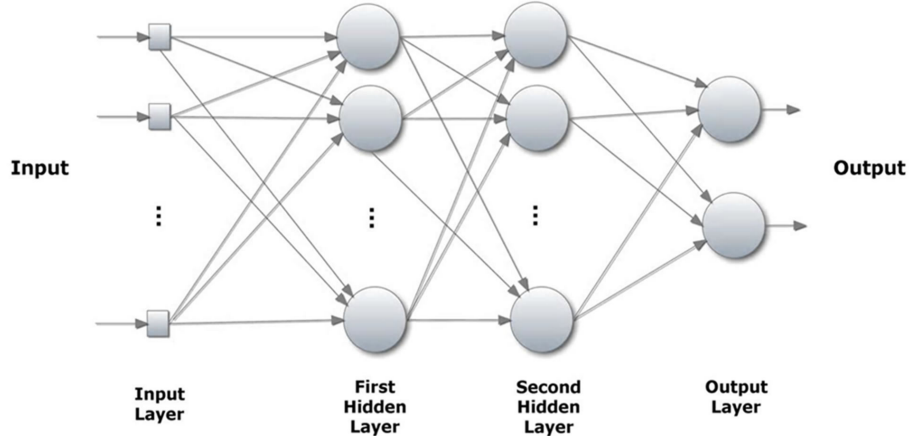


FIGURE 3.4: Structure of a multi-layer perceptron in [41].

A substantial amount of research presents the success of using MLPs in EMG signal classification. The advantage of using neural networks is their ability to represent both linear and non-linear relationships, and learn these relationships directly from the data being modelled [42]. In [27], Muceli and Farina use eight MLPs to estimate several hand movements. Different MLPs were used for different

angles with the aim of obtaining an accurate estimation for each degree of freedom. Similarly in [43], Aung and Al-Jumaily used a neural network to estimate the shoulder and elbow joint angles from the recorded EMG signals. The network consists of an input layer, which consists of four nodes for the EMG signals from the anterior deltoid, posterior deltoid, biceps brachii and triceps brachii muscles. The second layer is a hidden layer consisting of 20 nodes. The last layer, the output layer, provides the estimated joint angle for the upper limb. The system is trained using several individual movements, and the results are then simulated on a virtual human model. The evaluation results show that the developed MLP is able to represent the relationship between the EMG signals and the joint angle successfully and a simulation was able to mimic the human arm movements.

Finally, in [30], Jiang *et al.* investigated the possibility of using EMG from one arm to estimate the arm kinematics of the other arm using MLPs, an application aimed at unilateral amputees. The surface EMG features were the inputs to the MLPs, which used the joint angles as training targets. A dedicated MLP approach was considered, where a MLP for each degree of freedom was used. Training was divided into two parts. When the EMG from the same side as the kinematics was used for training, it was called ipsi-lateral training. When the EMG from the opposite side was used for training, it was called contra-lateral training. This paper was the first that demonstrated the feasibility of estimating wrist and hand kinematics of transradial amputees using surface EMG during mirrored movements with simultaneous and proportional activations of the three wrist degrees of freedom.

3.4 Transient properties of the EMG signal

As discussed in Section 2.4, one of the disadvantages of using the EMG signal to classify body movements is that the signal is non-stationary. Fatigue is a factor which affects the EMG signal with time. If the contraction of a muscle is sustained for a certain period of time, the muscle begins to twitch less frequently. Studies indicate that the build up of excessive hydrogen ions slows down the waveform of the motor unit action potential [44]. Other factors which may degrade the performance of a trained control scheme include skin impedance, electrode shift and posture. In this section, several attempts to reduce the effects of these factors in the interpretation of the EMG signal will be analysed.

In their attempt to eliminate the effects of deterioration of the EMG signal due to fatigue, Artemiadis *et al.* [45] created a method that detects fatigue and switches to the model which best fits these properties. This is done by defining a set of EMG classes, where each class corresponds to cases where the EMG recordings has some specific characteristics. A probabilistic framework was designed in order to assign a class to each of the recorded muscles which is related to the time-varying signal features. The results show that this method could estimate the human arm motion with high accuracy.

In a similar manner, posture changes can also cause degradation of the EMG signal. A study by Scheme *et al.* [46] examined the adverse effects of the limb position on a myoelectric control system. EMG data relating to eight different motions was collected and position-specific classifiers were trained with this data. The results indicate that EMG classification error is strongly dependent on limb position. As a result, it was concluded that it would be insufficient to train a control system in a single position and expect it to translate well to multi-position use. In [47], Fougner *et al.* proposed two possible solutions: training in multiple limb positions and measuring the position. By training in multiple positions, the pattern recognition system is informed about the patterns in each position. This expands the boundaries to each class to include position variation. By measuring the position using accelerometers, the classifier can compensate for the effect on the EMG signal.

Another factor which may cause a different EMG recording than that expected is electrode displacement. Hargrove *et al.* [48] attempted to simulate the electrode shift due to socket limb misalignment and determine the effect it has on the classification accuracy. It was confirmed that performance deteriorates with displacement of electrode position, with error rates of over 30 per cent with slight shifts of the electrode. In [43], Aung and Al-Jumaily suggest normalisation of the time domain parameters in order to overcome the conditions of the EMG measurements and placement of electrodes. It also compensates for the fact that the EMG signal obtained from the subjects vary from one person to another. The formula for normalisation is given by Equation 3.8, where Y_{norm} is the normalised EMG output, $Y_{max_{norm}}$ and $Y_{min_{norm}}$ are the maximum and minimum value of the normalised output, and Y_{max} and Y_{min} are the maximum and minimum value of the EMG

signal before normalisation.

$$Y_{norm} = \frac{(Y_{max_{norm}} - Y_{min_{norm}})(Y - Y_{min})}{Y_{max} - Y_{min}} + Y_{min_{norm}} \quad (3.8)$$

In reality, it is not practical to include the combination of all the factors discussed in one training set to produce a fully robust control scheme. What is possible, however, is an adaptive control scheme which updates the training set periodically to compensate for these factors. Nishikawa *et al.* were one of the first to propose a method which allows the correction of bad performance. The controller uses a real-time learning method which is divided into three units: the analysis unit, which extracts useful information for discriminating movements from EMG, the adaptation unit which learns the correlation between the EMG signal and the control command and adapts to operator's characteristics, and finally the trainer unit which generates the training data and makes the adaptation unit learn in real-time. Pilarski *et al.* [49], on the other hand, make use of a reinforcement learning method to learn a control scheme that adapts to transient changes as long as the user reinforces the system periodically. As a result, the system was able to learn a two-joint task, and demonstrated the ability to change over time according to continued user input.

3.5 Previous work

This project continues on the work done by Bezzina in [1] and Grech in [2]. Bezzina's work involved the acquisition of a set of EMG recordings from five muscles and the corresponding joint motion data from the motion capture system in the laboratory in order to replicate movement in the shoulder, elbow and wrist. These recordings were used to obtain the state space model which relates EMG data to joint angles. The technique adopted in order to obtain the state variables of the state space model was the Expectation Maximisation (EM) algorithm. When tested with cross validation for 30 second trials, the model resulted in average correlation coefficients (CC) of 0.63 ± 0.15 , 0.50 ± 0.2 and 0.41 ± 0.16 for the shoulder, elbow and wrist angles respectively. The average root mean square error (RMSE) values obtained were $20.05^\circ \pm 6.88^\circ$, $49.85^\circ \pm 26.92^\circ$ and $13.75^\circ \pm 2.29^\circ$ in the same order. Some limitations of this attempt include the fact that the model could only be used by the person who trained it, and no compensation for the transient properties of

the EMG signal was considered. Also, the system was not tested for real time operation.

As a continuation to Bezzina's work, Grech's dissertation [2] was split in three parts. The first part involved a detailed study on the non-stationary aspects of the EMG signal, with the main focus being the issue of fatigue. These tests confirmed that the median frequency provides an indication on the level of fatigue in the musculature. In the second part of the project, the EMG-to-joint angle state space model from the past dissertation was improved by trying a new algorithm, the Numerical Subspace State Space Identification (N4SID) algorithm to find the state variables. Tests using both the N4SID and EM algorithm concluded that the N4SID algorithm is the best option for this application. In this project, only the elbow joint was considered, as more focus was given to considering fatigue and real time operation. The EMG signal was recorded from the biceps muscle. For non-cross-validation trials estimated through the N4SID algorithm across constant-speed trials, an average RMSE of $19.88^\circ \pm 2.989^\circ$ and an average CC of 0.893 ± 0.028 were achieved. When forward cross-validating the models estimated through the N4SID algorithm across constant-speed trials, an average RMSE of $22.86^\circ \pm 2.085^\circ$ and an average CC of 0.881 ± 0.034 were achieved. In the final part of the project, a real-time system was implemented using the CataLyst-5T robotic arm. The result showed that movements were replicated with a system delay amounting to 0.5s, which was probably due to mechanical limitations of the robotic arm. Also, since it was discovered that fatigue did not affect the subject's performance for no-load exercise lasting up to four minutes, no compensation for EMG's time-variation property was implemented.

3.6 Concluding Analysis

This literature review presented a thorough discussion on the different systems in literature related to this project. Three techniques used to represent the EMG-to-joint angle relationship were investigated and works which used these methods were analysed. Furthermore, the properties which affect the EMG signals were discussed, and different approaches found in the literature to compensate for these effects were reviewed. Finally, a short overview of the previous projects by Bezzina and Grech was presented so as to seek the areas which can be improved.

In this project, the main aim will be to improve the performance of the EMG-to-joint angle model for the elbow joint. This will be done by analysing the pre-processing signal techniques for the state space model and testing the model with both biceps brachii and triceps brachii EMG. Also, two other models will be designed, a MLP and a linear regression model. The proposed MLP, which through the literature review was found to be commonly used and produces satisfactory results, allows the simultaneous and proportional control needed between the EMG signal and joint angles. This technique will also be implemented to analyse whether it can improve on the results obtained by Bezzina and Grech. The methodology used by Aung and Al-Jumaily's work [43] will form the foundation of this project as results showed a very low classification error. One should note however that this work was limited to single joint movements only. The linear regression model will also be investigated, as although it was found to achieve lower accuracy than the MLP [28], it requires less training time.

The two models will be tested using both the biceps brachii EMG and triceps brachii EMG as inputs, with the output being the elbow joint angle. Once the best model which indicates the best relationship between EMG data and joint angle data is selected, this can be tested and developed by adding more degrees of freedom, adding signals from different muscles and testing the system in real-time. The same real-time system apparatus as that implemented by Grech in [2] will be used.

Chapter 4

Analysis of the EMG-Joint angle system

4.1 Introduction

This chapter aims to give a brief description of the components involved in the EMG-to-joint angle system as operated by Grech [2]. Due to the fact that in the previous project by Grech, there was a notable delay between the elbow movement and the robotic arm's reproduction of the movement, several tests were carried out on each component of the system to identify the cause of the delay. Results are illustrated and a discussion of the results ensues for all tests performed on the robot system and the EMG-to-joint angle model.

4.2 The offline data acquisition system

First of all, for system identification, where the goal in this case is to find a model or a relationship between the EMG signals and the elbow joint angle, data needs to be collected to be used for training the model, that is to find the optimal model parameter estimates that link the inputs (EMG signals) with the outputs (joint angles). Figure 4.1 shows the complete data acquisition process. The ZeroWire EMG acquisition box is used to collect EMG data from the user while the positional data is acquired simultaneously to the EMG data using the Vicon camera system. The system is equipped with several position trackers, to extract the Cartesian co-ordinates at several points on the upper limb. In order to calculate the joint angle, inverse kinematics equations are applied, as will be derived in Section 4.2.3. Since the position data from the Vicon system is acquired at 100Hz, the EMG data is downsampled from 1kHz to 100Hz so that an EMG amplitude sample is assigned to each joint angle sample calculated.

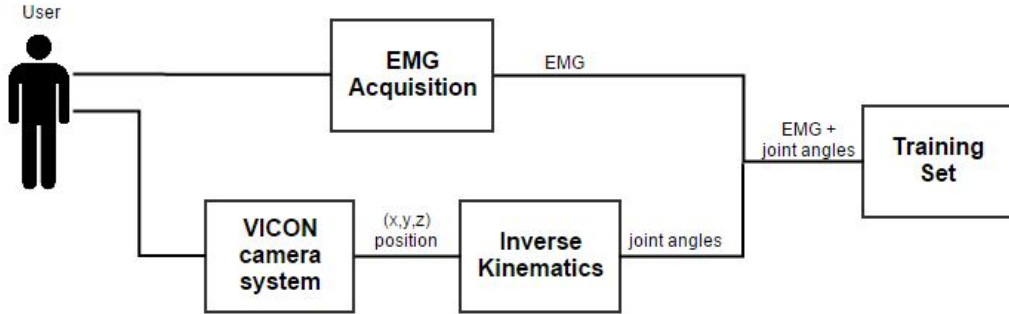


FIGURE 4.1: Offline data acquisition system diagram

4.2.1 ZeroWire EMG acquisition box

As discussed in Section 2.5, there are two different types of EMG electrodes which can be used to detect EMG signals from the human body. In this project, the Aurion ZeroWire EMG acquisition set located in the Biomedical Engineering Lab at the University of Malta was used, as can be seen in Figure 4.2. The advantage of using these surface EMG electrodes is that the ground electrode has been abolished and hence there is no risk of unreliable signals caused by incorrect positioning of the referential electrode [50].

The amplifier box is coupled to a series of eight wireless EMG probes communicating through Wi-Fi. Readings are sampled at 2kHz from each electrode. Each electrode incorporates its own preprocessor which performs high-pass filtering at 10Hz and low pass filtering at 1kHz. When accessed serially, data is transferred at 2kHz from the box. On the other hand, in our case this communication is formed indirectly through the Vicon acquisition hardware, at a downsampled rate of 1kHz [2].



FIGURE 4.2: ZeroWire EMG amplifier box and probes [50]

4.2.2 Vicon motion capture system

Motion capture is the process of recording the movement of objects or people. Vicon is a motion capture system that specialises in gathering position data for any movement analysis application using highly reflective markers. Figure 4.3 shows such a system which was used in this project which is situated at the Biomedical Engineering Laboratory at the University of Malta. The markers are placed in precise positions on the subject, and the infra-red cameras relay the position of each marker in the three-dimensional environment.



FIGURE 4.3: Vicon motion capture system at the Biomedical Engineering Lab

The system incorporates eight infra-red cameras, essential to obtain the kinetics of a moving entity. The ZeroWire wireless EMG system can also be integrated into the system thus allowing multi-modal human motion analysis. This provides valuable data which is used for system identification to be performed in this project.

The system captures the position of the markers at 100Hz and stores all the data together with any EMG readings taken at 1000Hz through the ZeroWire EMG system, as already mentioned. Two other components of the Vicon system are the calibration wand and the sync/connection box. The calibration wand is used to calibrate the cameras while accounting for sensor edge distortion to ensure synchronised overlay across the entire volume. The sync box provides a single communication point between the cameras and the PC [51].

4.2.3 Inverse kinematics

Kinematics is defined as geometry of motion, providing tools for describing the structure and behaviour of robot mechanism [52]. In a robotic arm, given the angle of each joint, the forward kinematic equations are used to find the location of the end effector of the arm as Cartesian coordinates. The inverse kinematics problem refers to the reverse process where the robotic arm's joint angles are found given the Cartesian co-ordinates. In the case of estimating the elbow joint angle, three markers are used. Figure 4.4 shows the position of these markers, and the notation used in calculating the joint angle. This method can be used to find any joint angle, as long as the co-ordinates of three markers around the angle are known.

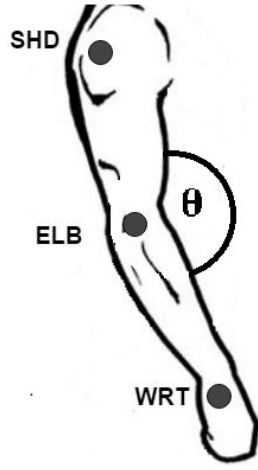


FIGURE 4.4: Position of the Vicon markers [53][edited]

As was done in the previous project by Grech [2], given the x, y, z positions of the three markers, placed at the shoulder (SHD), elbow (ELB) and wrist (WRT), the elbow joint angle was found using the dot product:

$$A = (x_{SHD} - x_{ELB})(x_{WRT} - x_{ELB}) + (y_{SHD} - y_{ELB})(y_{WRT} - y_{ELB}) + (z_{SHD} - z_{ELB})(z_{WRT} - z_{ELB}) \quad (4.1)$$

$$B = \sqrt{(x_{SHD} - x_{ELB})^2 + (y_{SHD} - y_{ELB})^2 + (z_{SHD} - z_{ELB})^2} \quad (4.2)$$

$$C = \sqrt{(x_{WRT} - x_{ELB})^2 + (y_{WRT} - y_{ELB})^2 + (z_{WRT} - z_{ELB})^2} \quad (4.3)$$

$$\theta(^{\circ}) = \cos^{-1} \left(\frac{A}{B \times C} \right) \quad (4.4)$$

4.3 Overview of the real-time system

4.3.1 Introduction

Following the offline procedure, where a static dataset of the EMG data and the position data is acquired, the parameters of the state-space model can be estimated. In the real time system these parameters are used so that the EMG data, downsampled to 100Hz is fed as input to the model which then gives the joint angle as output. This angle is then fed to the controller such that the robotic arm's corresponding angle changes in sync with that of the human subject. Figure 4.5 shows a diagram which describes the real-time operation of the system.

On a more technical level, EMG data is acquired from the user through the ZeroWire EMG acquisition box and transmitted over TCP (Transport Control Protocol). A C++ program automatically configures and activates the EMG acquisition box and also caters for the transfer of this data to MATLAB. The signal is then processed and undergoes the conversion from EMG amplitude to the joint angle through the state space model as described in Section 3.3.1. After further downsampling, the angles from the model are transferred to a Simulink model which controls the robotic arm's movement. There is also the possibility of converting the joint angles calculated to Cartesian co-ordinates using forward kinematic equations.

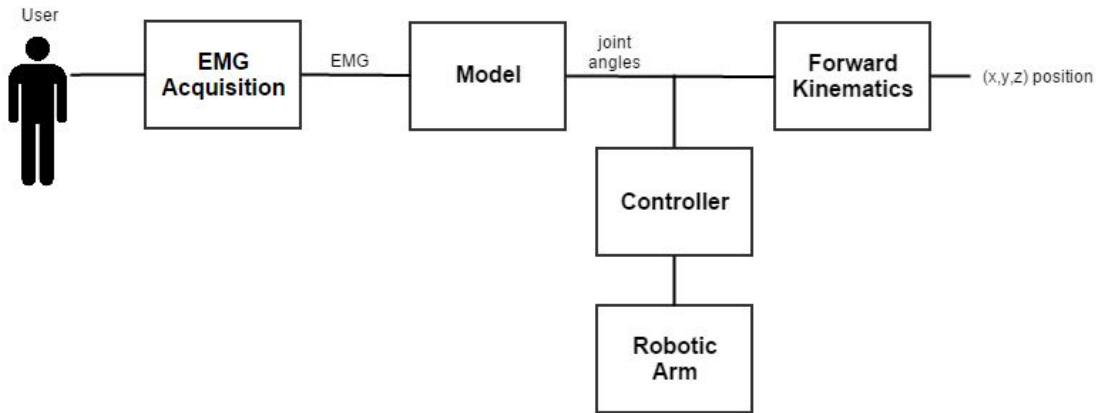


FIGURE 4.5: Online data acquisition system diagram

4.3.2 CRS Catalyst-5T robot system

The CRS Catalyst-5T is a five degree-of-freedom robot system which has five joints powered by five motors, as can be seen in Figure 4.6. The system includes the C500C controller which contains a PID controller operating about each motor. Incremental encoders for each joint provide continuous information on motor position. Once the arm has been homed, the controller uses this information to accurately position the arm within the work-cell. The specifications for each joint can be seen in Table 4.1. Functioning as a closed architecture controller, advanced algorithms in robotics such as adaptive control cannot be performed. However, when operated in open architecture mode, a different controller designed by the user is implemented, which sends currents directly to the motors.

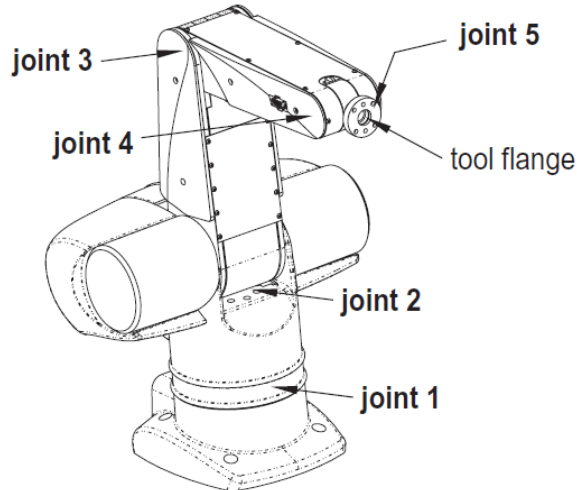


FIGURE 4.6: CRS Catalyst-5T robot system [54]

TABLE 4.1: Joint specifications for the CataLyst-5T arm [55]

Axis	Range of motion	Maximum Speed
Joint 1	$\pm 180^\circ$	$210^\circ/s$
Joint 2	0° to $+110^\circ$	$210^\circ/s$
Joint 3	-125° to 0°	$210^\circ/s$
Joint 4	$\pm 180^\circ$	$551^\circ/s$
Joint 5	$\pm 110^\circ$	$1102^\circ/s$

4.3.3 Robot Simulink model

As described in Section 4.3.2, the robotic arm can be controlled either by using the closed architecture controller, or else using an open architecture controller. As an open mode architecture was chosen for this project, the controller was designed in Simulink and implemented with QuaRC, instead of using the built-in controllers in the C500C system. The controller used in this project provides direct control over all the joint angles of the robot.

Figure 4.7 illustrates the entire joint-space position control process. A change in the joint angle constant blocks provides a reference step input to a sigmoid block which serves to smooth the joint movement of the robotic arm as otherwise damage may be caused by sudden large step inputs to the robotic arm itself, and also to the driver circuitry [55]. The time taken for the sigmoid signal to reach the reference signal is defined by two limits: the velocity limit $j3_vel$ and the acceleration limit $j3_acc$ for the elbow joint. In joint-based control, only the joint being commanded will be moving. Since there is coupling between the joints and motors, if the position of a motor is controlled directly, then multiple joints will be actuated.

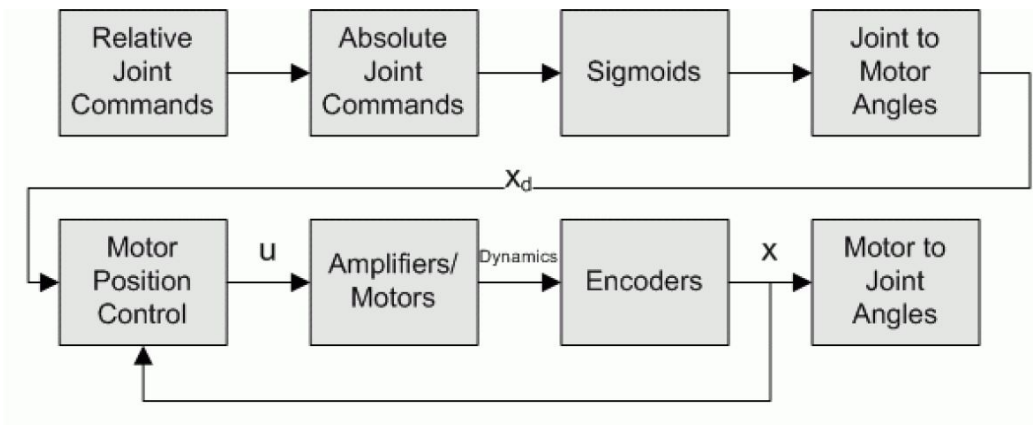


FIGURE 4.7: Joint-level position control flow diagram [55]

4.3.4 Forward kinematics

As was explained in Section 4.3.1, forward kinematic equations are used to calculate the end-effector Cartesian co-ordinates once the joint angles are known. In the case of the elbow and shoulder joint angles, since the movement is in a two-dimensional environment, only the x and y co-ordinates of the wrist position are calculated, as can be seen in Figure 4.8. In this diagram, SHD refers to the shoulder position marker, ELB refers to the elbow position marker while WRT represents the wrist marker. This method can be applied to shoulder and elbow movement in any two-dimensional space, not necessarily the x-y space.

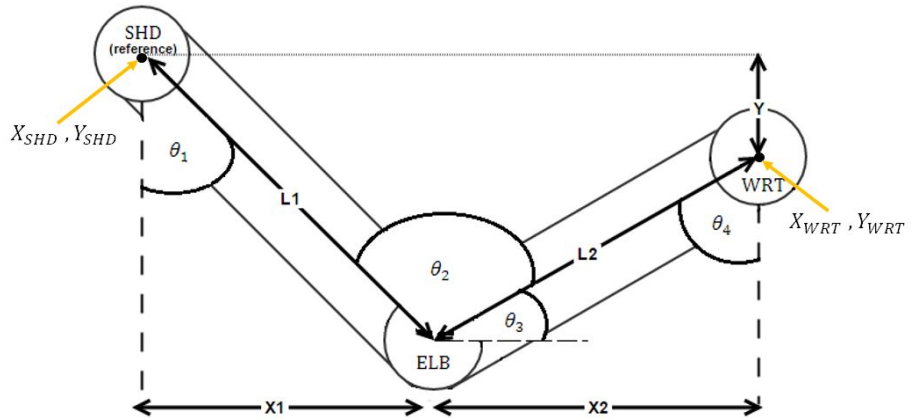


FIGURE 4.8: Forward kinematics derivation

Assuming no movement in the x direction, and that L_1 represents the length of the upper arm and L_2 represents the length of the forearm, using geometry principles, the co-ordinates of the wrist, X_{WRT} and Y_{WRT} can be deduced. From the diagram, θ_1 is the known shoulder angle and θ_2 is the known elbow angle.

Firstly an equation for θ_3 in terms of the shoulder and elbow joint angles is found:

$$\begin{aligned}\theta_3 &= 180^\circ - [(90^\circ - \theta_1) + \theta_2] \\ &= 90^\circ + \theta_1 - \theta_2\end{aligned}\tag{4.5}$$

An equation relating θ_3 to the elbow and shoulder joint angles is derived using Equation 4.5:

$$\begin{aligned}\theta_4 &= 90^\circ - \theta_3 \\ &= 90^\circ - (90^\circ + \theta_1 - \theta_2) \\ &= \theta_2 - \theta_1\end{aligned}\tag{4.6}$$

Considering the horizontal plane:

$$\begin{aligned}
 X_{WRT} &= X_{SHD} + X_1 + X_2 \\
 &= X_{SHD} + L_1 \sin(\theta_1) + L_2 \sin(\theta_4) \\
 &= X_{SHD} + L_1 \sin(\theta_1) + L_2 \sin(\theta_2 - \theta_1)
 \end{aligned} \tag{4.7}$$

Assuming that the shoulder angle does not exceed 90° , the vertical displacement can be calculated:

$$\begin{aligned}
 Y_{WRT} &= Y_{SHD} + Y \\
 &= Y_{SHD} - L_1 \cos(\theta_1) + L_2 \cos(\theta_4) \\
 &= Y_{SHD} - L_1 \cos(\theta_1) + L_2 \cos(\theta_2 - \theta_1)
 \end{aligned} \tag{4.8}$$

In the case that the shoulder angle exceeds 90° , the X_{WRT} and Y_{WRT} equations are exchanged, as the configuration remains the same, however rotated by 90° . It is important to note that in order to find the absolute end-effector co-ordinates, the shoulder and elbow co-ordinates must be known, else, knowing L_1 and L_2 , only the relative co-ordinates can be found.

4.4 Testing the Catalyst-5T robot system

This section describes several tests carried out on the Catalyst-5T robot system by setting a range of inputs. The response of these inputs was recorded so as to identify the optimal speed for the most accurate movement interpretation. These tests were performed so as to investigate the claim made by Grech [2] that a delay of 0.5 seconds existed since the robot could not mechanically keep up with fast movements at 0.5Hz.

4.4.1 Tests

In the first test, with the robotic arm positioned in the arm-up position (-90°), the input command was set to the lowest possible position (30°). Thus in this way, joint 3 of the robotic arm was displaced by 120° . The full range of the robotic arm's elbow joint can be seen in Figure 4.9. In order to obtain the best performance, the velocity and acceleration limits of the elbow joint were set at their maximum possible values ($j3_vel = 300^\circ/s$, $j3_acc = 500^\circ/s^2$). The output response to the input signal can be seen in Figure 4.10(a). The output reaches the angle requested

in 1s, which implies an average speed of $120^\circ/\text{s}$. Analysing the waveform, it was observed that the output waveform has only a slight delay in its start up. This implies that the time taken to reach the target position is due to the sigmoid function in the controller, which limits the velocity and acceleration so as to avoid high frequency changes which are generally hard on motors and amplifiers.

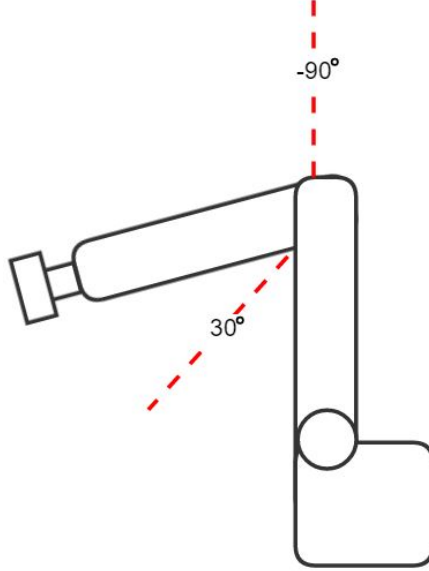
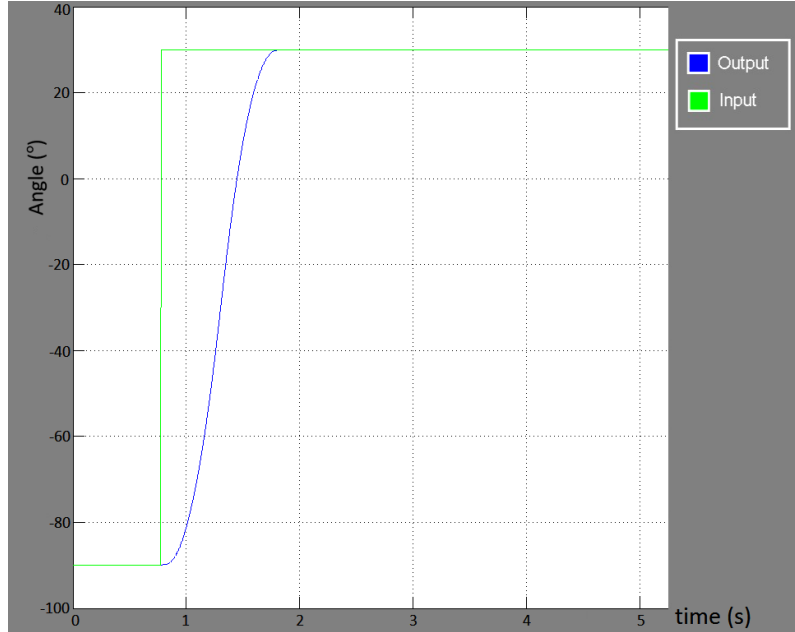
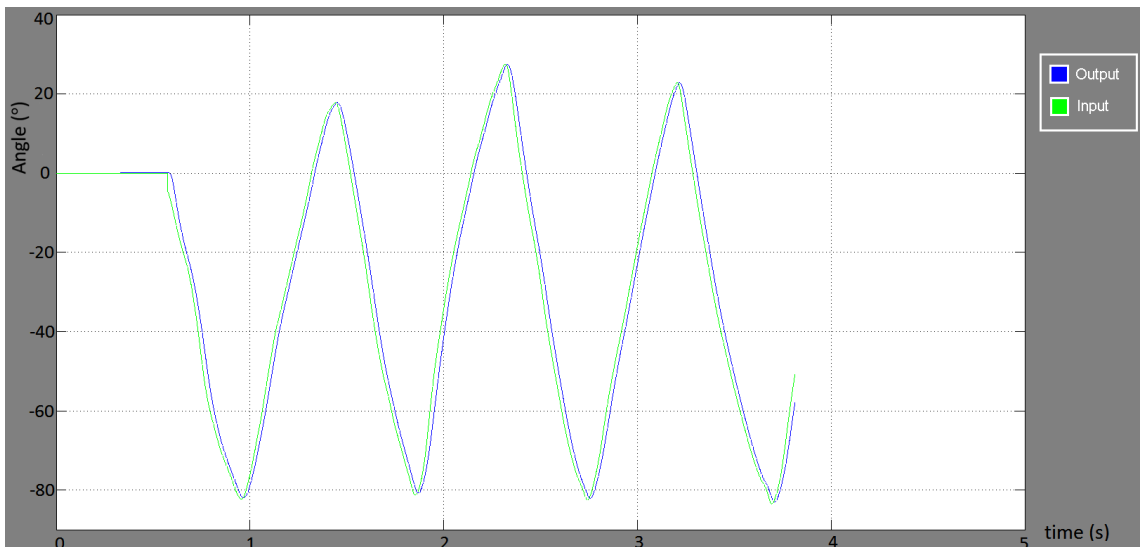


FIGURE 4.9: Range of robotic arm's elbow joint

In the second test, the flexion/extension elbow movement was analysed to see whether the robotic arm can follow typical human elbow movements with pre-defined parameters such as shape and speed of movement. Several elbow movements were recorded using the Vicon system and fed as an input to the robotic arm. Several cycles were performed at different speeds. It was noticed that the robotic arm followed the sinusoidal movement at rate of 0.5Hz accurately, as can be seen in Figure 4.10(b). The output lagged behind the input with a constant delay of 100ms due to the sigmoid function in the controller.



(a) Testing the step response of the robot system



(b) Testing the flexion-extension elbow movement

FIGURE 4.10: Testing the CRS Catalyst-5T robot system

In the final test, the currents sent to the motors were observed, so as to make sure that the robot system is operating below the saturation levels (-5A and 5A). When moving the elbow joint at a speed of 3 rad/s (0.48Hz), the current waveforms in Figure 4.11 were observed. The red waveform is joint 3's motor current wave. The light blue and pink waveforms are the currents which result from moving joints 4 and 5 indirectly along with joint 3. The conclusion from this experiment was that at 3 rad/s, the system is operating well below the saturation levels (-5A and 5A).

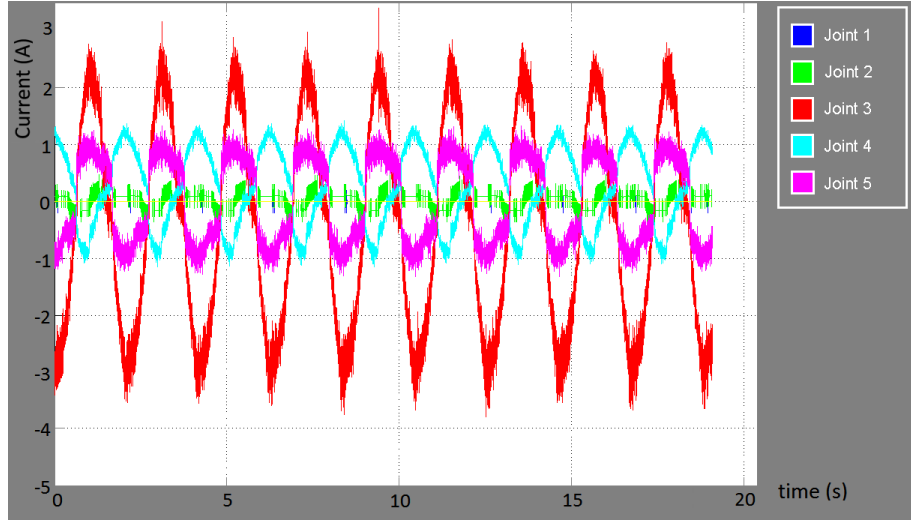


FIGURE 4.11: Analysing the currents sent to the motors

4.4.2 Discussion of Results

Considering all the tests that were performed, several conclusions can be made:

- Operating the robot system with movements having a frequency of 2-3 rad/s is the best compromise between accuracy and imitating movements that are realistic. Robot operation at higher speeds results in a lower accuracy, while lower speeds result in very unrealistic movements.
- When operating at this frequency, the current levels are within saturation levels.
- Although several joints are not commanded to move directly, their motors are supplied current so as to complement the movement of the commanded joint.
- Giving a direct angle command to joint 3, this will be reached within 1 second from the time the input is given. This means that a one second delay will exist if two angles 120 degrees apart are set as inputs right after each other. For a sinusoidal input, this does not apply, and the delay will be limited to 0.1 seconds.
- In the context of Grech's dissertation [2], it was noted that the 0.5s elbow-robotic arm delay was not fully a result of a delay in the robot controller's performance. Although the cause of the delay cannot be deduced from this analysis, possible reasons could be data transfer rates and program running times.

4.5 State space model

The state space model which was implemented by Grech [2] was also analysed so as to determine the errors in the joint angle occurring when supplying this model with biceps brachii EMG as done in [2] and triceps brachii EMG. The former analysis will be compared with that of Grech in [2] while the latter will be carried out to see whether there is any advantage of taking into consideration the triceps brachii EMG data when estimating the elbow joint angle. The movements recorded were performed at a constant 0.5Hz rate.

4.5.1 Experimental and Analysis procedure

As described in Section 3.3.1, the state space model is a linear system used to represent everyday processes. One may question why this model is used, when most phenomena are non-linear. One reason for using this method with a stochastic input is that many processes are well approximated by linear finite dimensional systems and that sometimes, complex behavior can be captured by choosing the order of the system high enough [56]. Literature [28, 37, 45] has also shown that such a linear model could represent well the EMG-to-joint angle relationship.

The Numerical Subspace State Space System Identification (N4SID) numerical algorithm is used to estimate the state space model's parameters. It becomes useful in the parameterisation of high-order multi-variable systems, with the difference that *a priori* parameterisation can be avoided. Moreover, the algorithm is non-iterative and does not involve non-linear optimisation. [2]. The MATLAB function *n4sid(data,nx)* estimates an nx order state space model, using measured input-output data, *data*. Using the Vicon system, ten trials, each 40 seconds long were recorded with constant-speed arm movement. Each cycle includes a full extension and flexion of the forearm, as can be seen in Figure 4.12. A metronome was used to keep the arm velocity constant. Three markers were used to determine the arm's position: at the shoulder, elbow and wrist, as can also be seen in Figure 4.12. Inverse kinematic equations were then applied to these three co-ordinates so as to find the angle of the elbow as described in Section 4.2.3.

Several tests were then performed so as to determine the optimal parameters of the state space model. The performance measures used were the root mean square

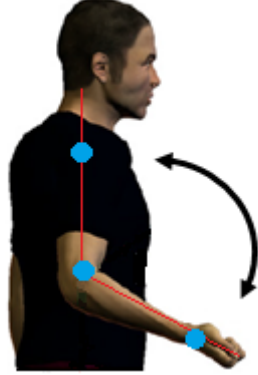


FIGURE 4.12: Elbow flexion/extension motion and markers' position [57] [Edited]

error (RMSE) and the correlation coefficient (CC). Equations 4.9 and 4.10 below define the RMSE and the CC respectively [2].

$$RMSE = \sqrt{\frac{\sum_{t=1}^n (y_t - \hat{y}_t)^2}{n}} \quad (4.9)$$

$$CC = \frac{\sum_{t=1}^n ((y_t - \bar{y}_t)(\hat{y}_t - \bar{\hat{y}}_t))}{\sqrt{\sum_{t=1}^n (y_t - \bar{y}_t)^2 \sum_{t=1}^n (\hat{y}_t - \bar{\hat{y}}_t)^2}} \quad (4.10)$$

The RMSE measures the square root of the mean of the difference between the actual joint angle y_t and the estimated joint angle \hat{y}_t for n samples. The result is a value in degrees ($^\circ$). On the other hand, the CC measures the correlation between the actual and estimated joint angles. It sums the differences between the actual joint angle and its mean \bar{y}_t and the estimated joint angle and its mean $\bar{\hat{y}}_t$, divided by the square root of the product of the squares of these values. The CC gives a value between +1 and -1 inclusive, where 1 is total positive correlation, 0 is no correlation, and -1 is total negative correlation. This value has no units as it is a ratio of values having the same unit.

An indication on the performance of the model across the ten trials is found by testing both without and with cross-validation (CV). When testing without cross-validation, the parameters were estimated using the whole 40s trial, and the model's performance was then tested on the same 40s. The procedure was then repeated for all trials, and an average of the RMSE and the CC was calculated. When testing with forward cross-validation, the parameters of the state space model were estimated using the first 20s of data, and tested on the remaining 20s for all ten trials. In reverse cross-validation, the second half of the data was used

for training while the first 20s were used for testing for all ten trials. The RMSE and the CC for cross-validated testing were then found by finding the mean result of the two methods.

4.5.2 Order variation and filter changes

As discussed in Section 2.4, one of the weaknesses of the EMG signal is that it is subject-specific, such that it varies considerably in amplitude according to the subject. Although Grech's principles were used as a guideline for analysing the state space model, tests to confirm that certain parameters are optimally chosen were performed so as to process the EMG signal accordingly. Hence, the first test involved testing several cut-off frequencies for the low-pass Butterworth filter. The average RMSE of the non cross-validated trials was considered as a measure of performance, and the results were plotted as can be seen in Figure 4.13. The result shows that the lowest error can be achieved when implementing the low-pass Butterworth fourth order filter with a cut-off frequency of 4 Hz. This is in accordance with the filter that Artemiadis and Kyriakopoulos [37] used when estimating the state space parameters.

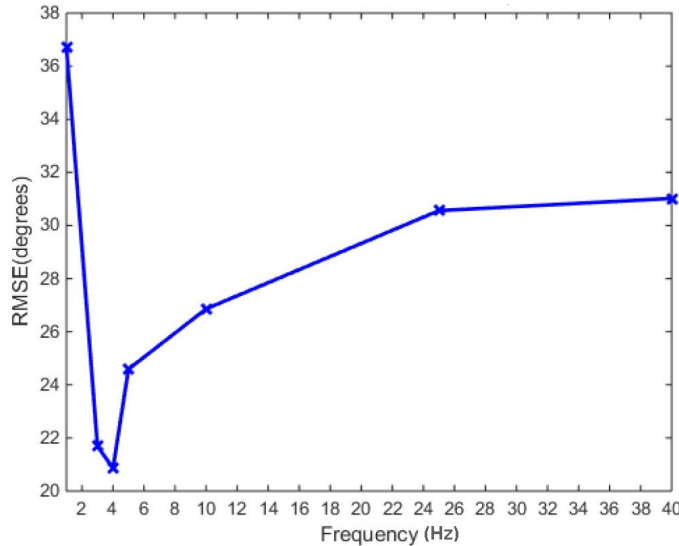


FIGURE 4.13: Effect of changing filter cutoff frequency

Using this cut-off frequency, a second test was performed in order to confirm the optimal order of the state space model. The box-plot graph in Figure 4.14 shows the distribution of the RMSE values achieved for each order in terms of five standard values, the minimum, first quartile, median, third quartile and maximum value. Whilst order 2 seems to be the best performing order in terms of the RMSE,

when a one-way analysis of variance test (ANOVA) was performed, it was observed that only orders 1, 6, 7 and 8 have a mean which is significantly different from an order of 2.

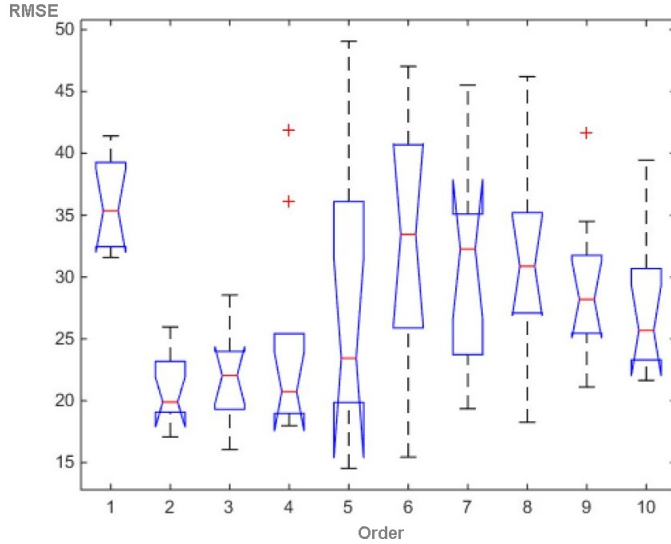


FIGURE 4.14: Effect of order variation on the RMSE

4.5.3 Results without cross-validation

The first test performed to calculate the RMSE and the CC for the ten trials was a non cross-validation test. Both the biceps brachii and triceps brachii EMG were tested separately as inputs to the state space model, with the output joint angle found using the Vicon system. The whole 40s trials were used for estimating the parameters, and the model's performance was tested using the same 40s. This procedure was repeated for all trials.

Table 4.2 shows the results when testing the biceps brachii and triceps brachii EMG as inputs without cross-validation across ten different constant-speed trials. The table is split in two, with the left side displaying results for the biceps brachii EMG, and the right side displaying results for the triceps brachii EMG. The non cross-validated results were found by calculating the mean and standard deviation for each input. Figure 4.15 and Figure 4.16 show the actual joint angle plotted with the estimated joint angle for the biceps brachii EMG input and the triceps brachii EMG input respectively for Trial 7.

TABLE 4.2: Non cross-validation results for model

Trial number	Biceps brachii EMG		Triceps brachii EMG	
	RMSE($^{\circ}$)	CC	RMSE($^{\circ}$)	CC
1	23.18	0.716	20.92	0.730
2	23.72	0.657	20.46	0.749
3	18.93	0.758	22.72	0.630
4	19.61	0.771	25.44	0.582
5	17.07	0.821	23.09	0.628
6	25.96	0.579	23.80	0.644
7	19.07	0.774	20.95	0.740
8	20.01	0.794	24.32	0.684
9	19.77	0.808	22.87	0.702
10	21.29	0.726	23.99	0.622
Mean \pm SD		20.86 \pm 2.54	0.740 \pm 0.07	22.86 \pm 1.56
				0.671 \pm 0.06

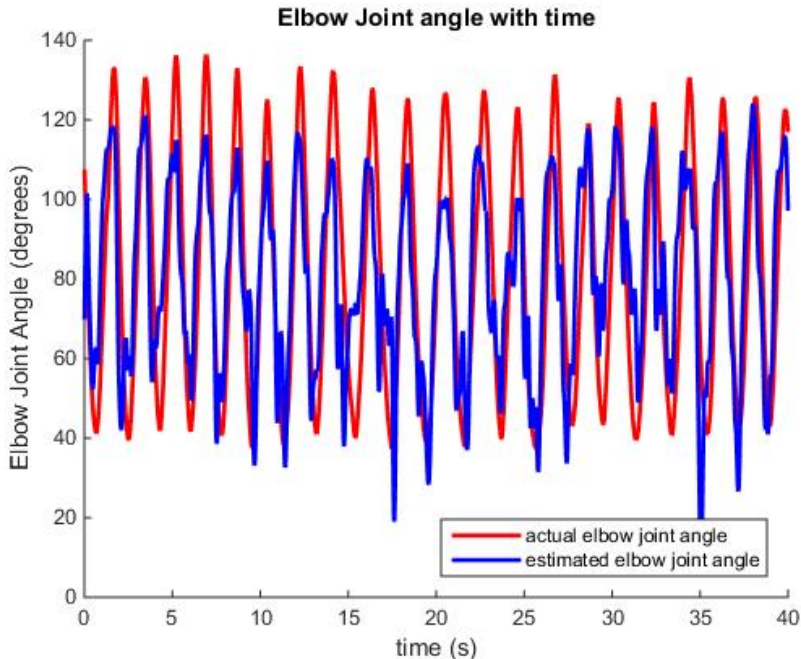


FIGURE 4.15: Actual and estimated elbow joint angle using biceps brachii EMG for Trial 7

4.5.4 Results with cross-validation

The performance of the N4SID algorithm was also tested with cross-validation, particularly using the forward-reverse cross-validation method. The first 20s of each trial were used to estimate the state space parameters, and then these parameters were used on the last 20s of each trial so as to obtain the output joint angle. The actual and the estimated joint angle were then used to calculate the RMSE and

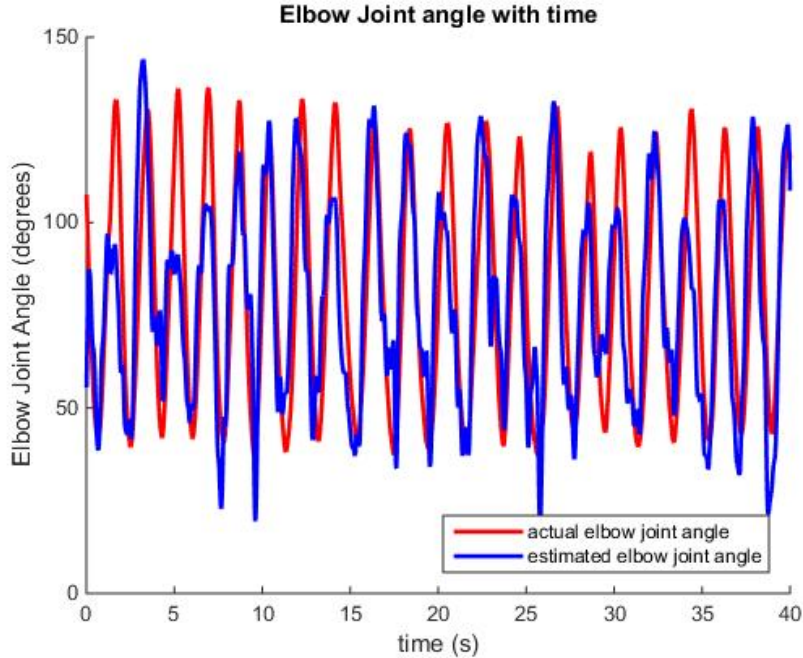


FIGURE 4.16: Actual and estimated elbow joint angle using triceps brachii EMG for Trial 7

the CC of each method. The final cross-validated RMSE and CC were calculated by finding the mean of the forward and reverse cross-validated results.

Table 4.3 and Table 4.4 display the results when testing the different inputs with cross-validation across the ten different trials. The tables are split in two, the left side detailing the results following forward cross-validation, whilst the right side refers to results with reverse cross-validation on the same trials. The aforementioned results include the RMSE and CC for each trial and the final row includes the average and standard deviation over the ten trials.

On the other hand, Figure 4.17 shows a plot for the actual and estimated joint angles for Trial 7 during forward cross-validation of the state space model identified using the N4SID algorithm, when using EMG signals from the biceps brachii. Figure 4.18 shows a similar plot, this time for the reverse cross-validation test when using EMG signals obtained from the triceps brachii.

TABLE 4.3: Cross-validation results for biceps brachii EMG

Trial number	Forward CV		Reverse CV	
	RMSE(°)	CC	RMSE(°)	CC
1	25.78	0.650	38.24	0.448
2	35.83	0.540	27.84	0.782
3	20.77	0.828	26.22	0.741
4	25.50	0.721	24.12	0.739
5	27.46	0.696	17.10	0.859
6	26.11	0.595	27.45	0.550
7	20.89	0.739	19.65	0.779
8	23.24	0.768	27.23	0.724
9	29.61	0.794	24.97	0.846
10	25.91	0.749	40.61	0.247
Mean \pm SD	26.11 \pm 4.16	0.708 \pm 0.085	27.34 \pm 7.27	0.672 \pm 0.196

TABLE 4.4: Cross-validation results for triceps brachii EMG

Trial number	Forward CV		Reverse CV	
	RMSE(°)	CC	RMSE(°)	CC
1	18.26	0.802	24.88	0.633
2	23.15	0.707	21.93	0.679
3	18.39	0.793	25.81	0.492
4	24.61	0.632	26.14	0.541
5	24.63	0.649	24.13	0.616
6	23.02	0.678	25.19	0.610
7	19.48	0.782	24.13	0.649
8	24.27	0.694	27.61	0.597
9	24.28	0.695	23.46	0.686
10	18.09	0.784	32.23	0.350
Mean \pm SD	21.82 \pm 2.74	0.722 \pm 0.060	25.55 \pm 2.82	0.585 \pm 0.102

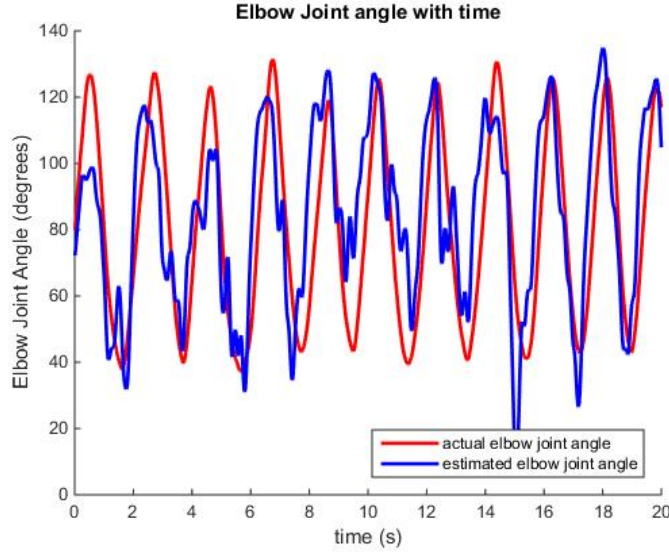


FIGURE 4.17: Biceps brachii results (forward cross-validation) for Trial 7

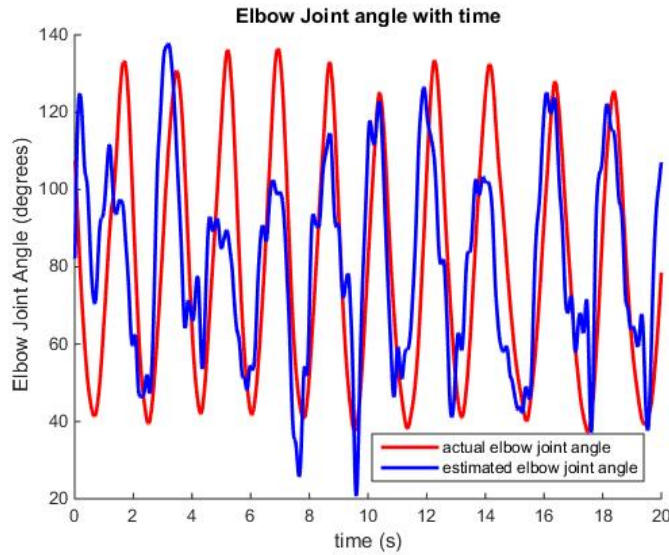


FIGURE 4.18: Triceps brachii results (reverse cross-validation) for Trial 7

4.5.5 Discussion of Results

A number of conclusions can be drawn from the results obtained. Considering the results in Table 4.2 there was no significant difference in the performance of the models when using biceps brachii or triceps brachii EMG. This conclusion was made by looking at the average RMSE and CC obtained for the different trials where results for both inputs lie within the deviation range calculated. Considering each input individually, the low standard deviation across trials with relation to their respective averages indicates that the RMSE and CC measures did not vary substantially across trials.

Analysing the results presented in Table 4.3 and Table 4.4, the RMSE and CC values are quite similar when comparing both the forward and reverse cross-validation methods. However, the reverse cross-validation RMSE and CC values were slightly worse than their forward cross-validation counterpart. This shows that for this subject, any time-varying features in the EMG signal, such as fatigue, seem to affect the performance of the model. In contrast with the non cross-validated results, the RMSE for the triceps brachii EMG was found to be lower than that for the biceps brachii EMG.

A summary of all the performance measures can be seen in Table 4.5. Set A shows the results achieved in this analysis, while Set B shows the results obtained by Grech [2] using the same method. Only the results with the biceps brachii EMG used as input can be compared as the triceps brachii EMG was introduced for the first time in this analysis. Results for the RMSE are comparable to each other, as the values obtained in both sets lie within each other's deviation range. However the CC obtained in the first set is worse off than that in the second set. This indicates that the estimated joint angle obtained by Grech had a stronger linear relationship with the actual joint angle than in the analysis carried out in this section.

TABLE 4.5: State Space model analysis - Summary of results

Method	Set A		Set B	
	RMSE(°)	CC	RMSE(°)	CC
Biceps brachii, no CV	20.86 ± 2.54	0.74 ± 0.07	19.88 ± 2.99	0.89 ± 0.03
Triceps brachii, no CV	22.86 ± 1.56	0.67 ± 0.06		
Biceps brachii, CV	26.73 ± 5.80	0.69 ± 0.15	23.67 ± 3.80	0.88 ± 0.03
Triceps brachii, CV	23.69 ± 3.31	0.65 ± 0.11		

4.6 Summary

In this chapter the complete EMG-to-joint angle system was described by distinguishing between the offline and online components of the system. The offline component is used to estimate the state space parameters, while the online system is used for real-time operation. The claim made in [2] by Grech about a notable delay between the elbow movement and the robotic arm's reproduction of the movement was investigated by analysing both the robotic arm's online performance and the model's offline performance and results show that the robotic arm's response accounts for a 0.1s delay. In the next chapter, two other models will be designed as an attempt to reduce the error between the actual and estimated joint angles. Furthermore, the possibility of using both the biceps brachii and triceps brachii EMG simultaneously to improve performance will be investigated.

Chapter 5

System Identification

5.1 Introduction

Three types of models, specifically state-space models, linear regression models and neural network based models have been identified in the literature review as being a suitable option to convert EMG data directly to output joint angles. The former was discussed and analysed in detail in Chapter 4. This chapter will now analyse and compare the model fit using linear regression models and neural networks and identify whether any of these is a good alternative to state-space models.

5.2 Data acquisition and Pre-processing

Ten trials, each 40 seconds long, of the input-target pairs were recorded so that they can be used to estimate the parameters of the model and test its performance. For elbow flexion and extension, EMG data was recorded from the biceps brachii and triceps brachii. The EMG data was recorded using the ZeroWire EMG acquisition box in parallel with the position co-ordinates of three markers on the elbow, shoulder and wrist using the Vicon system. The joint angles were calculated using the three co-ordinates, and set as the target elements. Figure 5.1 shows the placement of the electrodes and position markers on the subject.

Before the EMG signal was fed to the model, it was processed to remove movement artefacts and increase the signal-to-noise ratio. The raw EMG signals from different muscles were detected using one channel for every signal. The distance between electrodes was minimised to prevent crosstalk. The recorded signal was then filtered by the EMG acquisition box as described in Section 4.2.1 and stored for analysis.



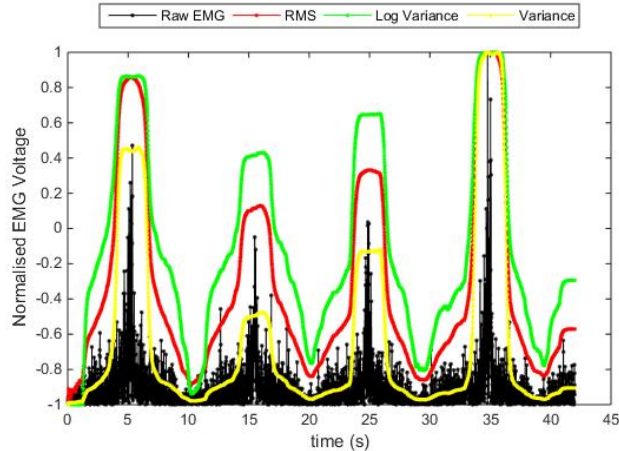
FIGURE 5.1: Electrode and position marker placement

The pre-processing procedure includes rectification of the signal, and then a non-linear function is applied to the signal to convert it to an amplitude envelope. Afterwards, a low-pass filter with a cut-off of 1Hz is introduced, as suggested by Aung and Al-Jumaily [43]. Finally the processed signal is normalised, with the maximum and minimum value determined from two trials which were not used to estimate the parameters or test the model. Using the same data would lead to a wrong performance estimation, since the parameters would over-fit to the specific data [28]. Hence, in this case eight trials were used for analysis.

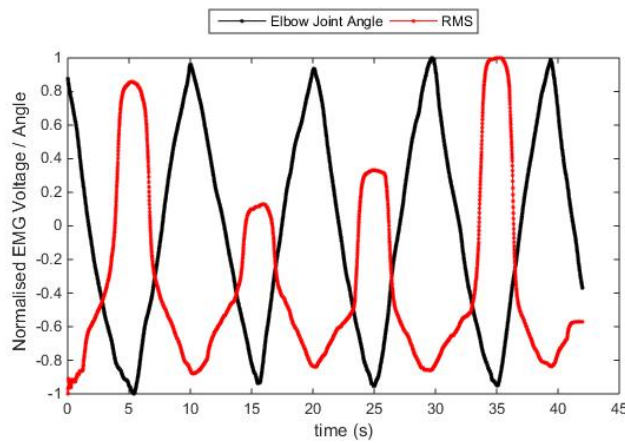
5.2.1 Effect of feature transformation and window size

The effect of feature transformation applied on EMG data was discussed in Section 3.3.2.1, where Hahne *et al.* tested the application of variance, log-variance and root-mean square (RMS) on EMG, and used the coefficient of determination (R^2) value as a performance measure. Figure 5.2(a) shows the relationship between the biceps brachii EMG voltage and the three features applied on it for four triangular cycles. One can note that although the movement is repeated for four times, the EMG values for each cycle are not identical. Figure 5.2(b) shows the relationship between the elbow joint angle and the RMS feature for the same period.

A similar test to that performed by Hahne *et al.* [28] was carried out, however the RMSE was used to measure the performance of the MLP model. Figure 5.3 shows the average results of the four-fold cross-validation test for the three features, together with the effect of the window size over which the feature is applied on. The RMS feature is the best performing feature for all window sizes, especially for window sizes of 150 and 200 samples.



(a) Relationship between features and biceps brachii EMG



(b) Relationship between RMS feature and elbow angle

FIGURE 5.2: Pre-processing biceps brachii EMG data

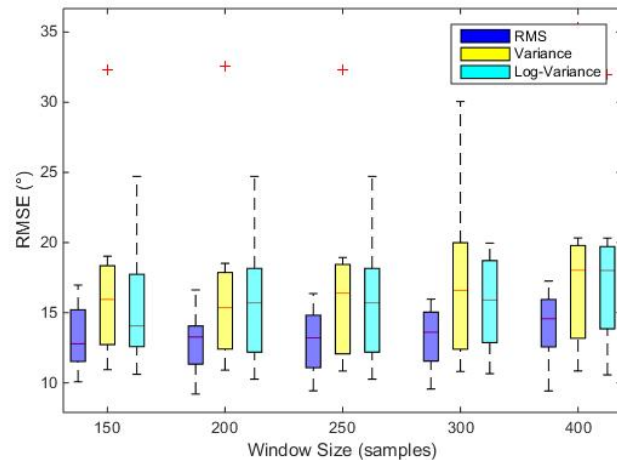


FIGURE 5.3: Comparing how performance, in terms of RMSE, varies with window size and feature used

5.3 Linear regression

Linear regression representation is a technique which can be used to fit a model and predict the response once an input is supplied. As described in Section 3.3.2, regression methods describe the relationship between an output (dependent) variable and one or more predictor (explanatory) variables using a linear representation.

5.3.1 Procedure

MATLAB's Statistics and Machine Learning Toolbox was used to create a model which can convert EMG data to represent the elbow joint angle. The input EMG data and the target joint angles were placed in a table, in two separate columns, where each row represented one observation. The *fittm* command was used to construct a least-squares fit of a model to the input data. By default, this command creates a linear model which contains an intercept and a linear term for each predictor.

After estimating the intercept value and the predictor constants, the model was analysed using two tests: without cross-validation and with cross-validation. In the first method, a trial of 40s was used to estimate the model parameters, and the same data was used to test the model. This was repeated for all eight trials. In the second method, a four-fold cross-validation was performed. Six trials were used to find the unknown parameters and the remaining two trials were used for testing. This procedure was repeated for four times, each time testing on two new trials. In this way, the model's ability to generalise to new data was tested.

Three measures were used to rate the performance of the model: the root mean square error (RMSE), the correlation coefficient (CC) and the coefficient of determination (R^2) value. The RMSE and CC parameters were defined in Section 4.5.1. Equation 5.1 defines the R^2 parameter, where y_t represents the target joint angle, \hat{y}_t represents the estimated joint angle, \bar{y}_t represents the mean of the target joint angles and n is the number of samples.

$$R^2 = 1 - \frac{\text{Mean square value}}{\text{Variance}} = 1 - \frac{\sum_{t=1}^n (y_t - \hat{y}_t)^2}{\sum_{t=1}^n (y_t - \bar{y}_t)^2} \quad (5.1)$$

Since anatomical joint movements are controlled by the actions of both agonist and antagonist muscles, more than one muscle may be involved in performing a single

joint movement. As one muscle contracts, causing the movement to occur, the other relaxes. In [58], Rahman *et al.* studied the shoulder and elbow muscles to find the appropriate pairs of agonist and antagonist muscles involved in shoulder and elbow movements. The muscles active in elbow flexion and extension were deduced to be the biceps brachii and triceps brachii. Hence, a multivariable regression method was used as can be seen in Equation 5.2

$$\mathbf{Y} = p_1 \mathbf{X}_1 + p_2 \mathbf{X}_2 + c \quad (5.2)$$

In this case both the biceps brachii EMG \mathbf{X}_1 and triceps brachii EMG \mathbf{X}_2 were set as inputs, with p_1 and p_2 acting as the predictor constants for the biceps brachii and triceps brachii EMG inputs respectively, and c representing the intercept value. \mathbf{Y} represents the elbow joint angle in this case.

5.3.2 Results without cross-validation

In the first test, the predictor parameters and intercept constant were first found for each trial using MATLAB's Statistics and Machine Learning Toolbox. Using the same input EMG and the determined parameters, the output elbow joint angle was calculated. Hence the RMSE, CC and R^2 values were determined. Table 5.1 displays the results when using multivariable linear regression, using both the biceps brachii and triceps brachii EMG as inputs. Results were consistent across all trials, proving that a linear relationship for each trial was successfully created. Figure 5.4 shows the actual and estimated elbow joint angles for Trial 6.

TABLE 5.1: Linear regression non cross-validation results

Trial number	Biceps brachii and Triceps brachii EMG		
	RMSE(°)	CC	R^2
1	19.33	0.865	0.663
2	15.39	0.902	0.769
3	9.75	0.946	0.883
4	9.38	0.949	0.889
5	15.27	0.887	0.729
6	10.84	0.932	0.849
7	13.47	0.913	0.801
8	11.12	0.938	0.862
Mean \pm SD		13.07 \pm 3.45	0.916 \pm 0.030
		0.806 \pm 0.081	

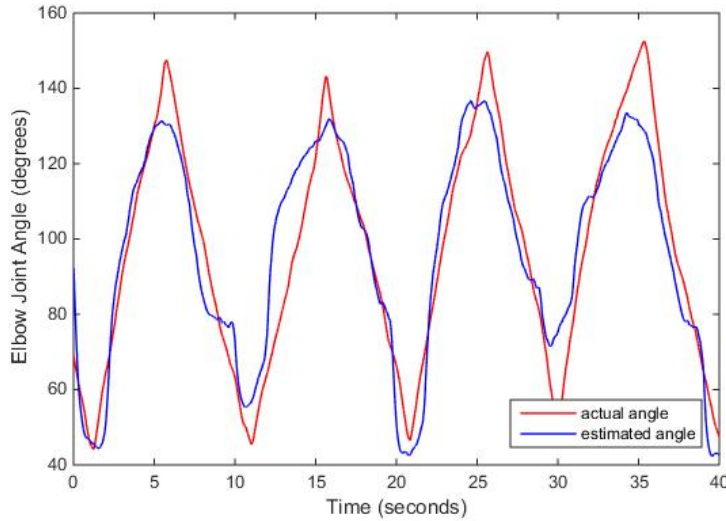


FIGURE 5.4: Actual and estimated angles for Trial 6

5.3.3 Results with cross-validation

In the second test, the predictor parameters and intercept constant were first found using six trials. Using the input EMG from the remaining two trials and the determined parameters, the output elbow joint angle was calculated. This process was repeated four times, picking two new trials from the set for testing the model. The RMSE, CC and R^2 values were then determined for each fold. Table 5.2 displays the results for the four-fold cross-validation procedure and the mean value for all performance measures. The first column shows the trials used to test the model. Results show inconsistency across the different trials tested, with values for the RMSE and R^2 varying considerably. The actual and estimated elbow joint angles for the third fold can be seen in Figure 5.5, where the model was estimated using Trials 1, 2, 3, 4, 7 and 8 and tested on Trials 5 and 6.

TABLE 5.2: Linear regression cross-validation results

Trials	Biceps brachii and Triceps brachii EMG		
	RMSE(°)	CC	R^2
1,2	60.44	0.787	0.263
3,4	20.62	0.856	-1.046
5,6	22.32	0.899	-2.004
7,8	23.23	0.934	-3.609
Mean \pm SD	31.65 \pm 19.22	0.869 \pm 0.063	-1.599 \pm 1.631

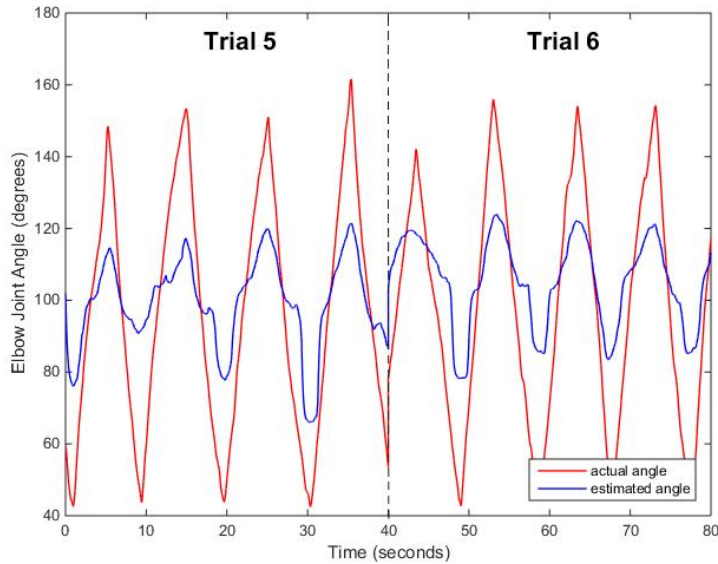


FIGURE 5.5: Actual and estimated angles for Trials 5 and 6

5.3.4 Discussion of Results

When testing the linear regression model without cross-validation, the model estimated the elbow joint angle quite accurately, with a 7° improvement in RMSE over the state-space model RMSE. However, the results when testing the model with four-fold cross-validation were inferior, especially for one of the folds. These results indicate that as the characteristics of the EMG signals may change, the estimated model remains no longer suitable to translate new EMG data into the true corresponding elbow joint angle.

5.4 Multi-layer perceptron

Artificial neural networks consist of simple elements inspired by biological elements which can be trained to perform a certain function by adjusting the values of the connections (weights) between elements. One such configuration is a multi-layer perceptron, which was described in detail in Section 3.3.3. For this project, this neural network was used to create a model which maps EMG data into joint angles. The reason which makes a multi-layer perceptron ideal for this application is the fact that it consists of non-linear activation functions which are perfect for complex and stochastic inputs.

5.4.1 Procedure

The network is trained so that a particular EMG input leads to a specific target joint angle. Such a situation is shown in Figure 5.6. The network is adjusted, according to the difference between the output and the target, until the output matches the target. The error between the target elements and the output is used to adjust the weights according to the back-propagation algorithm as discussed in Section 3.3.3. The process is repeated until the value of these weights converge.

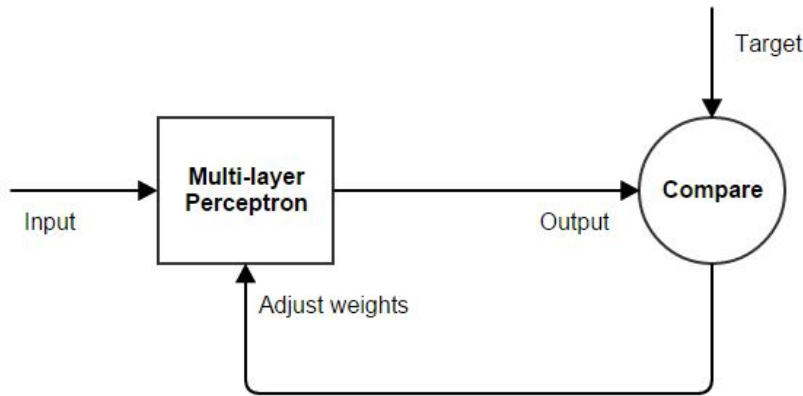


FIGURE 5.6: Training the MLP

MATLAB's Neural Networks Toolbox is used to represent and train the network. A single perceptron cannot do very much, as it can only represent linearly separable functions. However, several perceptrons can be combined into multiple layers that have great power. The Neural Networks Toolbox makes it easy to create and understand such large networks. The Neural Fitting application was used to generate a script of code which uses several in-built functions to create a network which incorporates all the data necessary to build a MLP. One can choose between three back-propagation neural networks (BPNN) algorithms to train the network. In this case the Levenberg-Marquardt algorithm was used as suggested by Aung [43] as this is the fastest method.

Since the neural network starts with random initial weights, the results differ slightly every time it is run. The random seed is set to avoid this randomness when finding the best parameters for training the system. This was removed when the best configuration was determined. In addition, another MLP was designed from first principles, which finds the weights of the network manually using the back-propagation algorithm. However, the application was used as it provides better flexibility in adding inputs and hidden layer nodes.

After defining the architecture of the network and training the MLP, the weights of the configuration were stored, and two tests on the model were carried out: testing without cross-validation and testing with cross-validation. The performance measures used were identical to those used on the linear regression model, so that their performance could be compared.

5.4.2 Defining the architecture of the network

The architecture of a network can be defined by the number of layers the network has, the number of neurons in each layer, each layer's transfer function, and how the layers connect to each other. Beside defining the number of neurons in the network's output layer, the number of neurons in the hidden layer needs to be determined after running several tests on the architecture. If a linear mapping needs to be modelled, a linear transfer function should be used. However, a linear configuration cannot perform a non-linear computation. Using a non-linear transfer function makes the configuration capable of representing a non-linear relationship between the input and the output. A sigmoid transfer function is an example of a non-linear transfer function which can be used to model a complex, stochastic input. The Neural Networks Toolbox uses the *tansig* function defined in Equation 5.3 as an alternative to the sigmoid function, as it is a good trade off where speed is prioritised over the exact shape of the transfer function [59].

$$\text{tansig}(n) = \frac{2}{1 + e^{-2n}} - 1 \quad (5.3)$$

Multiple feed-forward layers are used to represent complex relationships, as they give the network greater freedom. Almost any function can be represented using a two-layer network: a sigmoid layer feeding another sigmoid output layer [60]. A bias is included with each neuron, as it can represent relationships between inputs and outputs more easily. A neuron without a bias always has a net input of zero to the transfer function when all of its inputs are zero. On the other hand, a neuron with a bias can learn to have any value under the same conditions by learning an appropriate bias value [59].

The number of neurons in the hidden layer was optimised with cross-validation. Including very few neurons can lead to high errors as the data being predicted becomes too complex for a small number of nodes to capture. On the other hand,

too many neurons over-fit the training data and as an effect cause the model to not generalise well when presented with new data. A test on a range between one and 20 hidden neurons demonstrated that the performance did not improve with more than three neurons and deteriorated when using more than five neurons. Similar results were also declared by other studies [28, 30]. Thus the number of hidden neurons for elbow joint angle estimation was fixed to three, as can be seen in Figure 5.7, and the number of weights in the network was hence thirteen.

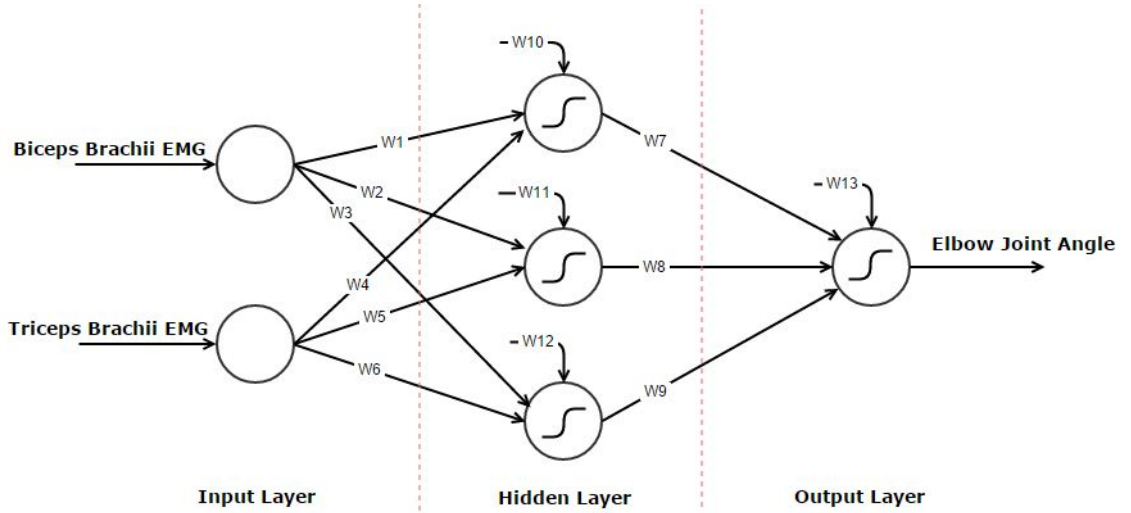


FIGURE 5.7: MLP structure for elbow movement

5.4.3 Results without cross-validation

In the first test, the thirteen weights were found for each trial and using the same input EMG and weights, the output elbow joint angle was calculated. The RMSE, CC and R^2 values were determined to evaluate the performance of the model. Table 5.3 displays the results when using both the biceps brachii and triceps brachii EMG as inputs. An average RMSE of 8.57° , CC of 0.964 and R^2 of 0.922 was obtained. Figure 5.8 shows the actual and estimated elbow joint angles for Trial 2.

TABLE 5.3: MLP elbow angle non cross-validation results

Trial number	Biceps brachii and Triceps brachii EMG		
	RMSE(°)	CC	R²
1	7.72	0.980	0.958
2	8.25	0.973	0.945
3	10.83	0.945	0.878
4	9.14	0.952	0.897
5	7.87	0.971	0.940
6	8.89	0.961	0.916
7	7.03	0.972	0.942
8	8.85	0.955	0.901
Mean \pm SD		8.57 \pm 1.15	0.964 \pm 0.012
			0.922 \pm 0.028

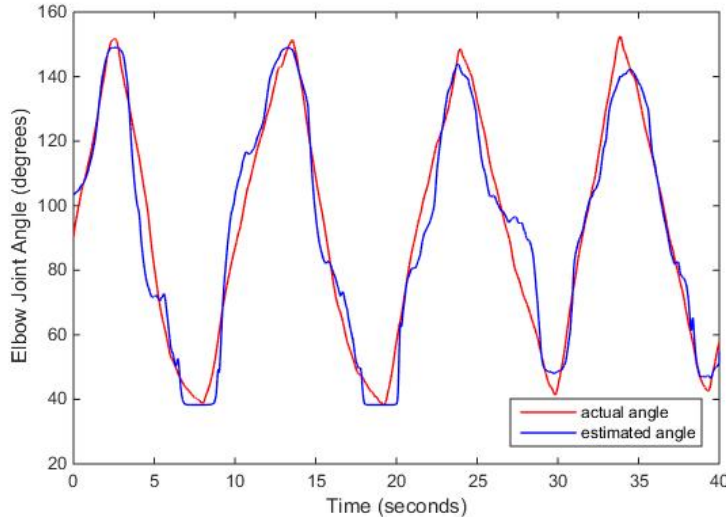


FIGURE 5.8: Actual and estimated angles for Trial 2

5.4.4 Results with cross-validation

In the second test, a four-fold cross-validation test was performed, where the weights were found by training the network using six trials. Using the input EMG from the remaining two trials and the determined weights, the output elbow joint angle was calculated. In this way, the model's ability to generalise to new data was investigated. The RMSE, CC and R² values were determined so as to evaluate the performance of the model. Table 5.4 displays the results for the cross-validation procedure and the mean value for all performance measures. The first column shows the trials used to test the model.

TABLE 5.4: MLP elbow angle cross-validation results

Trial number	Biceps brachii and Triceps brachii EMG		
	RMSE(°)	CC	R²
1,2	21.48	0.889	0.526
3,4	13.28	0.908	0.783
5,6	12.95	0.929	0.848
7,8	12.91	0.930	0.786
Mean \pm SD	15.16 \pm 4.22	0.914 \pm 0.020	0.736 \pm 0.143

It can be noted that the results for the first fold are considerably inferior to the remaining three folds' results. However, on average results were better than those achieved in the previous models. The actual and estimated elbow joint angles for the third fold can be seen in Figure 5.9, where the model was estimated using Trials 1, 2, 3, 4, 7 and 8 and tested on Trials 5 and 6.

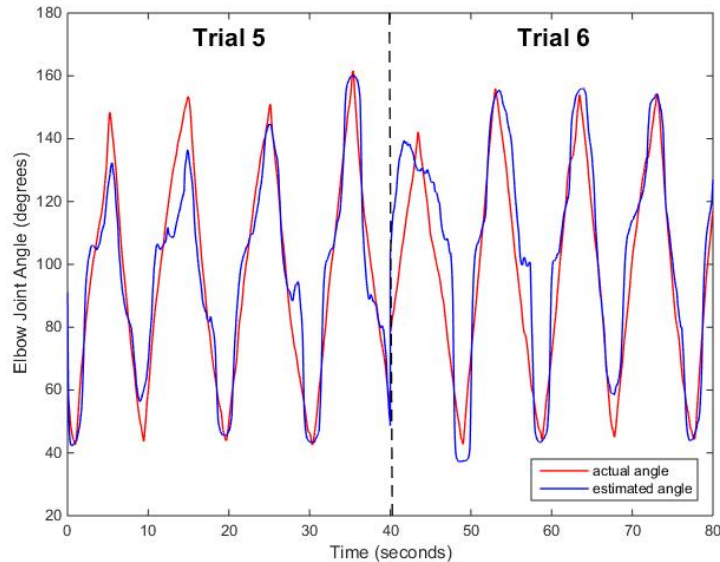


FIGURE 5.9: Actual and estimated angles for Trials 5 and 6

5.4.5 Discussion of Results

Observing the results obtained without cross-validation, the MLP learns effectively the data it is trained on, as the performance across all the trials varies slightly. When testing the MLP with cross-validation, one fold produces worse results than the remaining three folds. However, the results obtained in both tests are superior

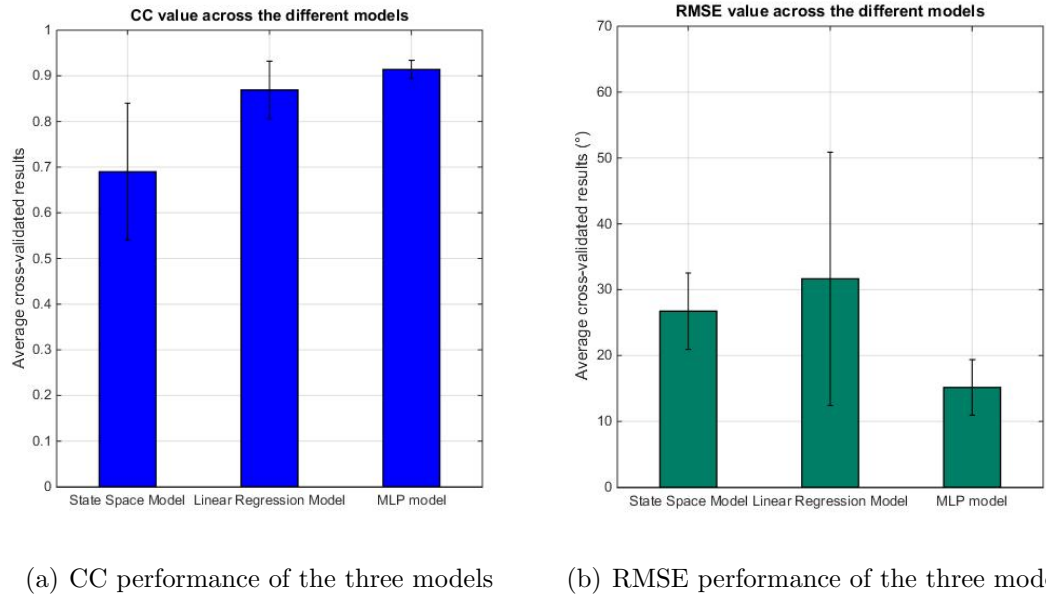


FIGURE 5.10: Comparing performance of the three models

for all performance metrics over both the state-space model and linear regression method. This is shown evidently in Figure 5.10.

The first graph, Figure 5.10(a) shows the CC performance for the three models, where the MLP model performs slightly better than the linear regression model. The second graph, Figure 5.10(b) shows the RMSE obtained over all three models. The MLP performed superiorly to the other methods, and also more consistently, with the lowest standard deviation. This outcome shows that using a non-linear method such as the MLP is a better option for estimating the joint angle using EMG signals.

5.5 Summary

In this chapter, two different modelling techniques were compared for independent myoelectric control. The methods were compared under carefully designed experimental paradigms in order to assess their performance in terms of accuracy and robustness. The RMS transformation of the EMG signal was chosen to linearise the relationship between EMG and joint angles. Research [28] suggested that linear methods can achieve good results comparable to parametric non-linear algorithms. However, in this case it was noted that the linear regression method was unable to generalise to new data. Whereas in [28], the average cross-validated

R^2 value obtained was around 0.6, in this case a value of -1.6 was obtained. On the other hand, more accurate results were confirmed using the MLP. The average cross-validated R^2 value obtained was 0.736, which compares well with the results obtained by Hahne *et al.*, with a value of 0.7.

Considering the next step to model different shoulder and elbow movements, and implement the model in real-time, both models were evaluated. The MLP method is relatively fast during evaluation, but training can be slow. A major advantage of the linear regression method is the considerable reduction in computational demand for training and evaluation. However, accuracy plays an important role in such an application, and hence the MLP method was chosen. A study on reducing the training size of the MLP will be discussed in the upcoming chapter.

Chapter 6

Modelling different joint movements

6.1 Introduction

Following the analysis of different system identification methods for the estimation of upper arm joint angles from EMG signals, the multi-layer perceptron (MLP) approach was found to be the best choice. In this chapter, six different movements in three two-dimensional planes will be modelled and tested, including three simultaneous joint movements. Figure 6.1(a) shows the reference which was considered in this project for defining the different planes while Figure 6.1(b) shows the muscles used and the respective electrode placement. A description of the method used to create a model for each of the six different movements recorded is also provided. Furthermore, the results achieved in the offline training procedure will be demonstrated, followed by a discussion on the results obtained.

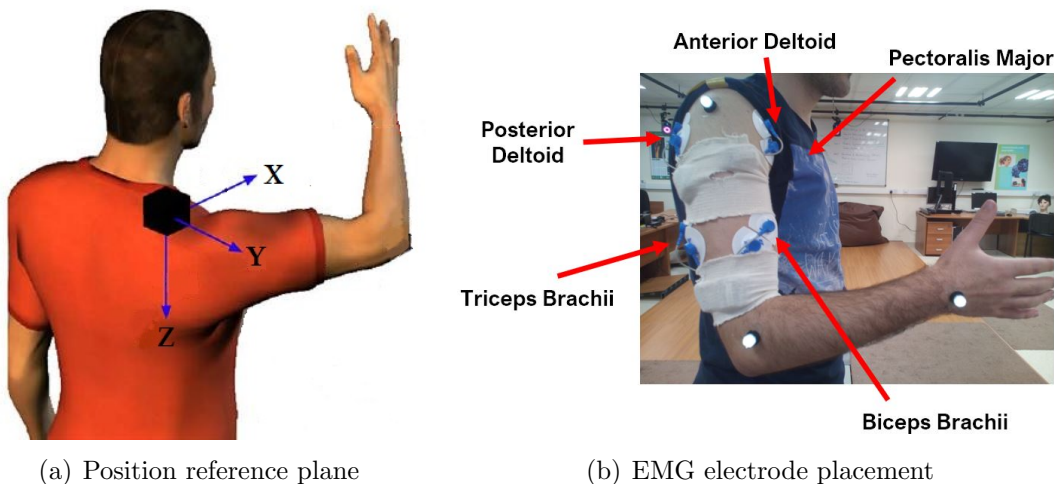


FIGURE 6.1: EMG electrode and plane references [37] [Edited]

6.2 Single joint movements

The first three modelled movements were single joint movements in three different planes. These included shoulder movement in the x-z plane, x-y plane and the y-z plane as shown in Figure 6.2. This diagram also shows the position of the markers used for each movement. Ten trials, each 40s long were recorded for each movement, and as was done in the previous exercise, two trials were used to set the normalisation values for the EMG signals. The Vicon motion capture system was used to record the position of three markers so that the joint angle can be calculated as described in Section 4.2.3.

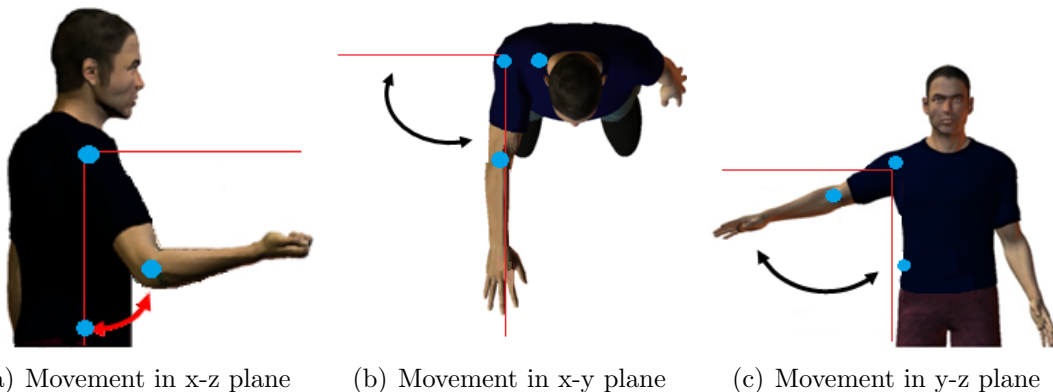


FIGURE 6.2: The three types of shoulder single joint movements [57] [Edited]

For the x-z plane shoulder movement in Fig 6.2(a), the same MLP structure as that in Figure 5.7 was used, however instead of using the biceps brachii and triceps brachii as the pair of input EMG channels, the anterior and posterior deltoid channels were used. The output in this case was the shoulder angle. The three position markers were placed on the shoulder, elbow and on the hip.

The next modelled movement was in the x-y plane as can be seen in Figure 6.2(b). In the training session, the three position markers were placed on the shoulder, elbow and on the chest. The reason why a marker was placed on the chest instead of on the hip was that the angle being calculated in this case was in the x-y plane. Two EMG probes were used to record signals at the posterior deltoid and pectoralis major. As in the previous movement, a two-input MLP structure was used, however using the pectoralis major EMG and posterior deltoid EMG as inputs. The final modelled movement was in the y-z plane as demonstrated in Figure 6.2(c). For the training session, the three position markers in this case were placed on the

shoulder, elbow and on the hip. A two-input MLP structure was used, the inputs being the anterior and posterior deltoid EMG signals.

For every single joint movement, the root mean square (RMS) feature was applied on the rectified EMG of each channel before training the network, as was discussed in 5.2. As in the previous tests, the model was tested without cross-validation and with cross-validation. The root mean square error (RMSE), correlation coefficient (CC) and the coefficient of determination (R^2) performance metrics were used.

6.2.1 Results

6.2.1.1 Movement in the x-z plane

Initially, the model was tested with the data used to train the MLP network. This test without cross-validation was repeated for all the eight trials. The average RMSE achieved was $10.01^\circ \pm 1.52^\circ$, with an average CC of 0.955 ± 0.015 and an average R^2 value of 0.902 ± 0.035 .

The second test carried out was a four-fold cross-validation test. The goal of this analysis was to investigate the generalisability of the estimated model in translating muscle activity to the corresponding joint angles when working on new unseen data. This consists of training the network using six trials, testing using the remaining two trials, and then repeating this procedure four times for different trials. The results obtained can be seen in Table 6.1. The first column lists the trials on which the model was tested. Results were consistent over all the folds, resulting in small standard deviation values. Figure 6.3 shows the actual and estimated shoulder angles for Trials 5 and 6.

TABLE 6.1: Shoulder angle in x-z plane cross-validation results

Trial number	Anterior Deltoid and Posterior Deltoid EMG		
	RMSE(°)	CC	R^2
1,2	14.17	0.912	0.819
3,4	11.11	0.947	0.882
5,6	11.31	0.951	0.900
7,8	12.77	0.936	0.870
Mean \pm SD	12.34 ± 1.43	0.936 ± 0.018	0.868 ± 0.035

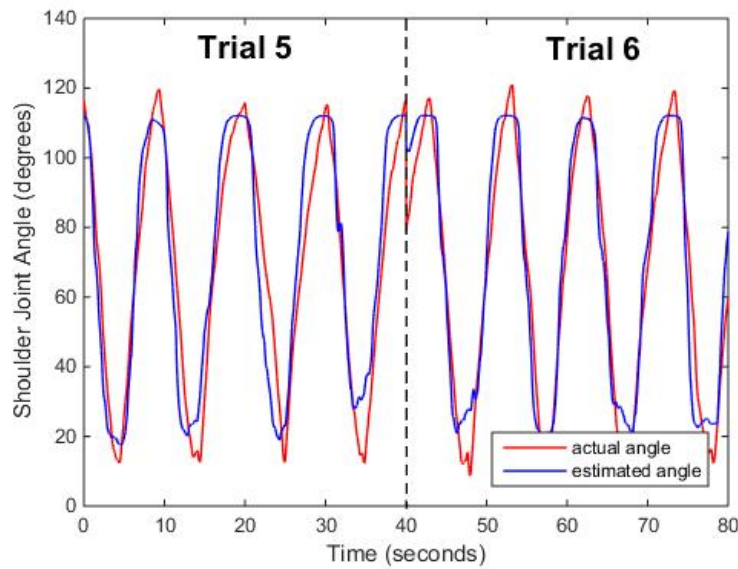


FIGURE 6.3: Actual and estimated angles for Trials 5 and 6

6.2.1.2 Movement in the x-y plane

First of all, the model was tested with the data used to train the MLP network. This test without cross-validation was repeated for all the eight trials. The average RMSE achieved was $4.95^\circ \pm 0.91^\circ$, with an average CC of 0.953 ± 0.019 and an average R^2 value of 0.896 ± 0.046 .

Subsequently, a four-fold cross-validation test was performed. The results obtained can be seen in Table 6.2. The first fold was observed to perform superiorly to the remaining folds across all performing measures. Figure 6.4 shows the actual and estimated shoulder angles for Trials 1 and 2.

TABLE 6.2: Shoulder angle in x-y plane cross-validation results

Trial number	Pectoralis Major and Posterior Deltoid EMG		
	RMSE($^\circ$)	CC	R^2
1,2	6.92	0.935	0.873
3,4	10.78	0.905	0.679
5,6	9.19	0.892	0.714
7,8	8.36	0.906	0.786
Mean \pm SD	8.81 ± 1.61	0.910 ± 0.018	0.763 ± 0.086

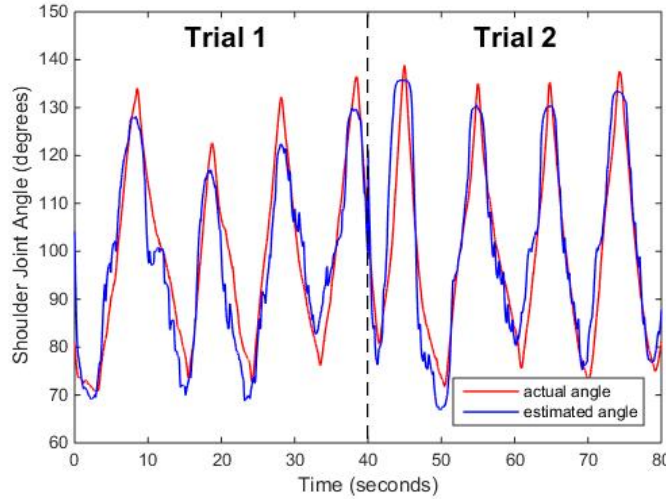


FIGURE 6.4: Actual and estimated angles for Trials 1 and 2

6.2.1.3 Movement in the y-z plane

The first test was a non cross-validation test. The average RMSE achieved was $4.34^\circ \pm 0.55^\circ$, with an average CC of 0.979 ± 0.004 and an average R^2 value of 0.957 ± 0.010 .

The second test was a cross-validation test. The results obtained can be seen in Table 6.3. The first column lists the trials on which the model was tested. Results obtained were very consistent across the trials for all performance measures. Figure 6.5 shows the actual and estimated shoulder angles for Trials 1 and 2.

TABLE 6.3: Shoulder in y-z plane cross-validation results

Trial number	Anterior and Posterior Deltoid EMG		
	RMSE($^\circ$)	CC	R^2
1,2	5.34	0.971	0.938
3,4	5.30	0.967	0.927
5,6	5.16	0.971	0.940
7,8	5.92	0.969	0.923
Mean \pm SD	5.43 ± 0.33	0.970 ± 0.002	0.932 ± 0.008

6.2.2 Performance as a function of training set size

Keeping the size of the multi-layer perceptron's training set as small as possible is beneficial as it reduces the model's training time and makes it easier for the model

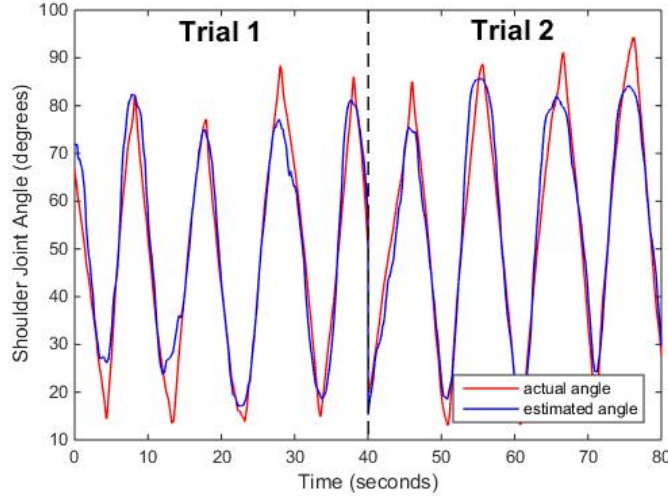


FIGURE 6.5: Actual and estimated angles for Trials 1 and 2

to be used in practice. In the previous analysis, six trials were used to train the neural network in a four-fold cross-validation method. An experiment was then performed to investigate how model performance varies as the number of trials used for training is varied in single joint movements. Specifically, since 8 trials of 4000 samples each were available, 2 trials were left for testing purposes and the remaining 6 trials were used for training. This was repeated in a four-fold cross-validation manner, each time testing on 2 new trials. The analysis investigated how performance varies as the number of training trials was reduced from 6 down to 1 with the average results shown in Table 6.4. It must be noted that the test was carried out using the elbow movement and the shoulder movement in the x-z plane.

TABLE 6.4: MLP average elbow and shoulder angle performance

Number of trials	Average for elbow angle			Average for shoulder angle		
	RMSE(°)	CC	R ²	RMSE(°)	CC	R ²
6	15.157	0.914	0.736	12.338	0.936	0.868
5	19.679	0.898	0.449	12.245	0.936	0.845
4	23.116	0.861	-0.029	12.773	0.933	0.835
3	25.918	0.847	-0.612	13.078	0.931	0.821
2	24.590	0.845	-0.349	12.949	0.931	0.844
1	22.781	0.828	-0.307	14.053	0.923	0.812

The results for the RMSE are depicted in Figure 6.6. One can note that for the elbow angle, training using six trials is essential to obtain the best results. Training with five instead of six trials results in a decrease in performance of 4.52° which

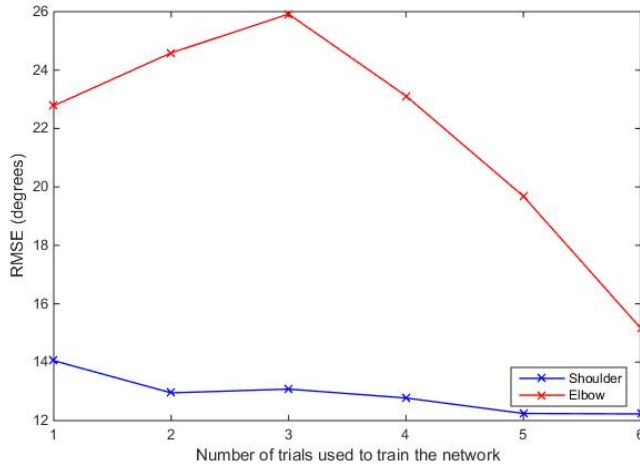


FIGURE 6.6: The RMSE obtained for different training set sizes

is substantial. On the other hand, when training the network for shoulder angle estimation, it was noticed that using a training set size of less than six trials does not cause a significant drop in performance for all performance measures.

6.3 Simultaneous joint movements

Following the modelling of different single joint movements, three simultaneous shoulder and elbow movements were modelled in three different planes using the MLP approach. Figure 6.7 shows the three types of modelled movements and the position of the markers for each movement. As in the previous case, ten trials, each 40s long were recorded for each movement. The Vicon motion capture system was used to record the position of four markers so that the two joint angles can be calculated. The elbow joint angle was calculated as described in Section 4.2.3, while for the shoulder joint angle, the angle between the hip/chest, shoulder and elbow markers was calculated using the same method.

The first movement, simultaneous elbow and shoulder movement in the x-z plane combines the elbow flexion/extension and the shoulder flexion/extension movements as can be seen in Figure 6.7(a). To capture this movement, both the elbow and shoulder angle were recorded simultaneously, together with four EMG channels: biceps brachii, triceps brachii, anterior deltoid and posterior deltoid. In this case, the MLP structure in Figure 6.8 was implemented, with four input nodes, three neurons in the hidden layer, two output nodes and 23 weights labelled W1 to W23.

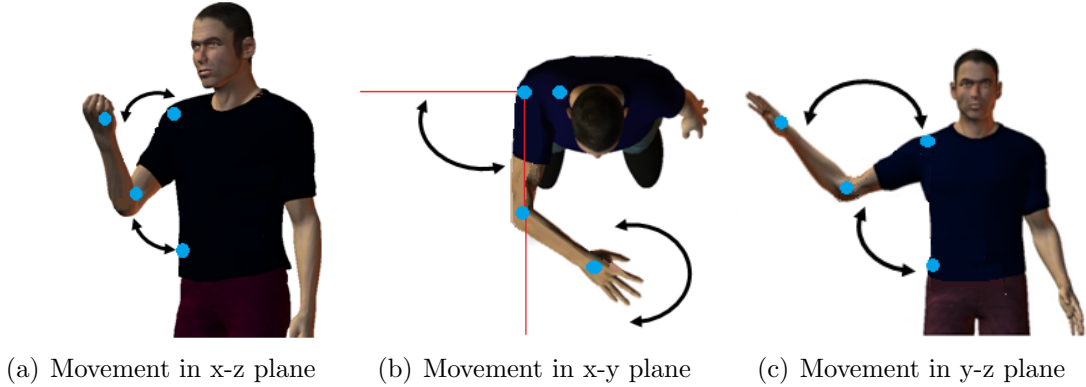


FIGURE 6.7: The three types of simultaneous joint movements [57] [Edited]

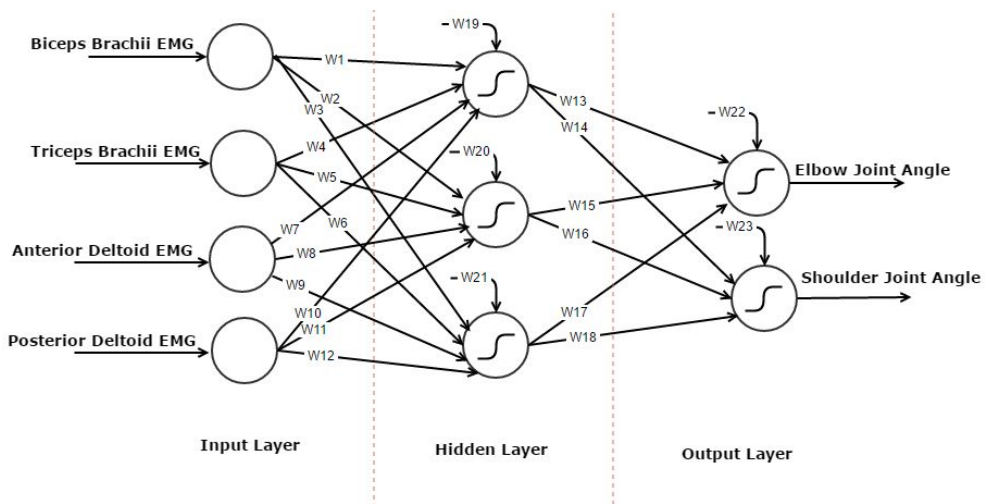


FIGURE 6.8: MLP structure for simultaneous control

The second modelled movement was simultaneous elbow and shoulder movement in the x-y plane, as can be seen in Figure 6.7(b). To capture this movement, both the elbow and shoulder angle were recorded simultaneously, together with three EMG channels: biceps brachii, triceps brachii and posterior deltoid. The anterior deltoid EMG was left out in this case as the anterior deltoid muscle is active throughout the movement in keeping the arm in its high vertical position. Hence including this EMG would not be useful in replicating the horizontal movement. Figure 6.9 shows the joint angles and EMG voltages for one of the trials recorded for this movement. For this model, the MLP structure in Figure 6.8 was used, however with three input nodes, three neurons in the hidden layer and two output nodes.

The final modelled movement, simultaneous elbow and shoulder movement in the y-z plane can be seen in Figure 6.7(c). This movement was repeated for several cycles, where both the elbow and shoulder angle were recorded simultaneously,

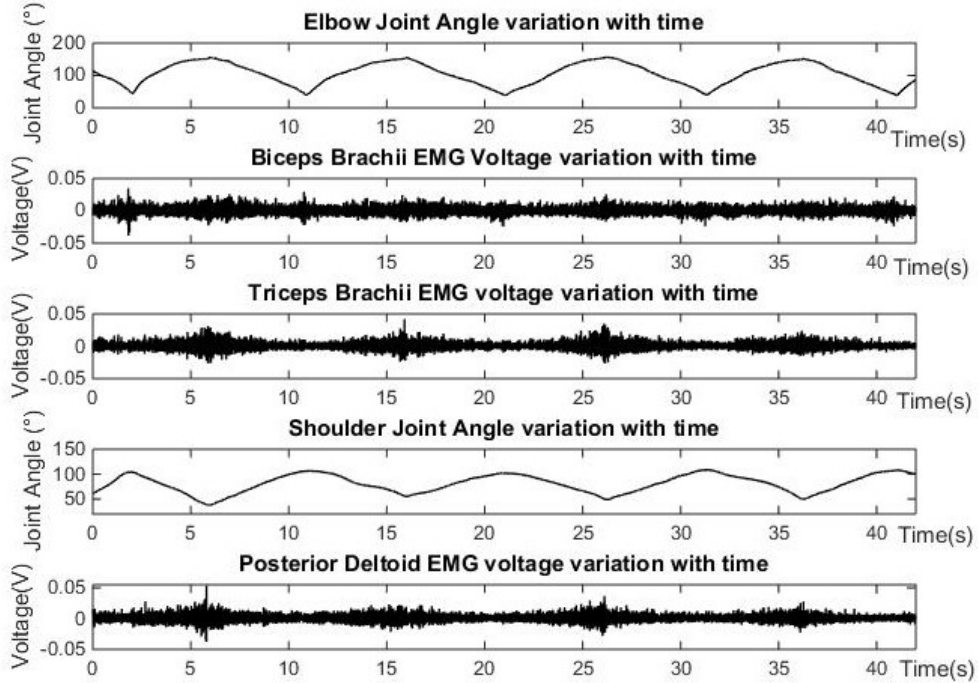


FIGURE 6.9: The three EMG sources with the corresponding joint angle

together with three EMG channels: biceps brachii, triceps brachii and anterior deltoid. As in the last movement, the MLP structure in Figure 6.8 was used, however with three input nodes, three neurons in the hidden layer and two output nodes.

For all of the movements, after pre-processing the EMG data using the RMS feature, the weights were calculated and the model was tested without cross-validation and with cross-validation. The RMSE, CC and R^2 parameters were used once again to evaluate the performance of the models.

6.3.1 Results

6.3.1.1 Movement in the x-z plane

In the first test without cross-validation, the average results were calculated over eight trials for both the elbow and shoulder angles. For the elbow angle, the average RMSE achieved was $7.13^\circ \pm 0.80^\circ$, the average CC was 0.984 ± 0.004 and the average R^2 value was calculated to be 0.966 ± 0.008 . For the shoulder angle, the average RMSE achieved was $3.62^\circ \pm 0.57^\circ$, the average CC was 0.983 ± 0.006 and the average R^2 value was calculated to be 0.967 ± 0.013 .

The results when testing the model with cross-validation can be observed in Table 6.5. One can note that results were consistent across each fold. The actual and estimated shoulder and elbow joint angles for Trials 7 and 8 when testing with cross-validation can be seen in Figure 6.10.

TABLE 6.5: Simultaneous movement in x-z plane cross-validation results

Trial number	Elbow Movement			Shoulder Movement		
	RMSE(°)	CC	R ²	RMSE(°)	CC	R ²
1,2	8.26	0.979	0.955	6.99	0.955	0.819
3,4	9.28	0.977	0.951	7.23	0.940	0.883
5,6	8.63	0.979	0.955	8.49	0.933	0.720
7,8	9.97	0.972	0.919	6.50	0.941	0.872
Mean	9.03	0.977	0.945	7.30	0.943	0.823
± SD	±0.75	±0.003	±0.018	±0.85	±0.009	±0.074

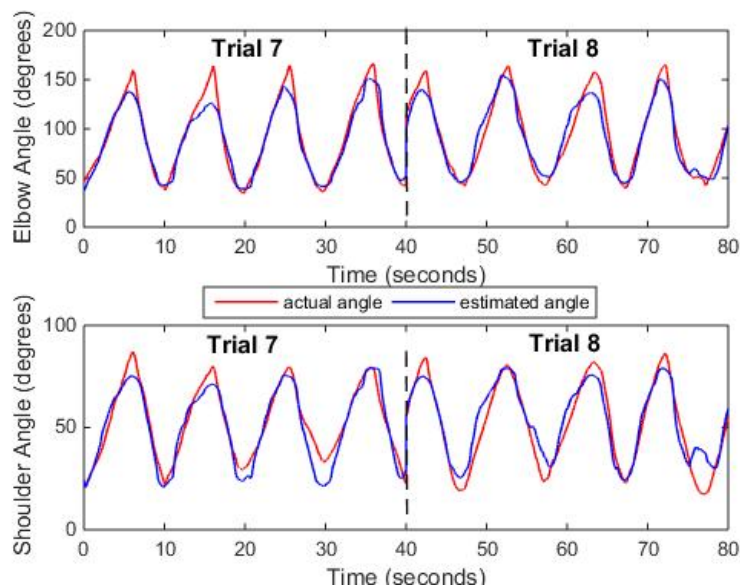


FIGURE 6.10: Actual and estimated joint angles for Trials 7 and 8

6.3.1.2 Movement in the x-y plane

The two tests were repeated for the simultaneous shoulder and elbow movements in the x-y plane. When testing without cross-validation, the average results were calculated over eight trials. For the elbow angle, the average RMSE achieved was **6.82° ± 0.87°**, the average CC was **0.977 ± 0.006** and the average R² value was calculated to be **0.952 ± 0.012**. For the shoulder angle, the average RMSE

achieved was $5.92^\circ \pm 1.23^\circ$, the average CC was 0.955 ± 0.015 and the average R^2 value obtained was 0.902 ± 0.035 .

The results when testing the model with a four-fold cross-validation test can be observed in Table 6.6. Although the average RMSE for the elbow and shoulder angles was very similar, the RMSE across the folds varied with high standard deviations. A similar trait was noted for the R^2 values, with standard deviation values for the shoulder angle estimation being very high. The actual and estimated shoulder and elbow joint angles for Trials 1 and 2 can be seen depicted in Figure 6.11.

TABLE 6.6: Simultaneous movement in x-y plane cross-validation results

Trial number	Elbow Movement			Shoulder Movement		
	RMSE(°)	CC	R^2	RMSE(°)	CC	R^2
1,2	10.65	0.953	0.890	9.47	0.895	0.726
3,4	15.94	0.954	0.689	10.73	0.869	0.164
5,6	11.66	0.958	0.866	15.35	0.894	0.065
7,8	9.42	0.959	0.903	12.23	0.919	0.309
Mean	11.92	0.956	0.837	11.94	0.894	0.316
± SD	± 2.84	± 0.003	± 0.010	± 2.54	± 0.020	± 0.291

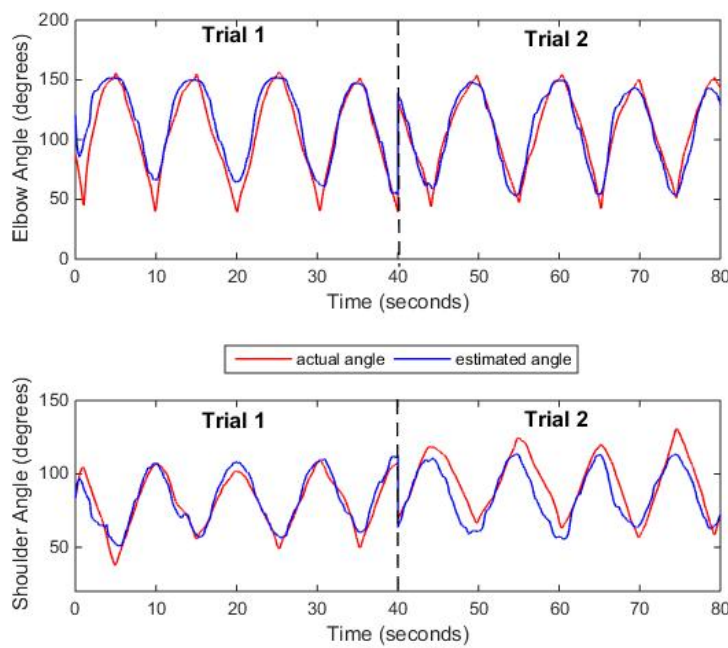


FIGURE 6.11: Actual and estimated joint angles for Trials 1 and 2

6.3.1.3 Movement in the y-z plane

The two tests were repeated for the simultaneous shoulder and elbow movements in the y-z plane. When testing without cross-validation, the average results were calculated over eight trials for both the elbow and shoulder angles. For the elbow angle, the average RMSE achieved was **13.84° ± 2.90°**, the average CC was **0.934 ± 0.026** and the average R² value was calculated to be **0.847 ± 0.068**. For the shoulder angle, the average RMSE achieved was **5.75° ± 1.76°**, the average CC was **0.962 ± 0.020** and the average R² value was calculated to be **0.920 ± 0.042**.

The results when testing the model with a four-fold cross-validation test can be observed in Table 6.7. Performance was noted to be inferior to the single joint movement in the same plane, especially for the elbow joint angle estimation. The actual and estimated shoulder and elbow joint angles for Trials 3 and 4 can be seen in Figure 6.12.

TABLE 6.7: Simultaneous movement in y-z plane cross-validation results

Trial number	Elbow Movement			Shoulder Movement		
	RMSE(°)	CC	R ²	RMSE(°)	CC	R ²
1,2	17.77	0.898	0.619	10.23	0.940	0.326
3,4	28.12	0.829	0.493	9.40	0.926	0.696
5,6	23.88	0.895	0.317	7.95	0.953	0.662
7,8	32.08	0.827	0.394	10.53	0.935	0.669
Mean	25.46	0.862	0.455	9.53	0.938	0.588
± SD	±6.12	±0.039	±0.131	±1.16	±0.011	±0.176

6.4 Discussion of Results

In this section a thorough analysis of the quantitative results and the plots obtained is carried out. The single joint movements and the simultaneous movements will be discussed separately. In the first case, where the shoulder angle was estimated when performing flexion and extension in the x-z plane, one can deduce from the non cross-validation results that the model was trained quite well. Performance remained consistent with the presentation of new data and was only slightly inferior to the non cross-validated results obtained.

The second modelled single joint movement was the flexion/extension movement

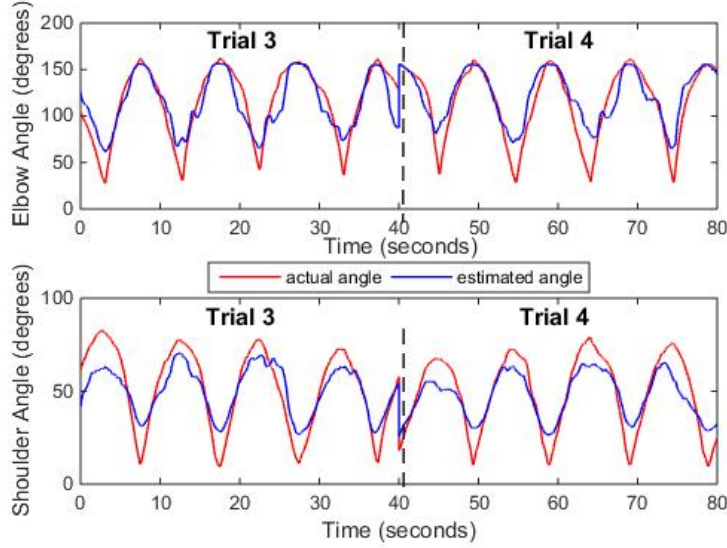


FIGURE 6.12: Actual and estimated joint angles for Trials 3 and 4

in the x-y plane. Results obtained without cross-validation were very good, which shows that the MLP was able to learn the characteristics of this data correctly. When testing with cross-validation, results were not as consistent as in the previous case, with the RMSE value varying from 6.92° to 10.78° over the four folds. The fourth fold was noted to perform superiorly to the other folds over all performance metrics. This shows that when training using the respective six trials of that fold, an adequate EMG-joint angle relationship was created, which was demonstrated when testing on the remaining two trials. For the shoulder adduction/abduction movement in the y-z plane, an accurate model was designed, which performed consistently in both tests with very small standard deviations over the RMSE, CC and R^2 values.

Comparing all the single joint movements covered in this project, as can be seen in Figure 6.13, there was a slight variance in CC values but quite a notable difference in the RMSE values. With an average RMSE of 5.43° with cross-validation, the shoulder movement in the y-z plane was the best performing single joint model in this project. Aung and Al-Jumaily in [43] also used the MLP approach to model the four single joint movements covered in this project, using all the biceps brachii, triceps brachii, anterior deltoid and posterior deltoid EMG signals in all cases. Unlike other publications, the RMSE obtained was less than 0.15° in all cases. It is not clear how such low errors were obtained, as only the mean square error was published, and we have no means to confirm these results.

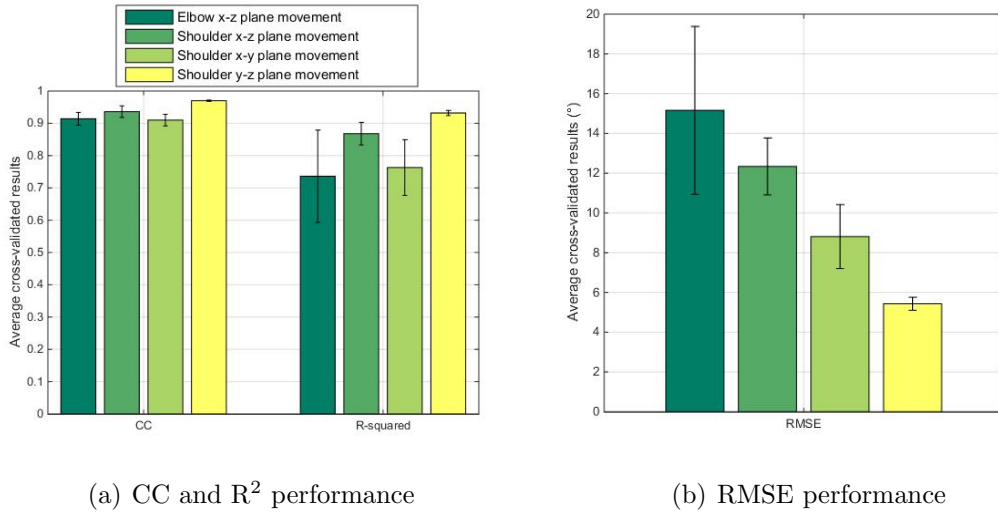


FIGURE 6.13: Comparing performance of the three single joint movements

In the case of the simultaneous elbow and shoulder flexion/extension movement in the x-z plane, excellent and consistent results were obtained across all trials for the non cross-validation test. When testing with cross-validation, results were superior for all performance measures for both shoulder and elbow angle estimation than the results obtained when separate MLPs were used in the previous analysis. This shows that although research [28] suggests using a separate MLP for each degree of freedom, for this type of movement it is beneficial to use a single MLP with two outputs. Results were consistent over all the trials tested, with low standard deviation results over all performance measures. On the other hand, when performing the simultaneous shoulder and elbow flexion/extension movement in the x-y plane, results were not consistent over all the cross-validation folds. In this case the shoulder angle estimation accuracy was inferior in the simultaneous movement rather than when the single joint movement was performed. In the last movement performed in the y-z plane results were contrasting. The shoulder angle was modelled quite accurately, however for the elbow estimation all the folds' performance metrics values varied significantly from each other.

Comparing the three simultaneous movements, Figure 6.14 shows the elbow and shoulder angle estimation performance for the three simultaneous movements. In this case the simultaneous movement in the x-y plane was the best performing movement with the lowest errors for both the shoulder and elbow estimation. Most of the previous simultaneous myoelectric control strategies that have been tested in amputees either rely on discrete gesture classification techniques [61, 62] or

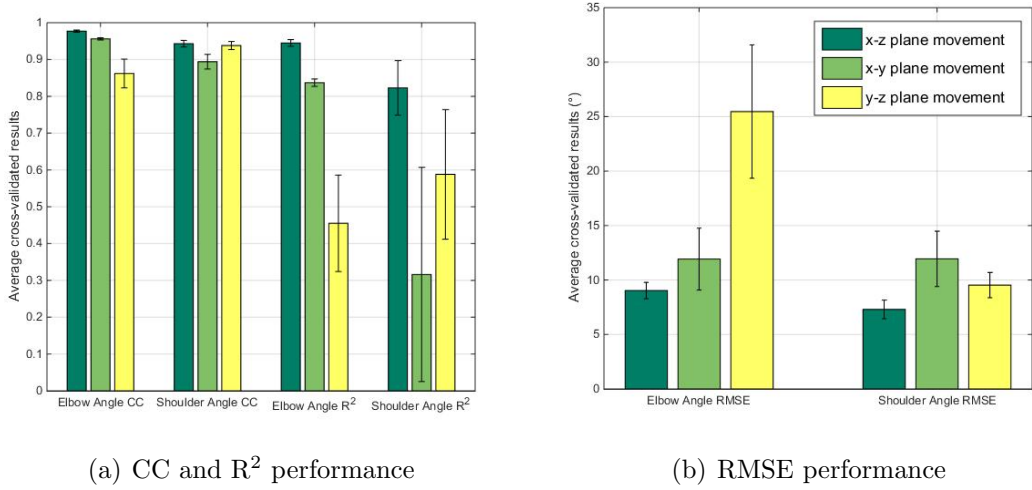


FIGURE 6.14: Comparing performance of the three simultaneous movements

else they use proportional techniques on estimating the wrist angles [27, 28, 30] rather than shoulder and elbow angles. Due to the novel factor of this project, a quantitative comparison of performance is not possible.

6.5 Summary

After choosing MLP neural networks as an appropriate EMG-joint angle estimation technique, in this chapter joint movements in different 2D spaces were modelled and their performance was evaluated. Six different models, one for each movement, including three simultaneous movements, were implemented and tested without and with cross-validation. Results show that EMG-to-joint angle modelling using a multi-layer perceptron can be applied to 2D movements in all three planes, however the best results were noted for shoulder adduction/abduction motion in the y-z plane and simultaneous shoulder and elbow vertical flexion/extension in the x-z plane.

The next chapter will investigate the possibility of having a robotic arm replicate some of these movements in real-time and hence highlighting possible applications of this work. The ability of the model to replicate intermittent movements will also be investigated.

Chapter 7

Real-time Application

7.1 Introduction

In the previous chapter six different models were implemented so as to estimate the joint angle position when performing three new single joint movements and three simultaneous joint movements involving the elbow and shoulder joints. This chapter presents the results obtained when a subset of these movements were replicated by a robotic arm in real-time. Apart from monitoring the robot's joint angles, an application was developed with the intention of having position control, in which case the robot arm's wrist was expected to follow the position in space of the subject's wrist. Details on the application and the results obtained are presented.

7.2 Elbow joint angle replication

In this project, the existing real-time system described in Section 4.3.1 and implemented by Grech [2] was used. Some minor changes were made in the C++ program and MATLAB script so as to upgrade the system to include more input EMG channels, as the one in [2] considered only one EMG signal input. The robotic arm used in this project is supplied with the CRS CataLyst-5T Simulink Library, which is basically a collection of custom S-functions designed for manipulation of the robot system in Simulink. For single joint replication, an in-built model titled ‘q_crs_pos_cntrl_joint.mdl’ [55] was used, where the angle of the joint being replicated can be controlled in real-time by providing the estimated joint angle.

7.2.1 Experimental Procedure

In order to assess the ability of the robotic arm in mimicking the elbow flexion/extension movement, the user and the robotic arm's elbow joint angles were compared. Before running the robotic arm, the Vicon camera system and the ZeroWire EMG acquisition box were used to create a new multi-layer perceptron (MLP) model, similar to what was done in Chapter 5. The model was created on the same day that the system was tested to ensure that the model remains valid for subsequent trials, since the characteristics of the EMG signal may vary slightly due to muscle fatigue or displacement of the probes location. This might not be required to run the system but was performed nonetheless to ensure the best possible results.

Using the model created, the CataLyst-5T robotic arm was run in real-time by using only the EMG data acquired from the biceps brachii and triceps brachii muscles. In the meantime the Vicon system was monitoring the position of the three reflective markers placed on both the subject and the robotic arm. This was done such that the angles of the user and the robotic arm are found using inverse kinematics and compared. To keep the angular ranges of the robot and human elbow equal, care was taken not to exceed the elbow angle range of 30° to 150° when performing the movement. Since the robotic arm has an elbow-up configuration and elbow flexion/extension is an elbow-down movement, the human angle needs to be transformed before it is sent to the robotic arm. To convert the robotic arm's elbow angle to that which represents the human elbow angle, it was subtracted from 180°, since upward movement of the robotic arm was made to correspond to upward movement of the human arm, and added by 30° [2].

7.2.2 Results

To evaluate the performance of the real-time system, five 30s trials were recorded and the root mean square error (RMSE), correlation coefficient (CC) and the coefficient of determination (R^2) between the human joint angle and robot joint angle were calculated for each trial. Since a delay of 0.5s exists between the human action and robot's replication, for the purpose of calculating the fore-mentioned parameters, the robot's joint angles were shifted by 0.5s to compensate for the delay. This is in accordance with what was done in [2] when a similar exercise was performed.

Table 7.1 shows the performance obtained for the five trials recorded. When testing the model offline, an average cross-validated RMSE of 18.34° was obtained. Figure 7.1 shows the resulting human and robotic arm elbow angles for Trial 1. It can be observed that the biggest errors are found at the points where the subject is changing the direction of his arm. One can attribute this phenomenon to the sigmoid functions in Simulink, which tend to slow down when a change in direction occurs, before actually following the direction [2]. In contrast, the human arm can change the direction of motion relatively fast. As was explained in Section 4.3.3, these functions serve to smooth the joint movement of the robotic arm as otherwise damage may be caused to the device.

TABLE 7.1: Human and robotic arm elbow angle performance

Trial number	RMSE($^\circ$)	CC	R^2
1	16.36	0.914	0.830
2	23.67	0.836	0.652
3	20.66	0.868	0.712
4	18.45	0.896	0.781
5	24.04	0.812	0.644
Mean \pm SD	20.64 ± 3.31	0.865 ± 0.042	0.724 ± 0.081

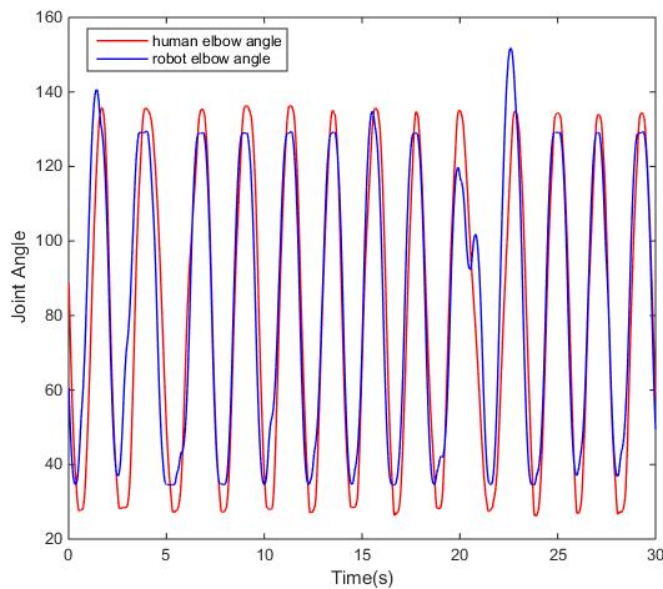


FIGURE 7.1: Human and robotic arm elbow angle for Trial 1

7.3 Simultaneous movement replication

Simultaneous control involves the control of more than one degree of freedom at the same time. In this project, three simultaneous movements which involved the elbow and shoulder in three different planes were modelled. As the robotic arm has an elbow-up configuration, while the human arm has an opposite configuration, it was not possible to control the robotic arm's angles and achieve an exact replication of both degrees of freedom. Hence, for simultaneous elbow and shoulder angle replication, it was decided to translate the joint angles to wrist position using the forward kinematics, and perform position estimation instead. In this case the goal is for the robotic arm to follow the human wrist position.

This required several changes to the real-time system. The training method and the MLP model were left unchanged, such that the model still estimates the elbow and shoulder joint angles. However, once the angles were calculated, the wrist position was calculated using the forward kinematics equations described in Section 4.3.4. Once the co-ordinates were calculated, these were sent to the Simulink model shown in Figure 7.2. This model is identical to the one used for angle control, except that an inverse kinematics block is added to convert the input co-ordinates to the robot's angles. Hence, in this case, only the end-effector's position will be controlled, with the robot's angles having no relation with the subject's elbow and shoulder angles.

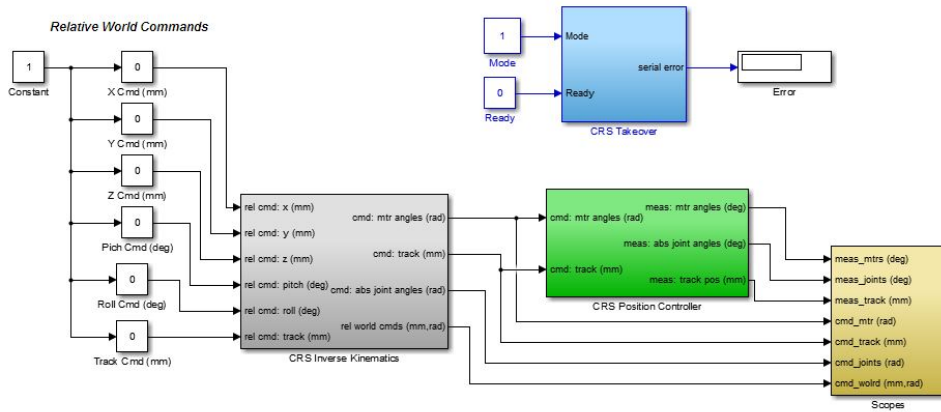


FIGURE 7.2: Robotic arm's position control Simulink model



FIGURE 7.3: Real-time wrist position control application

7.3.1 Application Procedure

In order to evaluate the real-time simultaneous movement replication performance, the simultaneous elbow and shoulder flexion/extension movement in the x-y plane was adapted to a typical movement performed every day. Three objects were placed on a horizontal plane, and the robotic arm followed the position of the subject's wrist when it moved and stopped in front of an object. As can be seen in Figure 7.3, the robotic arm was placed in front of the subject and it was configured so that it performs the mirrored position of the subject's wrist.

The same MLP structure as that used for simultaneous movement in the x-y plane was used, however, the pectoralis major EMG was used instead of the posterior deltoid EMG as can be seen in Figure 7.4. This was done as this movement was performed closer to the user's left arm, where the pectoralis major muscle becomes more involved than the posterior deltoid muscle. As was done for offline analysis, the Vicon camera system and the ZeroWire EMG acquisition box were used to gather position and EMG data simultaneously.

For the first time, the model was not trained with continuous movements only, but a protocol was developed which included one second stops in front of the three objects. This was done as an attempt to include intermittent movement, something which was not considered in the previous project [2] using the state space model. In fact, in [2], Grech established that a single state space model was unable to reliably convert EMG data to joint angle position for different speeds of movement.

It was further concluded that ‘multiple models or other compensatory methods would be required to cater for different speeds of movement’ [2].

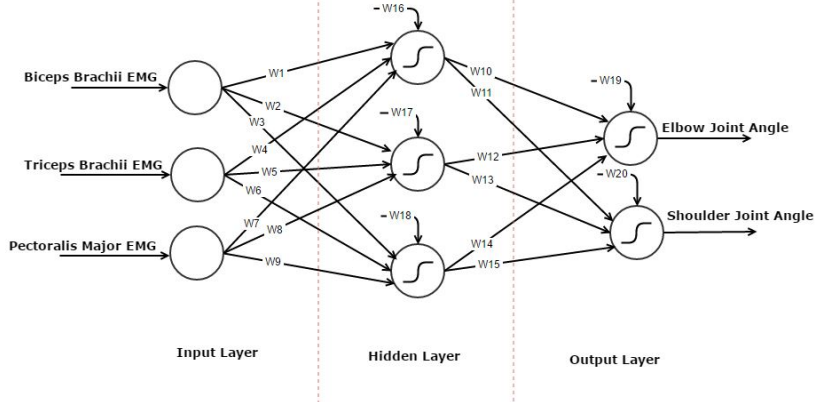


FIGURE 7.4: MLP structure for the real-time, simultaneous joint movement application

7.3.2 Results

The performance of the real-time system was evaluated by using the Vicon camera system to compare the position of the subject’s wrist and the robot’s end effector. The performance measures used were the RMSE and the CC for both the x and y positions. When training the model, care was taken not to exceed the 0-90mm range in the x-axis and the -270mm to 270mm range in the y-axis, as these are the position limits for the CRS Catalyst-5T robotic arm [55].

Table 7.2 shows the results obtained, where an average RMSE of 12.86mm and 48.69mm was obtained in the x and y directions respectively. Although it may seem that the performance in the x-axis was better than that in the y-axis, this is not the case, as one has to consider the fact that this axis had a range six times smaller than that of the y-axis. The CC measure is a better performance indicator in this case, and the results show a better overall estimation of the y-axis movement. Figure 7.5 shows a plot of the x position versus the y position for one cycle of movement in Trial 3.

Comparing these values with those obtained by Artemiadis and Kyriakopoulos [37] when using a state space model, results were very similar. In fact, the best result obtained in [37] for CC_x was 0.95 ± 0.03 while that for CC_y was 0.96 ± 0.03 , both of which fall within the standard deviation range of the results obtained in this

TABLE 7.2: Human and robotic arm simultaneous control performance

Trial number	$\text{RMSE}_x(\text{mm})$	$\text{RMSE}_y(\text{mm})$	CC_x	CC_y
1	15.98	39.60	0.862	0.960
2	9.99	72.51	0.960	0.945
3	16.21	35.97	0.867	0.971
4	11.98	42.84	0.916	0.947
5	10.12	52.02	0.934	0.932
Mean \pm SD	12.86 ± 3.06	48.59 ± 14.64	0.908 ± 0.043	0.951 ± 0.015

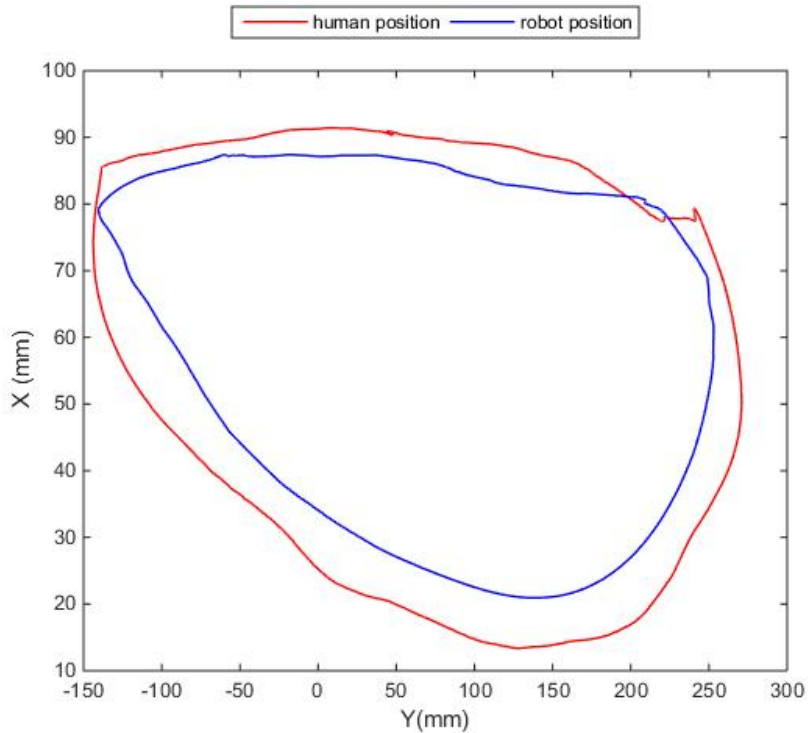


FIGURE 7.5: Human and robotic arm's x-y position for Trial 3

project. One needs to note that in this study, the z-axis and x-axis represent this project's x-axis and y-axis respectively.

This application can be used in many ways in the biomedical industry, especially in prosthetics for upper-limb amputees. An obvious extension of this exercise would be for object relocation. This would however require the inclusion of a gripper to the robotic arm, so that an object can be picked from a spot and placed in another location.

7.4 Summary

In this chapter, the MLP model which converts EMG data to joint angles was tested in real-time for both single joint movements and simultaneous elbow and shoulder movements. The elbow flexion/extension movement was evaluated by comparing the human elbow angle and the robot angle using the Vicon camera system. An average RMSE of $20.64^\circ \pm 3.32^\circ$ was recorded over five trials. Since the human elbow and shoulder angle could not be both replicated on the Catalyst-5T robot, for simultaneous movements, the wrist position was mimicked in real-time instead. An application for the simultaneous flexion/extension movement in the x-y plane was developed where the subject moves in the horizontal plane to choose an object, and the robotic arm replicates the same movement in real-time. Results for the elbow joint replication and simultaneous joint movement were compared to literature, and in both cases, similar results were obtained.

Chapter 8

Conclusion

The principal aim of this dissertation was to control a robotic arm using EMG signals, considering the simultaneous control of multiple degrees of freedom. A suitable model which maps EMG signals to joint angles was selected and extended to model several single joint and simultaneous joint movements. This chapter presents a summary of the work carried out in this dissertation, together with a concluding analysis and recommendations for future work.

8.1 Project Objectives and Achievements

The objective of this project was to implement a system that allows for proportional and simultaneous control of various degrees of freedom of a robotic arm in real-time using EMG signals from different muscles. In order for this to be accomplished, an initial study was carried out on the muscles of the shoulder and upper limb in Chapter 2, so as to help provide information on which muscles are activated for different kind of movements. This was useful when deciding which EMG channels to use when replicating several movements. The advantages and disadvantages of using EMG signals and the different types of EMG detection devices were also investigated.

Furthermore, a thorough literature review was conducted which focused on the different types of EMG-to-joint angle models used in research, previous projects, as well as the characteristics of an ideal myoelectric control system. Two types of myoelectric control systems were identified, the first involve gesture recognition of discrete movements while the second type consist of proportional continuous control. This project was focused on the second type of myoelectric control. Hahne *et al.* [28] proposed several methods for simultaneous and proportional myoelectric control

of the hand and the wrist. In particular they focused on finding the best way to linearise EMG data by applying several non-linear functions on the variance of the EMG data such as the logarithm and the square root. Similar tests were performed in this project so as to pre-process the EMG signal accordingly.

Through this review, three models were identified as suitable options for this project. These models were analysed for the estimation of the elbow angle during elbow flexion/extension. The first model investigated, which was also used in the previous project, was the state space model. As part of the analysis on the existing real-time system implemented by Grech [2], the robotic arm's response to a step input and sinusoidal inputs were investigated, so as to make sure that the robotic arm can move at certain speeds without delay. The state space model was tested with biceps brachii EMG and triceps brachii EMG and in the first case, the results obtained for the root mean square error (RMSE) were very similar to those achieved in [2]. The second model investigated, the linear regression model was found to be unable to generalise to new data and hence a third model, the multi-layer perceptron (MLP) was investigated. Aung and Al-Jumaily [43] used a MLP to identify the joint angles of separate single joint movements. The model built for this project was based on this work. Through several tests, the MLP was found to be the best performing model, and hence this model was extended to model different movements in different planes.

Six additional movements were modelled: three of them were single joint movements, while the remaining three movements were simultaneous elbow and shoulder movements. Different EMG signals from five different muscles were used in each case. First of all, three sequential joint movements were modelled. The average shoulder angle RMSE cross-validated results for these movements varied from 5.43° to 12.34° . The best performing simultaneous model was the simultaneous shoulder and elbow flexion/extension movement in the x-z plane with an average cross-validated RMSE result of $9.03^\circ \pm 0.33^\circ$ for the elbow angle estimation and $7.30^\circ \pm 0.85^\circ$ for the shoulder angle estimation. However, the overall best performing model was the shoulder movement in the y-z plane with an average cross-validated RMSE result of $5.43^\circ \pm 0.33^\circ$.

Finally the elbow movement in the x-z plane and the simultaneous elbow and shoulder movement in the x-y plane were replicated using the robotic arm in

real-time and their performance was evaluated. When estimating the elbow joint angle in the former task, an average RMSE of $20.64^\circ \pm 3.31^\circ$, correlation coefficient (CC) of 0.865 ± 0.042 and a coefficient of determination (R^2) of 0.724 ± 0.081 were obtained. In the latter case, since it was not possible to replicate both the elbow and shoulder angle at the same time using the Catalyst-5T robotic arm, the wrist position was mimicked by the robot's end effector. Hence the accuracy of the x and y positions in millimetres was evaluated. An average RMSE of $12.86\text{mm} \pm 3.06\text{mm}$ and $48.59\text{mm} \pm 14.64\text{mm}$ for the x and y end effector trajectories respectively were obtained. The CC value in the x direction was 0.908 ± 0.043 while that in the y direction was 0.951 ± 0.015 . A limitation in the previous project which was solved in this project was that of creating a model which is not restricted in speed by a metronome. At no point in this project were metronomes used while testing in real-time, and several times, the ability of the model to stop and continue was tested and the model reacted quite well. These results demonstrate the ability of the real-time robotic arm in replicating simultaneous human arm movement as was the objective of this dissertation.

8.2 Accomplishments and Recommendations

Even though all the objectives of this project were met, there are several aspects of the project which could be improved for the future. As part of the literature review, in Section 3.2.2, the criteria which must be effected to obtain an ideal myoelectric control system as described by Farina *et al.* [33] were presented. In this section, the criteria which were accomplished, or need to be fulfilled in the future will be discussed. These criteria must be satisfied in order to create a robust device which could be used commercially.

The first criterion requires control which is simultaneous and proportional. This was fulfilled in this project, where three simultaneous elbow and shoulder movements were modelled, one of which was tested in real-time. A further improvement would be including wrist and finger movements, as these were not catered for in this project. Secondly, the system is expected to be robust to the transient effects of the EMG signal. Although no tests on the system in this project were carried out to check the performance over different days of use, when the simultaneous joint model was tested a week after it was trained, reliable performance was still obtained. A systematic study needs to be carried out in this respect to verify

this preliminary observation. Furthermore the system needs to be tested for long durations where fatigue may come into effect. In that case a study needs to be carried out to see over which span of time this system can be used reliably and how to cater for issues such as fatigue. The third criterion enquires that the least possible number of electrodes must be used, and the system's performance must not be sensitive to their precise position. In replicating the movements, the number of electrodes was always kept to a minimum and the most dominant muscles for each specific movement were used.

The fourth point states that the training should be as short as possible and infrequent. One of the biggest issues in this project was the long training time involved so that a specific model for each movement can be made. Training the model to perform one movement can take up to two hours, which includes calibrating the Vicon camera system, performing ten trials, processing the position and EMG data into Excel files from the Vicon software, calculating joint angles, processing the EMG signal and finally training the network. When a test was carried out on the training set size of single joint movements, it was concluded that the training set size can be reduced for shoulder joint angle estimation, but not for elbow joint angle estimation. A solution for this issue would be to incorporate an online learning system, where the MLP's weights are adjusted in real-time, so that the system is trained whilst it is running.

The fifth criterion requires a computationally inexpensive system. This requires the model to be able to supply the estimated joint angles in the least possible time, such as not to create a bottleneck in the system. In this project this criterion was achieved, as the model was tested in real-time and the angles were supplied to the robotic arm at a continuous rate of 10Hz at all times. The final point states that motions should be replicated with a delay which is less than 0.2s. This was not achieved in this project as the delay between the user and robotic arm's movement was 0.5s.

Another issue which was tackled in the progress of this project was that of the robotic arm. Unfortunately, since the robotic arm has an elbow up configuration, simultaneous elbow and shoulder angle control could not be replicated in real-time, and hence wrist position control was implemented. Ideally, the model created

should be implemented on a robotic arm which can simulate the different shoulder and elbow movements.

The next logical step to further the work done in this project would be to incorporate all the models created into one model which can reproduce any movement in 3D space, as all possible movements in the different 2D planes have so far been investigated separately. Once this is complete, further testing on various subjects would be necessary to analyse the inter-variability of the system, and how it can be tuned for different users so that it can be used in practice.

Once all the points mentioned above are catered for, the system implemented in this project for reproducing different simultaneous elbow and shoulder movements would be ready to be developed as a fully functional prosthetic device.

References

- [1] P. Bezzina, “EMG Based Control of a Robotic Arm,” B.Eng. dissertation, University of Malta, Malta, 2013. 1, 24
- [2] S. Grech, “Analysis of EMG Signals for Real-Time Control of a Robotic Arm,” B.Eng. dissertation, University of Malta, Malta, 2014. 1, 24, 25, 26, 27, 28, 30, 35, 38, 39, 40, 47, 48, 78, 79, 80, 82, 83, 87
- [3] J. Basmajian, “Introduction,” in *Muscles Alive: Their Functions Revealed by Electromyography*, ch. 1, p. 10, The Williams & Wilkins Company, 1967. 4
- [4] “Candela Open Courses [online].” Available: https://courses.candelalearning.com/ap2x1/chapter/skeletal-muscle/#m46476-fig-ch10_02_02. [Accessed: 2016-05-09]. 5
- [5] “TeachPE [online].” Available: http://www.teachpe.com/anatomy/sliding_filament.php. [Accessed: 2016-05-09]. 6
- [6] H. Lodish, “Figure 17-30,” in *Molecular Cell Biology*, ch. 17, H Freeman and Company, 2008. 6
- [7] “Medical Blog [online].” Available: <https://ayeshaakhtar.wordpress.com/category/medical/>. [Accessed: 2016-05-09]. 7
- [8] “Anatomy and Physiology [online].” Available: <http://cnx.org/contents/FPtK1zmh@7.1:q0q5t3Jz@3/Muscles-of-the-Pectoral-Girdle>. [Accessed: 2016-05-09]. 7, 8
- [9] R. Drake, W. Vogl, and A. Mitchell, “Upper Limb,” in *Gray’s Anatomy for Students* (W. Schmitt, ed.), ch. 7, pp. 668–791, Churchill Livingstone, 2010. 8
- [10] Y. Sun, K. Yen, H. Kung, and Y. Tsai, “The muscular function for human knee movement revealed from electromyography: A preliminary study,” *Life Science Journal*, vol. 9, no. 1, pp. 453–456, 2012. 8
- [11] P. Artermiadis, “EMG-based Robot Control Interfaces: Past, Present and Future,” *Advances in Robotics and Automation*, vol. 1, no. 2, pp. 1–3, 2012. 8, 12

References

- [12] J. Cram and E. Criswell, “Introduction,” in *Cram’s Introduction to Surface Electromyography*, ch. 1, pp. 3–7, Jones and Bartlett Publishers, 2011. 9
- [13] J. Cram and E. Criswell, “Electrodes and Site Selection Strategies,” in *Cram’s Introduction to Surface Electromyography*, ch. 4, pp. 65–73, Jones and Bartlett Publishers, 2011. 10
- [14] “Omnilexica [online].” Available: <http://www.omnilexica.com/?q=electromyogram>. [Accessed: 2016-05-09]. 10
- [15] J. Basmaian, “Apparatus, detection and recording techniques,” in *Muscles Alive: Their Functions Revealed by Electromyography*, ch. 2, pp. 19–34, The Williams & Wilkins Company, 1967. 11
- [16] “King Medical [online].” Available: <http://kingmedical.com/media/catalog/product/cache/1/image/600x600/9df78eab33525d08d6e5fb8d27136e95/2/4/242.jpg>. [Accessed: 2016-05-09]. 11
- [17] “Motion-Lab [online].” Available: https://www.motion-labs.com/prod_access_finewire.html. [Accessed: 2016-05-09]. 11
- [18] S. Bitzer and P. van der Smagt, “Learning EMG control of a robotic hand: towards active prostheses,” in *Robotics and Automation, 2006. ICRA 2006. Proceedings 2006 IEEE International Conference on*, pp. 2819–2823, May 2006. 12
- [19] R. Okuno, M. Yoshida, and K. Akazawa, “Development of biomimetic prosthetic hand controlled by electromyogram,” in *Advanced Motion Control, 1996. AMC ’96-MIE. Proceedings., 1996 4th International Workshop on*, vol. 1, pp. 103–108 vol.1, Mar 1996. 12
- [20] C. Fermo, C. De Vincenzo, T. Bastos-Filho, and V. Dynnikov, “Development of an adaptive framework for the control of upper limb myoelectric prosthesis,” in *Engineering in Medicine and Biology Society, 2000. Proceedings of the 22nd Annual International Conference of the IEEE*, vol. 4, pp. 2402–2405 vol.4, 2000. 12
- [21] J. Naft, “Use of a Myoelectric Arm Orthoses to Improve Therapeutic and Functional Value for Patients with Severe Arm Dysfunction,” *Journal of Prosthetics and Orthotics (JPO)*, 2013. 12
- [22] H. Kazerooni, “Human-robot interaction via the transfer of power and information signals,” *Systems, Man and Cybernetics, IEEE Transactions on*, vol. 20, pp. 450–463, Mar 1990. 12

- [23] E. Cavallaro, J. Rosen, J. Perry, S. Burns, and B. Hannaford, "Hill-Based Model as a Myoprocessor for a Neural Controlled Powered Exoskeleton Arm - Parameters Optimization," in *Robotics and Automation, 2005. ICRA 2005. Proceedings of the 2005 IEEE International Conference on*, pp. 4514–4519, April 2005. 13
- [24] P. Artemiadis and K. Kyriakopoulos, "EMG-based teleoperation of a robot arm in planar catching movements using ARMAX model and trajectory monitoring techniques," in *Robotics and Automation, 2006. ICRA 2006. Proceedings 2006 IEEE International Conference on*, pp. 3244–3249, May 2006. 13
- [25] J. Vogel, C. Castellini, and P. van der Smagt, "EMG-based teleoperation and manipulation with the DLR LWR-III," in *Intelligent Robots and Systems (IROS), 2011 IEEE/RSJ International Conference on*, pp. 672–678, Sept 2011. 13
- [26] A. Fougner, O. Stavdahl, P. Kyberd, Y. Losier, and P. Parker, "Control of Upper Limb Prostheses: Terminology and Proportional Myoelectric Control; A Review," *Neural Systems and Rehabilitation Engineering, IEEE Transactions on*, vol. 20, pp. 663–677, Sept 2012. 14
- [27] S. Muceli and D. Farina, "Simultaneous and Proportional Estimation of Hand Kinematics From EMG During Mirrored Movements at Multiple Degrees-of-Freedom," *Neural Systems and Rehabilitation Engineering, IEEE Transactions on*, vol. 20, pp. 371–378, May 2012. 15, 21, 77
- [28] J. Hahne, F. Biebmann, N. Jiang, H. Rehbaum, D. Farina, F. Meinecke, K.-R. Muller, and L. Parra, "Linear and Nonlinear Regression Techniques for Simultaneous and Proportional Myoelectric Control," *Neural Systems and Rehabilitation Engineering, IEEE Transactions on*, vol. 22, pp. 269–279, March 2014. 18, 19, 20, 26, 39, 50, 58, 61, 76, 77, 86
- [29] J. Hahne, S. Dahne, H.-J. Hwang, K.-R. Muller, and L. Parra, "Concurrent adaptation of human and machine improves simultaneous and proportional myoelectric control," *Neural Systems and Rehabilitation Engineering, IEEE Transactions on*, vol. 23, pp. 618–627, July 2015. 19
- [30] N. Jiang, J. L. Vest-Nielsen, S. Muceli, and D. Farina, "EMG-based simultaneous and proportional estimation of wrist/hand kinematics in uni-lateral trans-radial amputees," *Journal of NeuroEngineering and Rehabilitation*, vol. 9, no. 1, pp. 1–11, 2012. 15, 22, 58, 77
- [31] A. Fougner, O. Stavdahl, and P. Kyberd, "System training and assessment in simultaneous proportional myoelectric prosthesis control," *Journal of Neuro-Engineering and Rehabilitation*, vol. 11, no. 1, p. 75, 2014. 15

- [32] M. Ahsan, M. Ibrahimy, and O. Khalifa, “Electromyography (EMG) signal based hand gesture recognition using artificial neural network (ANN),” in *Mechatronics (ICOM), 2011 4th International Conference On*, pp. 1–6, May 2011. 15
- [33] D. Farina, N. Jiang, H. Rehbaum, A. Holobar, B. Graimann, H. Dietl, and O. Aszmann, “The Extraction of Neural Information from the Surface EMG for the Control of Upper-Limb Prostheses: Emerging Avenues and Challenges,” *Neural Systems and Rehabilitation Engineering, IEEE Transactions on*, vol. 22, pp. 797–809, July 2014. 15, 88
- [34] K. Ogata, “Analysis of Control System in State-Space,” in *Modern Control Engineering*, ch. 11, pp. 711–725, Pearson Education Inc., 3 ed., 2010. 16
- [35] J. Han, Q. Ding, A. Xiong, and X. Zhao, “A State-Space EMG Model for the Estimation of Continuous Joint Movements,” *Industrial Electronics, IEEE Transactions on*, vol. 62, pp. 4267–4275, July 2015. 17
- [36] Q. Ding, A. Xiong, X. Zhao, and J. Han, “A novel EMG-driven state space model for the estimation of continuous joint movements,” in *Systems, Man, and Cybernetics (SMC), 2011 IEEE International Conference on*, pp. 2891–2897, Oct 2011. 17
- [37] P. Artermiadis and K. Kyriakopoulos, “EMG-Based Control of a Robot Arm Using Low-Dimensional Embeddings,” *Robotics, IEEE Transactions on*, vol. 26, pp. 393–398, April 2010. 17, 39, 41, 63, 83
- [38] P. Artermiadis and K. Kyriakopoulos, “A Switching Regime Model for the EMG-Based Control of a Robot Arm,” *Systems, Man, and Cybernetics, Part B: Cybernetics, IEEE Transactions on*, vol. 41, pp. 53–63, Feb 2011. 17
- [39] “Linear Regression [online].” Available: <http://www.stat.yale.edu/Courses/1997-98/101/linreg.htm>. [Accessed: 2016-05-09]. 18
- [40] J. Hahne, K. Muller, and D. Farina, “An Embedded System for Simultaneous and Proportional Myoelectric Control of Upper Limb Prostheses,” in *IEEE Engineering in Medicine and Biology Society, 37th Annual International conference*, August 2015. 19
- [41] J. Foroozesh, A. Khosravani, A. Mohsenzadeh, and A. Mesbahi, “Application of Artificial Intelligence (AI) Modeling in Kinetics of Methane Hydrate Growth,” *American Journal of Analytical Chemistry*, vol. 4, no. 11, pp. 616–626, 2013. 21
- [42] E. J. Rechy-Ramirez and H. Hu, “Bio-signal based control in assistive robots: a survey,” *Digital Communications and Networks*, vol. 1, no. 2, pp. 85 – 101, 2015. 21

- [43] Y. Aung and A. Al-Jumaily, "Estimation of Upper Limb Joint Angle Using Surface EMG Signal," *International Journal of Advanced Robotic Systems*, vol. 10, no. 369, pp. 1–8, 2013. 22, 23, 26, 50, 56, 75, 87
- [44] J. Cram and E. Criswell, "Anatomy and Physiology," in *Cram's Introduction to Surface Electromyography*, ch. 2, pp. 9–34, Jones and Bartlett Publishers, 2011. 22
- [45] P. Artemiadis and K. Kyriakopoulos, "An EMG-Based Robot Control Scheme Robust to Time-Varying EMG Signal Features," *Information Technology in Biomedicine, IEEE Transactions on*, vol. 14, pp. 582–588, May 2010. 23, 39
- [46] E. Scheme, A. Fougner, . Stavdahl, A. Chan, and K. Englehart, "Examining the adverse effects of limb position on pattern recognition based myoelectric control," in *Engineering in Medicine and Biology Society (EMBC), 2010 Annual International Conference of the IEEE*, pp. 6337–6340, Aug 2010. 23
- [47] A. Fougner, E. Scheme, A. Chan, K. Englehart, and O. Stavdahl, "Resolving the Limb Position Effect in Myoelectric Pattern Recognition," *Neural Systems and Rehabilitation Engineering, IEEE Transactions on*, vol. 19, pp. 644–651, Dec 2011. 23
- [48] L. Hargrove, K. Englehart, and B. Hudgins, "The effect of electrode displacements on pattern recognition based myoelectric control," in *Engineering in Medicine and Biology Society, 2006. EMBS '06. 28th Annual International Conference of the IEEE*, pp. 2203–2206, Aug 2006. 23
- [49] P. Pilarski, M. Dawson, T. Degris, F. Fahimi, J. Carey, and R. Sutton, "Online human training of a myoelectric prosthesis controller via actor-critic reinforcement learning," in *Rehabilitation Robotics (ICORR), 2011 IEEE International Conference on*, pp. 1–7, June 2011. 24
- [50] "Aurion [online]." Available: <http://www.aurion.it/ZeroWire%20Technical%20Features%20rev02.pdf>. [Accessed: 2016-05-09]. 28
- [51] "Vicon [online]." Available: <http://www.vicon.com/what-is-motion-capture>. [Accessed: 2016-05-09]. 29
- [52] H. Asda, "MIT OpenCourseware [online]." Available: <http://ocw.mit.edu/courses/mechanical-engineering/2-12-introduction-to-robotics-fall-2005/lecture-notes/chapter4.pdf>. [Accessed: 2016-05-09]. 30
- [53] "Learn-to-draw [online]." Available: <http://www.learn-to-draw.com/figure-drawing/03-draw-male-arm-proportions.shtml>. [Accessed: 2016-05-09]. 30

References

- [54] Thermo CRS, *CataLyst-5 Robot System User Guide*, July 2002. 32
- [55] Quanser, *CataLyst-5 Robot System - Position Control with QuaRC User Guide*, 1.1 ed. 32, 33, 78, 83
- [56] P. Van Overschee and B. De Moore, “Introduction, Motivation and Geometric Tools,” in *Subspace Identification For Linear Systems: Theory, Implementation, Applications*, ch. 1, Kluwer Academic Publishers, 1996. 39
- [57] R. Gopura, K. Kiguchi, and E. Horikawa, “A Study on Human Upper-Limb Muscles Activities during Daily Upper-Limb Motions,” *International Journal of Bioelectromagnetism*, vol. 12, no. 2, pp. 54–61, 2010. 40, 64, 70
- [58] M. Rahman, C. Ochoa-Luna, and S. M., “EMG Based Control of a Robotic Exoskeleton for Shoulder and Elbow Motion Assist,” in *Journal of Automation and Control Engineering*, vol. 3, August 2015. 53
- [59] The MathWorks, *Neural Network Toolbox: For Use with MATLAB*, 4 ed., 2002. 57
- [60] G. Brightwell, C. Kenyon, and H. Paugam-Moisy, “Multilayer neural networks: One or two hidden layers?,” in *Advances in Neural Information Processing Systems 9, Proc. NIPS*96*, pp. 148–154, MIT Press, 1996. 57
- [61] A. Young, L. Smith, E. Rouse, and L. Hargrove, “A new hierarchical approach for simultaneous control of multi-joint powered prostheses,” in *Biomedical Robotics and Biomechatronics (BioRob), 2012 4th IEEE RAS EMBS International Conference on*, pp. 514–520, June 2012. 76
- [62] A. J. Young, L. H. Smith, E. J. Rouse, and L. J. Hargrove, “A comparison of the real-time controllability of pattern recognition to conventional myoelectric control for discrete and simultaneous movements,” *Journal of NeuroEngineering and Rehabilitation*, vol. 11, no. 1, pp. 1–10, 2014. 76